University of Padova

DEPARTEMENT OF MANAGEMENT AND ENGINEERING

MASTER DEGREE IN INDUSTRIAL ENGINEERING

Integrated methodology for quality evaluation of molten metal in Al foundry

Supervisor: Ch.mo Prof. GIULIO TIMELLI

Advisor: Dott. SILVIO BARISON
             Dott. FILIPPO VOLTAZZA

Student: ANDREA GNESOTTO

Vicenza, December 2013

To my family and Elena,

who have always supported me in everything I have done.

ACKNWOLEDGEMENT

LIST OF ILLUSTRATIONS

LIST OF TABLES

TABLE OF CONTENTS

CV Andrea Gnesotto

INTRODUTCION

Aluminium industry has increased steadily in the last 20 years. This light metal has replaced many others in a lot of applications, especially in automotive field that produce the largest request for aluminium casting products. The applications have been increased by the industry requests for new solutions to save weight and improve performance. The weight of casting is continuously augmenting to save joining and welding operation costs, but the effect of defects on them is more critical due to the higher wall thickness.

Campbell said [1]: "Although the manufacturing path from the liquid to the finished shape is the most direct, this directness involves the greatest difficulty. This is because so much needs to be controlled simultaneously, including melting, alloying, moulding, pouring, solidification, finishing, etc. Every one of these aspects has to be correct since failure of only one will probably cause the casting to fail."

Therefore, with the purpose of improving the quality of castings, this thesis focuses on the first step to gain defects-free components: the control of melting stage. All defects formed before solidification stage could be carried to final product adding to any other subsequent casting process defect and will affect component behaviour. If defects coming from the melting stage cannot be distinguished from those coming from the following stages, the corrective actions could be useless or even harmful.

Actually, there is no a definitive and universal test capable of identifying and classifying the defects that can occur in aluminium alloy melts. These defects are dissolved hydrogen and the entrained aluminium oxides, known as bifilms, which have been held responsible for the failure of castings. This work tries to evaluate the most common quality assessment techniques, both in laboratory and in the foundry to find the best one in terms of cost, ease to use and quickness. The final aim is the achievement of a procedure to measure the melt cleanliness in industrial field, from smelters to casters. Economic potential is very high, considering all foundry costs due to the lack of quality that affect one of the most energy-demanding industries in Europe.

This work was developed within the of MUSIC project (MUlti-layers control&cognitive System to drive metal and plastic production line for Injected Components) that involves a lot of European universities and companies. The purpose of the project is to increase the quality in aluminium industry and this thesis is the first step to overcome the challenge.

SUMMARY

Aluminium casting theory related to this work is presented in Chapter 1. Particular attention is given to oxides formation and their relationship with porosity and hydrogen content. Then molten metal quality assessment techniques are presented and the contest of this work is explained.

In Chapter 2, the experimental procedure is described in detail both for laboratory and industrial tests. Quality indexes used for the reduce pressure test, filtration and hydrogen measurement are presented with operating conditions applied.
Once the method for each instrument was established in the laboratory, they were applied in the industrial environment to obtain the largest possible data sets for three different alloys in different conditions. Degassing was deeply studied, changing flow rate and duration, moreover effect of time processing on metal quality was also analysed. Finally foundry suppliers were evaluated using quality assessment method proposed.

In Chapter 3, the laboratory results and differences between quality indexes chosen were presented. Further industrial tests data for supplier evaluation, degassing and time processing were analysed.

The interpretation of results and their implications, are explained in Chapter 4. The "quality assessment methodology" is also presented.

Finally, Chapter 5 presents the conclusions and the possible economic implications of this work.

CHAPTER 1

LITERATURE REVIEW

Aluminium production has grown steadily in the last fifty years due to his considerable properties such as lightweight, ductility, recyclability, high strength, corrosion resistance, durability and formability. This unique combination of properties contributes to increase the number of aluminium applications, especially in aerospace and automotive industries. The necessity to reduce pollution and fuel consumption, increase performance, reduce production costs and gain high strength/weight ratio allowed the aluminium alloys to replace iron-based alloys in automotive field, as seen in Figure 1.1
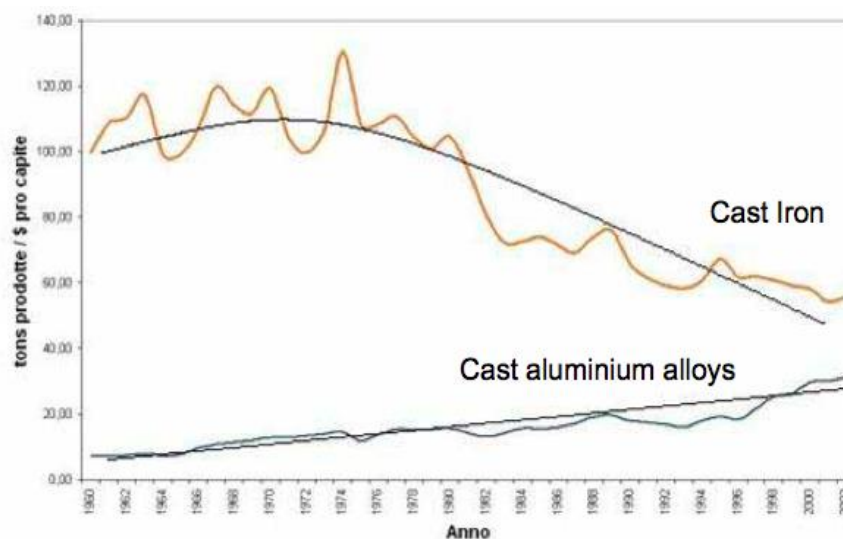
Figure 1.1: Cast iron and cast aluminium alloys technological evolution [2].

Foundry is the most important process to produce all those three-dimensional shape components widely used in the cars; automotive industry is the largest market for aluminium castings. Most important products are wheels, suspension arms, engine blocks, cylinder heads and pistons. The volume of cast aluminium components is projected to grow significantly year by year [3]. Aluminium castings are affected by a significant defectively, not only due to shrinkage and gas porosity, as it was supposed for decades, but particularly because of the presence of oxide bifilms, extremely thin but harmful defects

[1]. Bifilms have crack-like shape and may open to become porosity into final components. In both cases they are detrimental for the mechanical properties and responsible for many failures in products, for example poor strength, low fatigue properties and reduced elongation [4-6].

This study begins from the theory of Al oxide bifilms and it will try to evaluate most common quality assessment techniques to find the best way to measure the melt cleanliness in industrial field.

1.1 Casting processes

The most common casting processes can be classified by the type of mould, pattern, or pressure applied to fill the mould cavity with molten metal. Sand and shell casting are used for big pieces or complex geometry and utilize a permanent pattern, but the mould is disposable. Permanent moulds, called dies, are usually made by machined steel and are used for large volume production castings of medium size. Investment casting and lost foam processes utilize an expendable mould and an expendable pattern. The highest quantity of aluminium is used in die casting processes [7], and between them high pressure die casting (HPDC) is the most important, as seen in Figure 1.2. HPDC is characterized by forcing molten metal into die cavity with high pressure obtained with a piston. It is widely used in automotive industry because has the highest productivity, with a cycle time between 30 seconds and 60 minutes.
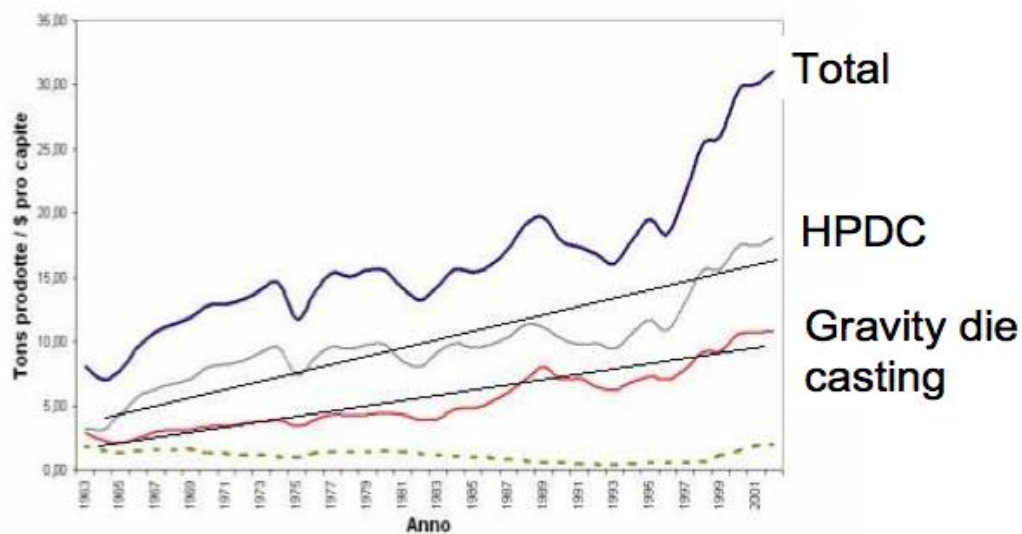
Figure 1.2: HPDC and gravity die casting technological evolution [2].

The geometry of pieces cannot be too complex due to extraction system of the die, for example undercut should be avoided and cores cannot be used. However, the microstructure is very fine due to rapid solidification, but a lot of defects could be introduced into final products due to turbulence, lubricant, process parameters and, of course, molten metal quality.

Aluminium production is double than other light metals and cast products consume 20% of aluminium, as world average [7]. Apart from lightness, other advantages of aluminium alloys for casting processes are lower melting temperatures compared to iron-based alloys that means less energy consumption, good surface finish (near-net shape) and negligible solubility for all gases except hydrogen. Mechanical properties are widely ranged and it can be further modified by alloying elements and/or heat treatment. Shrinkage is one of the major problem for aluminium castings because is relatively high, between 3,5 and 8,5% [8].

1.2 Metal quality

The metal quality is affected by three important features: non-metallic inclusions, trace elements and dissolved gasses. Inclusions in the aluminium alloy can cause premature failure of a component because they act as stress-raisers or they can break tools during machining due to their hardness. The most common inclusions observed in molten aluminium are oxides. They arrive in the melt from skin of material to be melted and further form as films during melting stage. If submerged, oxides float free and become suspended in the melt. In final castings these films are founded as massive film-like or dross-like inclusions [1]. These defects can make mechanical properties of castings unpredictable and in general lower than standard alloy values.

The control of the liquid metal should be the first quality check, due to the significant amount of oxide formed during melting process and coming from the charge. Ingots already contain a population of defects, introduced during previous processing that normally includes one or more pouring steps. However, an high number of oxides may be added if the melt is handled poorly, particularly if it is violently stirred, shacked or poured, but if during the final casting operation the melt is handled carefully, quiescently, defects should not form [1].

As previously said ,oxide films form during melting, but other interactions can occur between aluminium melt and its environment like the absorption of hydrogen or entrapment of other inclusions. Hydrogen is absorbed readily in liquid aluminium but is

much less soluble in the solid state and may form porosity if exceed solubility limit during solidification. Further alumina form quickly on exposed liquid aluminium surfaces and it is impossible to prevent its formation, but has an important part in the melting process, because it protects the metal below from further oxidation. However, if an oxide film is pushed into the melt its surface fold on itself in two non-wetting surface films that will trap between them a certain quantity of gas (Figure 1.3). This defect that will act exactly like a crack in the liquid and it is known as a 'double oxide film' defect or a 'bifilm' [1]. Therefore, defects can be introduced into the casting process from the melting stage, where hydrogen gas, inclusions and oxide films can be incorporated into the melt.
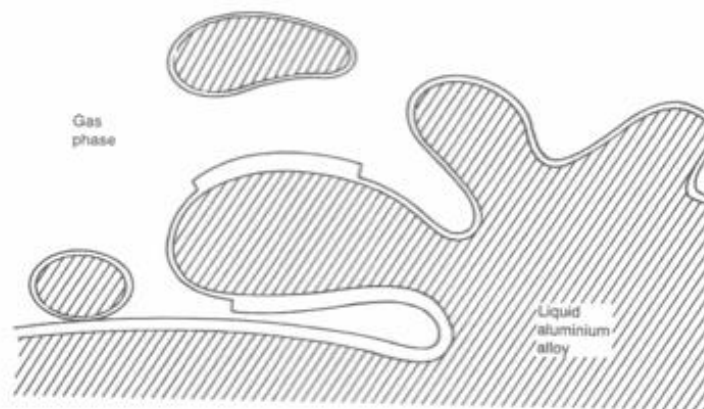
Figure 1.3: Surface turbulence; the most common mechanism of introducing bifilm into the melt [1].

1.3 Hydrogen content

Molten aluminium is inclined to considerable adsorption of hydrogen more than other gas, due to the small volume of its atom, which can cross alumina film on the surface and it can be taken into solution in the melt [1].

The main source for hydrogen is the dissociation of water vapour coming from fluxes, crucibles, refractories and charge materials. The atmosphere can also be a source of water vapour, especially on hot and humid days. The chemical reactions involved are:

$$2\,Al + 3H_2O \ \rightarrow Al_2O_3 + 3H_2 \tag{1.1}$$

$$^1/_2 \, H_2 \, (gas) \leftrightarrow H \, (in \, Al) \qquad\qquad (1.2)$$
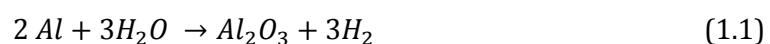
Equation 1.1 refers to splitting of water into oxygen, which combined with aluminium will form alumina, and hydrogen gas. Then gas is absorbed by melt as seen in equation 1.2. Figure 1.4 shows the solubility of hydrogen in pure aluminium [7]. It can be observed how the hydrogen content decreases with decreasing temperature. This decreased solubility in the solid phase may cause porosity due to precipitation of hydrogen gas.
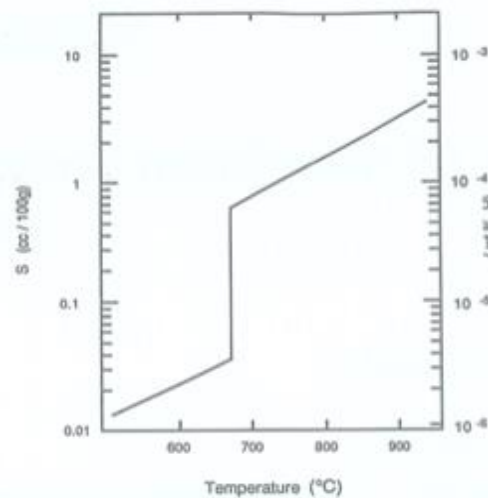
Figure 1.4: Solubility of hydrogen in pure aluminium as a function of temperature [7].

1.4 Oxides

1.4.1 Formation of oxide film

Aluminium tends to react with air to form oxide and such behaviour is the cause of many problems in melting and casting operations. Oxide film that forms on the surface of solid metal protects it from further oxidation, and at the same time may slow down the dissolution and release of hydrogen. In the case of liquid metal, formation of solid oxide layer is sudden and, when new solid forms on top of the melt, volume or length changes are required, so higher phases has to give way to grow. Therefore, with discontinuous films, the oxygen will penetrate through breaks, not by diffusion, and continue its path downward as time goes by. Such behaviour would be expected to occur during multi-layer growth of films on liquids because it has been observed during multi-layered oxides growth on solid metals [9].

Pure aluminium is very reactive with oxygen, so formation of first amorphous alumina layer starts within milliseconds. This film forms a protective layer over the molten aluminium because prevents the diffusion of aluminium and oxygen ions. Since amorphous films are entrained quickly and have little time to grow, are characterised by extreme thinness, usually measured in tens of nanometres and so are called '*young oxides*' [10] (Figure 1.5 a).

After incubation time the amorphous oxide film changes its structure discontinuously. At high temperature oxygen ions in the atmosphere cross the oxide-metal interface and causes the nucleation and growth of γ-Al_2O_3 crystalline phase under the amorphous layer. This process usually starts after 5 to 10 minutes at 750°C [10] and is increased by high temperature and inclusion content in the melt. During this period the films become thicker, from nanometres to micrometres or even millimetres thick and called '*old oxides*' [11], characterised by crystalline structure (Figure 1.5 b).

After crystallization, films grow inside thanks to diffusion of oxygen through the crystalline oxide layer and continuous exposure to high temperature. Therefore oxides finally turn from Υ to α Al_2O_3. During this transformation the 24% of their volume is loss due to the structure and morphology change from cubic spinel γ- Al_2O_3 to rhombohedral α-Al_2O_3. This results in a fracture of the oxide, in which oxygen slips and the process starts again.
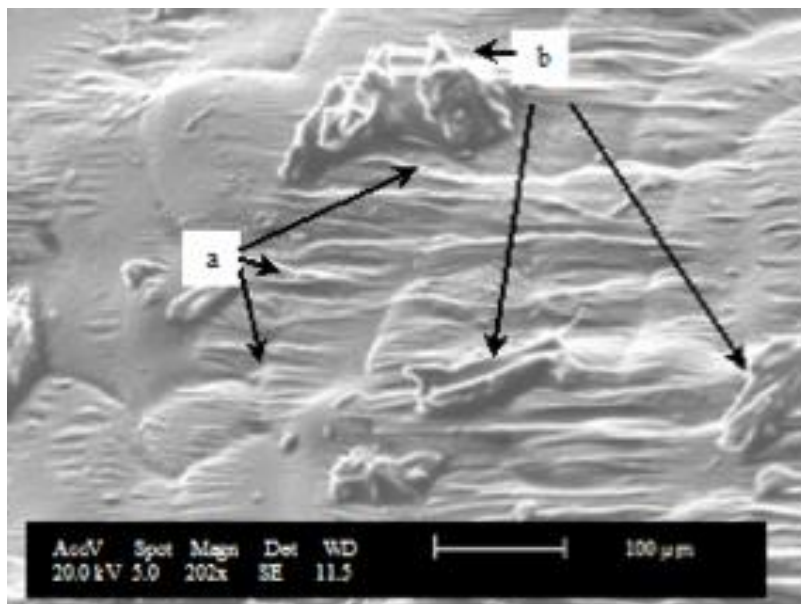
Figure 1.5: SEM pictures of (a) young and (b) old oxides [12].

The type of oxides formed depends on the melt composition. Elements such as copper, iron, and manganese could have a certain effect on oxidation process. For example in the presence of approximately 0.005% of magnesium, surface oxide is made by the mixed oxide $MgO.Al_2O_3$ also known as spinel, but above 2%, then the oxide film is expected to be only MgO [1]. Example of these oxides is seen in Figure 1.6 and 1.7.
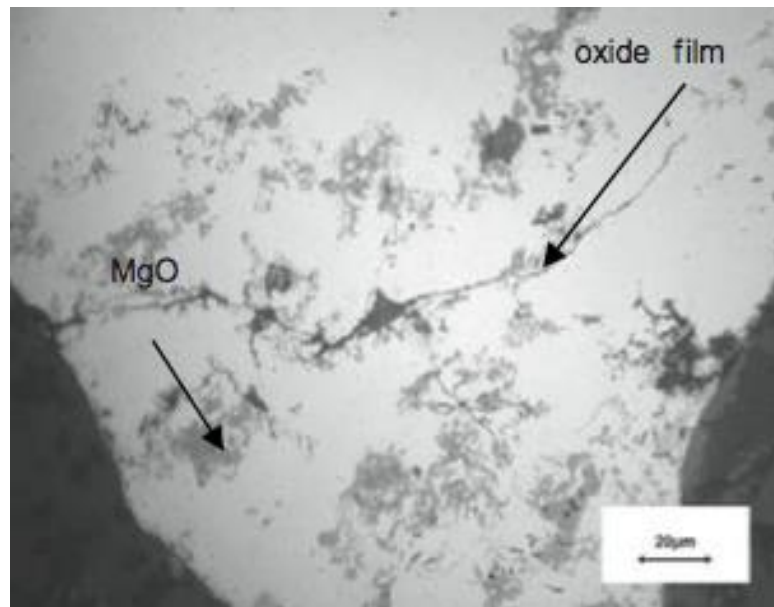
Figure 1.6: Optical micrograph of oxide film and MgO [4].
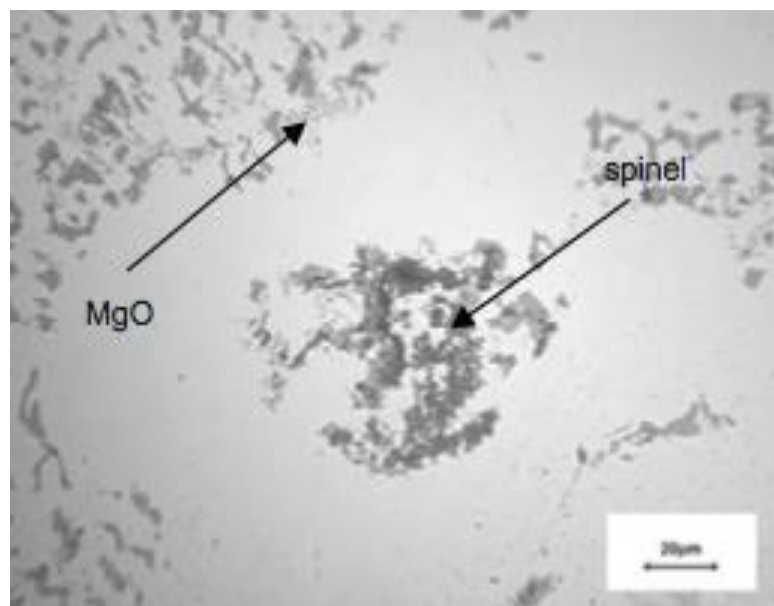
Figure 1.7: Optical micrograph of spinel and MgO [4].

1.4.2 Surface entrainment of bifilms

Thanks to the protective action of alumina film, molten aluminium can benefit from this oxide layer because oxidation cannot continue further into the melt. Since surface film is not submerged, oxides are not a problem [1]. During entrapment action, a single oxide cannot be submerged alone; it has to be folded one or more times and so two film surfaces will be brought into contact. This bifilm will act as a crack in the liquid [1]. During turbulent filling, handling, transfer or pouring, these cracks are submerged into the melt. This surface entrainment occurs if the velocity of the liquid aluminium exceeds the critical value of 0,5 m/s [1].

1.4.3 Ravelling and unravelling of Bifilms

If two films are folded together and incorporated into the melt are called bifilms, as said before, but bifilms could ravel into small compact features due to internal turbulence. In this form their size is reduced up to ten times from their original one and so they could be relatively harmless [1], as seen in Figure 1.8. However, during solidification, they may unravel back to their original starting shape to form a planar crack as shown in Figure 1.9. This behaviour is encouraged by hydrogen precipitation in the air layer between the films or/and shrinkage that reduces pressure on the films. Low mechanical properties observed as a result of hydrogen porosity or shrinkage porosity are due to the opening action of tangled bifilms.

Figure 1.8: Tangled oxide film.
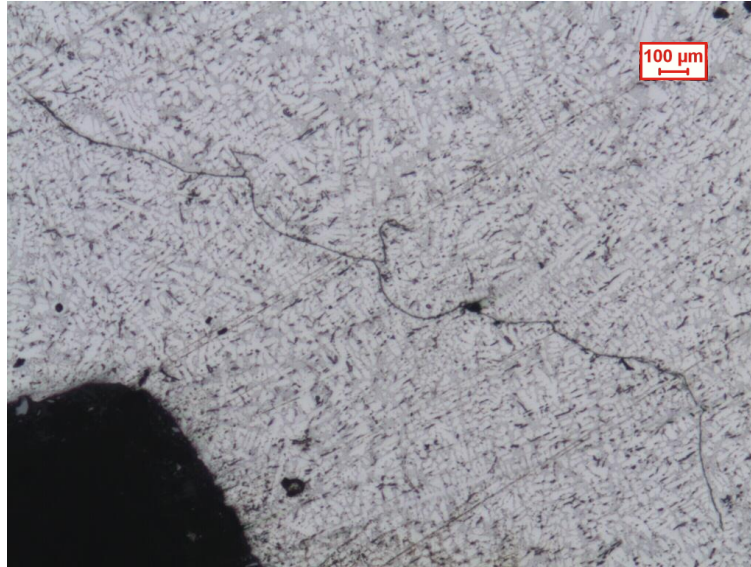
Figure 1.9: Unravelled oxide film.

1.5 Porosity

1.5.1 Nucleation

According to the laws of nucleation and growth [1], pore formation process follows the next steps: during solidification, hydrogen atoms are concentrated in the solidification front due to segregation, then embryo pores are formed and, if these pores have radius greater than critical size continue to grow until hydrogen atoms are available.

A description of pores formation in liquid was given by Fisher [13] for homogeneous nucleation. The formation of a pore of volume V requires work equal to $p_e V$, where p_e is the pressure of the liquid, so porosity has to push away surrounding liquid to reach volume V. This liquid-gas interface of area A needs a work equal to γA, where γ is the interfacial energy, to resist and grow. The gas requires a negative work of $-p_i V$, where p_i is the pressure of gas itself, to fill the bubble because pressure inside the bubble helps during the formation process [1]. Thus if the bubble is a sphere of radius r, the total energy will be [12]:

$$\Delta G = \gamma A + p_e V - p_i V \qquad (1.3)$$

Gathering the pressures the equation 1.4 is obtained:

$$\Delta G = \gamma A + \Delta p V \qquad (1.4)$$

Since A and V are the area and the volume of the bubble respectively, Equation 1.4 becomes:

$$\Delta G = 4\pi r^2 \gamma + \frac{4}{3}\pi r^3 \Delta p \qquad (1.5)$$

Finally, equating the equations 1.4 and 1.5 it follows that:

$$r^* = -\frac{2\gamma}{\Delta p} \qquad (1.6)$$

where r* is the critical radius for the homogeneous nucleation of a bubble, below which it is not possible to grow and survive; Δp is the e difference between internal pressure of the pore and pressure of the liquid, γ is the surface tension of the liquid.

By solving equation 1.6 using properties of A356 alloy, pressure required for nucleation is approximately 31000 atm [14]. Therefore homogeneous nucleation of pores is practically impossible to occur.

In castings, the nucleation of pores is expected primarily at heterogeneous sites. These include oxides and other non-metallic inclusions, which are present in almost all liquids metals. Surfaces of oxides and inclusions are rough and not wetted by the metal, so they work as preferential nucleation sites for bubbles; in fact, the presence of inclusions and oxides greatly enhances the porosity formation in aluminium alloys [15].

The energy relationship between homogeneous and heterogeneous nucleation is given by equation 1.7 [1]:

$$\frac{P_{het}}{P_{hom}} = 1{,}12\left[\frac{(2+cos\theta)(1-cos\theta)}{4}\right]^{\frac{1}{2}} \qquad (1.7)$$

where P_{het} and P_{hom} are the pressures required for heterogeneous and homogeneous nucleation, and θ is the contact angle between the solid particle surface and the liquid, which defines the extent of wetting. θ=180° refers complete non-wetting and θ=0 means wetting whereas, as shown in Figure 1.10.

As seen from Figure 1.11 and Equation 1.7, as the wetting angle decreases, the ratio of P_{het}/P_{hom} goes to unity that is the wetting condition for homogenous nucleation. If a surface is well wetted the nucleation becomes harder because there are less atomic sites on the surface compared to bulk liquid. Campbell [1] calculated required pressure for heterogeneous nucleation in an A356 alloy, which was approximately 1500 atmospheres, still to high to occur in a normal solidification process.
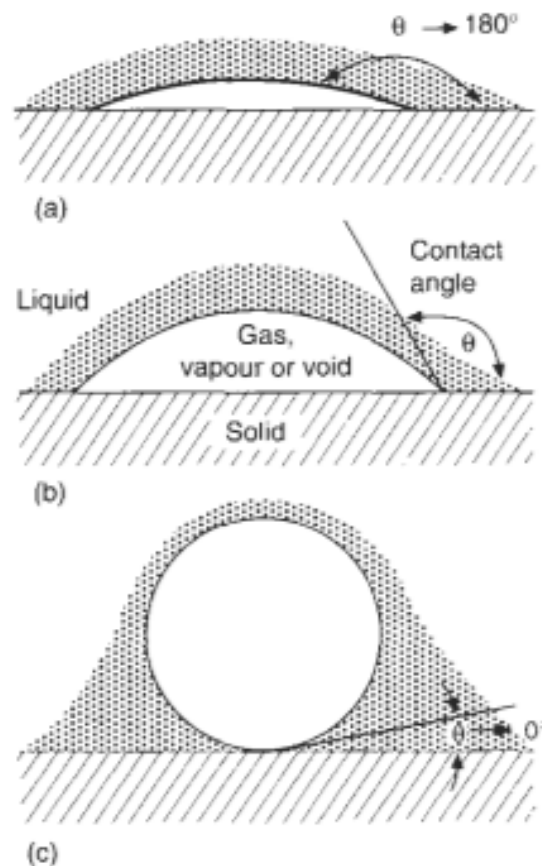
Figure 1.10: Geometry of a bubble in contact with a solid showing: a) a poor wettability, b) medium wettability and c) good wettability [1].
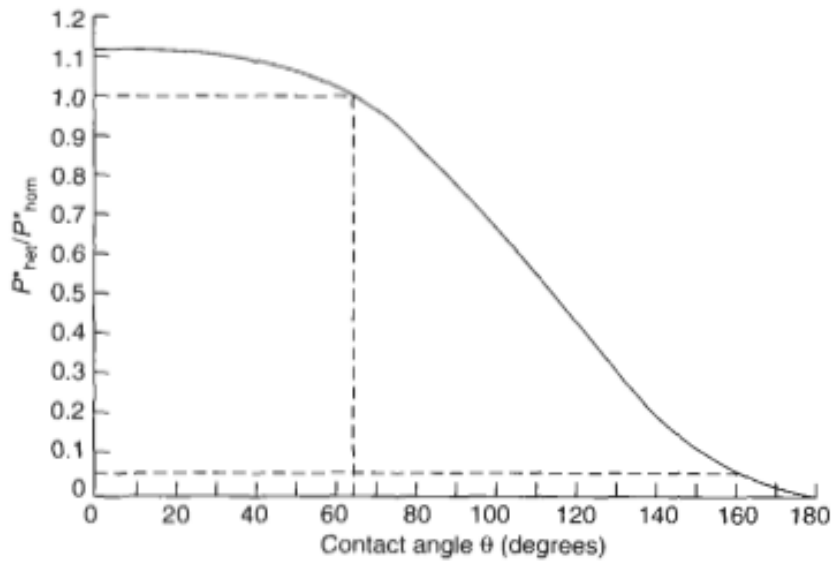
Figure 1.11: The relative difficulty of nucleating a bubble as contact angle with the solid changes from wetting to non-wetting [1].

1.5.2 The new approach to pore formation

Since both homogeneous and heterogeneous nucleation of pores requires too much energy to naturally occur, another factor that helps pores' formation and growth should exist. Campbell identified this factor as the presence of bifilms, because their opening involves negligible force compared to other type of nucleation. This theory overcome the classic thought that porosity results just from an incomplete liquid metal feeding which leads to volumetric shrinkage and/or reduced solubility of hydrogen upon solidification and assumes that bifilms are initiation source of porosity [1]. As previously said two oxide layers folded together with a gas between them form a bifilm. During solidification, precipitation by hydrogen in the gas between the oxides interfaces thus inflating the defect. In Figure 1.12 a and b, opening actions for simply folded and convoluted bifilm are shown. If enough hydrogen continues to precipitate, the bifilm will eventually grow into a spherical pore, as seen in Figure 1.12 c. Contrary, if the pore cannot grow freely in the liquid but grow later during freezing, takes interdedritic shape (Figure 1.12 d).
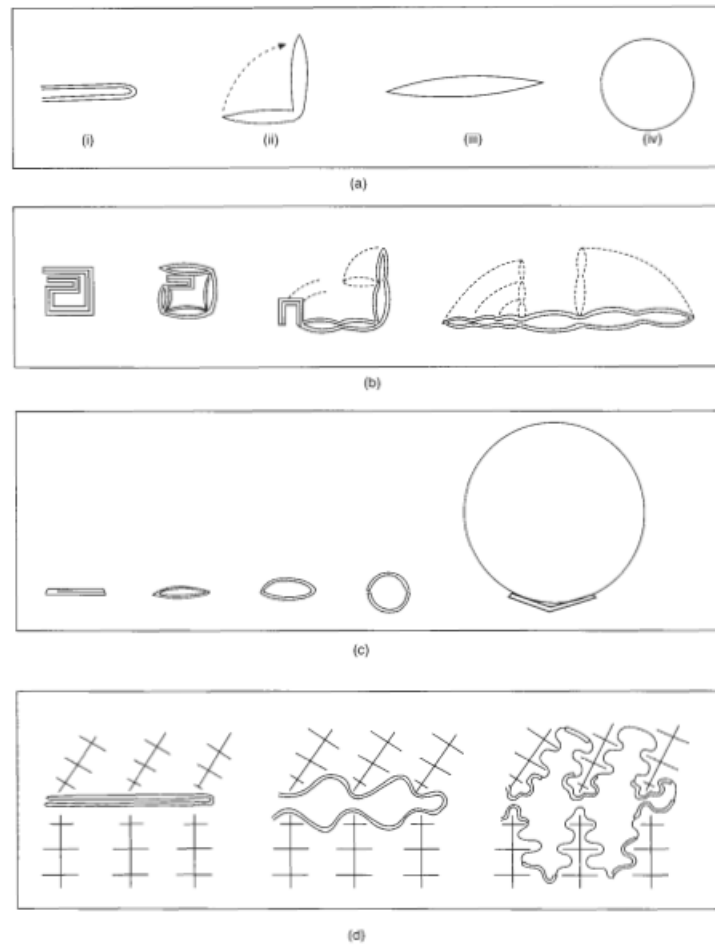
Figure 1.12: Inflating mechanism of bifilms [1].

Dispinar experimentally demonstrated evidence of this theory in his work [12]. Using the reduced pressure test technique, he manipulated the conditions during freezing so the bifilms opened sufficiently to be evaluated. Moreover he introduced Bifilm index to evaluate oxides presence and so molten metal quality. This is a value in millimetres calculated by adding all pores length counted cutting RPT sample (Figure 1.13).
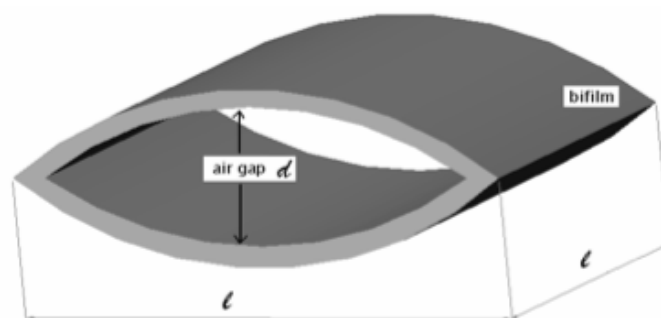
Figure 1.13: A schematic representation of a bifilm [12].

This work starts from the theory that folded oxide skins introduced into the melt were related to the porosity in castings. Then to evaluate metal quality utilizes some indexes, including Bifilm index.

1.5.3 Porosity type

Porosity formation in aluminium alloys can be classified according to size:

- Macroporosity (>100 µm)
- Microporosity (<100 µm)

or according to cause:

- Shrinkage porosity
- Gas porosity

Microporosity is characterized by small and dispersed cavities and usually occurs in long freezing range alloys, instead macroporosity occurs mainly in short freezing alloys or pure metals and large cavities are due to shrinkage phenomenon. Gas porosity are generally rounded and isolated, as seen in Figure 1.14. Common thought is that are caused by hydrogen rejection during solidification. Shrinkage porosity assumed interdendritc shape because liquid metal is not able to feed this region after solidification contraction, Figure 1.15.

However, it is impossible to completely separate effects of the shrinkage and gas in the formation of porosity because, for example, hydrogen can precipitate in the interdendritic region and bubbles may assume this shape [16].

However the diffusion mechanisms control the rate of gas deposition, therefore increasing the freezing rate the time available for growing will be reduced, and so the volume of gas porosity. Concluding, it should to be considered that a casting without porosities does not necessarily mean casting free from bifilms because their opening requires the right conditions, for example the vacuum application (RPT).
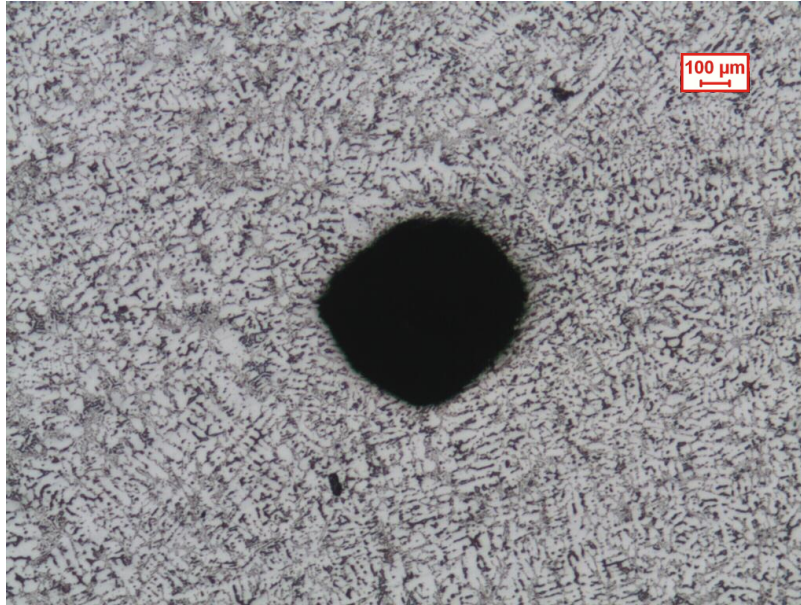
Figure 1.14: Gas macroporosity.
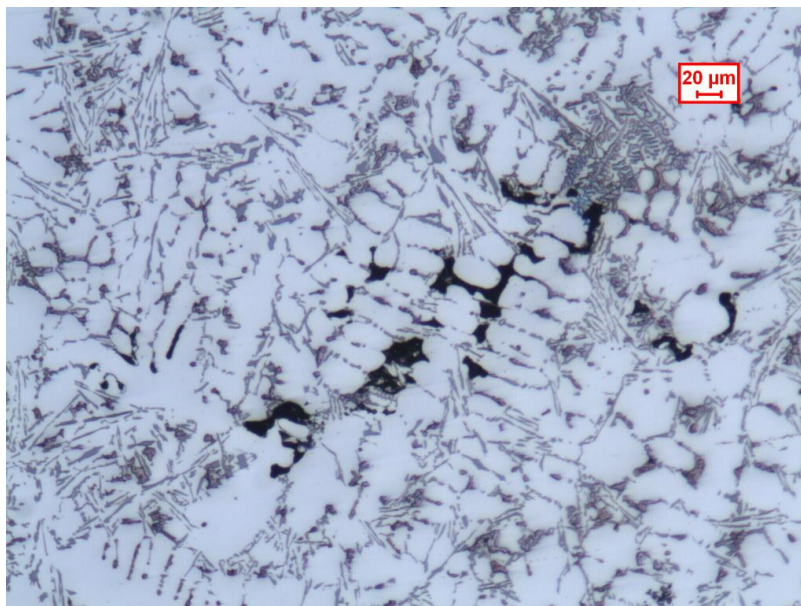
Figure 1.15: Shrinkage microporosity.

1) Shrinkage porosity

Shrinkage porosity is due to the density difference between the solid and liquid alloy phases. Since density in the solid is usually higher than in the liquid, during solidification the volume decreases and surrounding liquid flows in to compensate. This fluid flow may be impeded or even blocked by the solid part, so if sufficient liquid cannot flow in to feed the shrinkage, a large internal tensile stress develops that may be sufficient to form pores.

Out of five possible feeding mechanisms shown in Figure 1.16, interdendritic feeding is one of the most difficult ways for the formation of porosity defects. Especially in long freezing range alloys, feeding becomes progressively more difficult because of dendritic mesh growing that decrease channels size, as seen in Figure 1.17. In thin section, shrinkage is negligible (a), but becomes more critic if section increases (b), in fact thick ones usually contain hot spots or internally nucleated porosity, because the feeding is not sufficient (c).
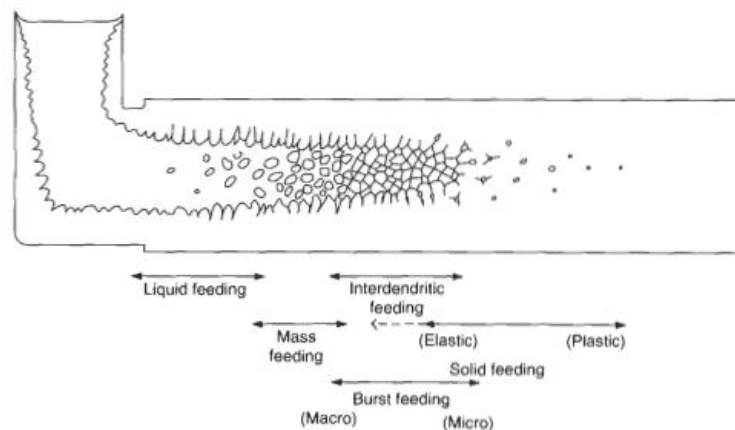
Figure 1.16: Feeding mechanisms in a solidifying casting [1].
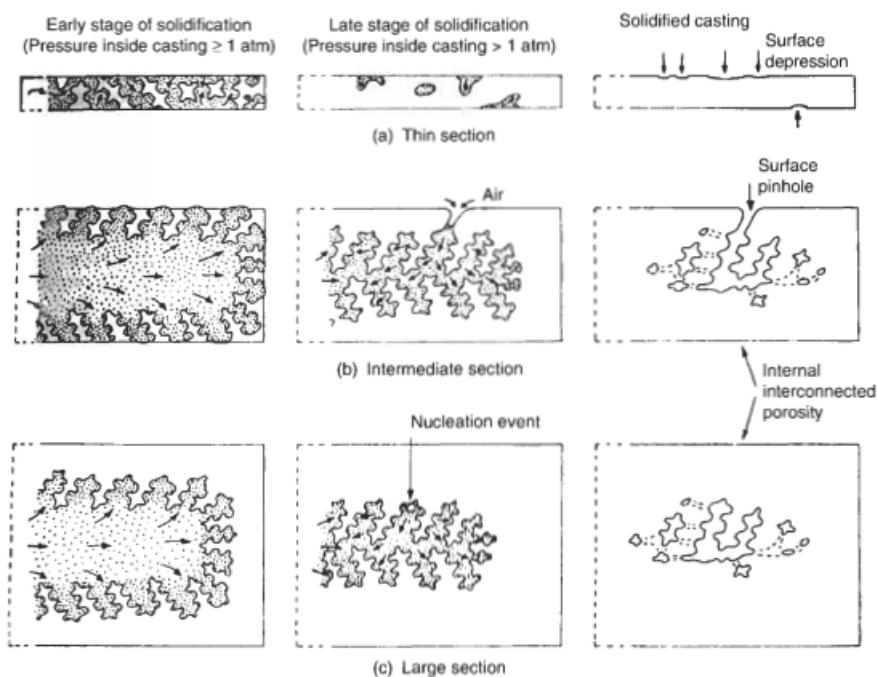
Figure 1.17: Volumetric shrinkage in long freezing range alloy depending on the thickness of casting [1].

2) Gas porosity

Hydrogen is the only gas with a significant solubility in aluminium and its alloys. The precipitation of this gas during solidification is due to the solubility difference of hydrogen in the solid and in the liquid state, as seen in Figure 1.4. Since it is low in the solid, some of the gas will be rejected from solution during solidification. This gas diffuses into the bifilms and expands the central gap. The consequent expansion of the bifilm may fill the interdentric spaces if dendrites are already grown and so they can be confused with shrinkage pores. They may also appear rounded depending on the fraction of eutectic phase that can change freezing from dendritic to planar.

1.5.4 Factors affecting porosity

In addition to hydrogen rejection and shrinkage, other many factors affect the complex mechanism of pore formation in aluminium alloys. Some of these are cooling rate, melt quality, melt handling, grain refinement and alloy composition. In this section such factors are discussed.

1) Hydrogen content

The initial hydrogen concentration in the melt is one of the most important factors influencing the amount of porosity formed. At high initial concentrations of hydrogen (Figure 1.18 a-b), pores form in the early stages of solidification and grow freely from growing dendrites.
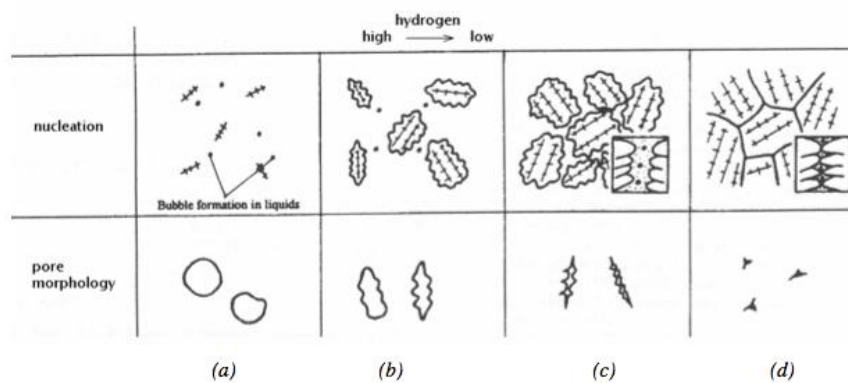
Figure 1.18: Effect of hydrogen content on pores morphologies [12].

At low initial concentrations, pores form later during solidification and they are usually small and have interdendritic shape due to grown restriction (Figure 1.18 c-d).

2) Inclusion content

Inclusion content is an important factor that can affect porosity. In fact when an inclusion is entrained, is suddenly wrapped by oxide film formed on the surface of melt [1], as seen in Figure1.19. In this way also air is entrapped by oxide layer and this is a good initiation site for hydrogen precipitation
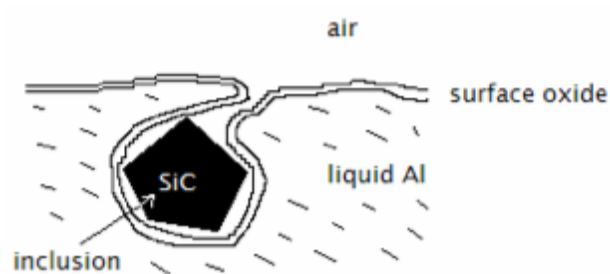
Figure 1.19: Schematic demonstration of entrainment of an inclusion [1].

3) Oxide structure

Protective effect of oxide film on the surface of the melt is strongly influenced by alloying elements. For example, by adding strontium to the melt, $SrO.Al_2O_3$ forms, which is less protective than amorphous Al_2O_3 [17due to different structure. At the same way if magnesium is present, it changes the oxide film from Al_2O_3 to spinel $MgAl_2O_4$ or to MgO that are weaker [18]. Therefore, hydrogen coming from air humidity may cross these oxide layers easier and porosity will increase.

4) Grain refinement

Porosity formation is also controlled by grain refinement. Grain refiners are added to alloys to increase the strength and toughness by changing the microstructure, in particular increasing number of dendrites and reducing their size. However, these variations also

18

change large pores to smaller discrete pores, but this alteration reduces only the size of the pores, not their number. In addition, some elements are able to shift the eutectic temperature, while others may affect the hydrogen solubility in aluminium (Figure 1.20) [19].
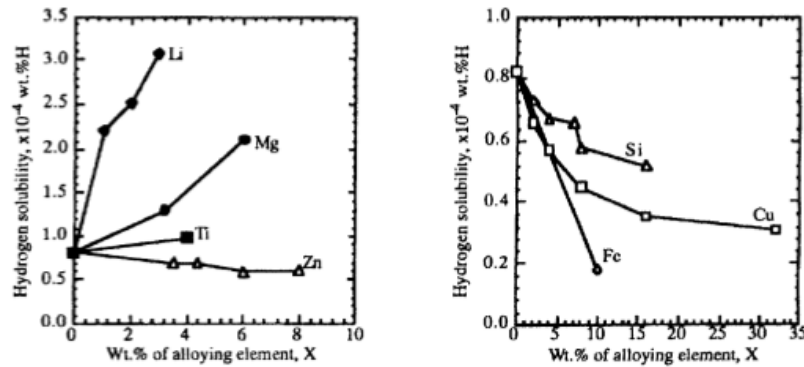
Figure 1.20: Effects of alloying elements on hydrogen solubility in liquid aluminium [19].

5) Cooling rate

Increasing the solidification rate reduces the time for diffusion of hydrogen into the bifilms. In this case porosity will decrease [20].

6) Intermetallics

Iron is one of the major impurities in Al-Si alloys, but it plays an important role in the mechanical behaviour of the alloy. Solubility of iron in in liquid aluminium is about 2 wt%, a relative high amount, but the solubility in the solid at its freezing point is only about 0.005 wt%. This means that the segregation ratio of iron is high and so the formation of iron-rich intermetallic phases is encouraged. These intermetallics not only may nucleate on oxide films present in the liquid metal, but they tend to unfurl bifilms, changing their shape from compact ravelled to large planar cracks [14, 21]. Therefore the bifilms on which iron phases may nucleate are responsible for the fracture founded in correspondence of Fe-rich phases in the castings.

1.6 Measurement of metal quality

The hydrogen content in liquid aluminium has been assumed to be a significant problem to obtain high quality castings, therefore many techniques have been developed to measure it. Several techniques used solidification under reduced pressure, where the densities of the samples solidified under vacuum were compared with the theoretical density, and then the amount of hydrogen was evaluated. The technique is quick and low cost, but quantitative assessment of the gas in solution is not so accurate.

Currently, methods like RPT (Reduced Pressure Test), NOTORP, Alscan and Hyscan are used to determine hydrogen content. These are based on circulation of an inert gas (N_2 or Ar) through the liquid with a probe, when hydrogen equilibrates insufflated gas partial pressure of hydrogen is measured and is related with its content. This technique is complex, expensive and slow.

Another possibility to measure hydrogen content is the use of a probe made by two electrodes and a membrane. The system measures the potential difference between the electrodes. Hydrogen can freely enter in the probe through the membrane and hinder formation of the electric arc between electrodes, so if the potential measured is low means that hydrogen is high and vice versa. The instrument used in this thesis was FOSECO Alspek-H®. Probe needs to be calibrated before the use, but using pre-calibrated sensor the measurement is quick and accurate. The only problem is the high cost.

1.6.1 Inclusion detection tecniques

During years, a number of techniques for inclusion detection in liquid aluminium have been developed, but they were usually slow, complicated and expensive to use in industrial field [12]. The main of them are listed below.

1) Limca

A sample of liquid aluminium is forced to flow through a small hole of diameter between 0.05 and 0.10 mm, then electrical potential across the hole is measured, as seen in Figure 1.21. This process is continuous in action and so it is able to monitor quality of metal for a certain period of time. The problem of this technique is that is limited to inclusions that can enter the hole, so the most important inclusions cannot be detected by the LIMCA test [12].
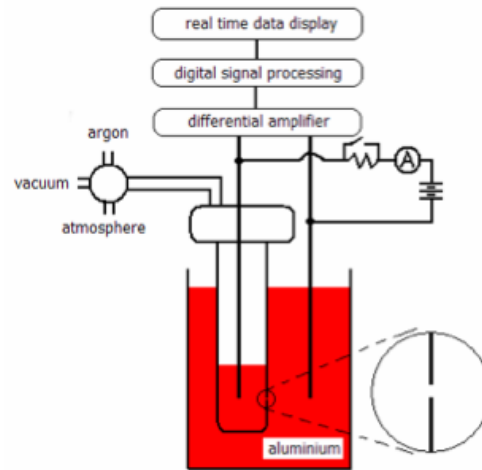
Figure 1.21: Schematic representation of LIMCA [22].

2) Podfa and Prefil

In PODFA and PREFIL tests, the molten metal is forced to pass through a fine filter. The metal is weighted and finally the filter is sectioned to identify inclusions using metallographic techniques. The interpretation of the metallographic sections needs to be ruled to quantify correctly number of inclusions and oxides. Actually there is not any differentiation between oxides morphology, so a long or thick one is counted exactly like a small or thin one.

However, PODFA measures the filter rate of blockage applying vacuum and it relates this with the melt quality, as shown in Figure 1.22. The weight of metal required for a reliable result is approximately 2 kg. Filtration techniques cannot detect nanometre thick films, not only due to micrometric pore size, but even because these oxides are not structurally rigid and so wrap around the filter or pass through it reaming undetectable. It should be noted that tangled micrometric oxides can also pass through the filter and so lost of information about melt cleanliness if all filter surface is not scanned.

In this thesis filtration technique is applied, but in a completely new way to assess molten metal quality overcoming main defects of existing methods.
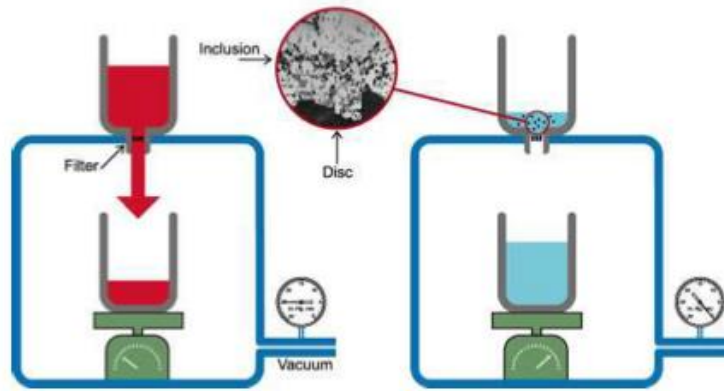
Figure 1.22: Schematic representation of PODFA test [22].

1.6.2 RPT

The reduce pressure test or RPT has been generally considered as a poor reliability test due its failure to measure correctly hydrogen content. Anyway it is a good test to estimate the *porosity potential* of the melt. But the great strength of RPT is the possibility to monitor the porosity level considering both inclusions and hydrogen [12]. In addition, this test is also simple, low cost and quick.

The test consists of solidification under a reduced pressure of a specimen taken from the melt, as shown in Figure 1.23.
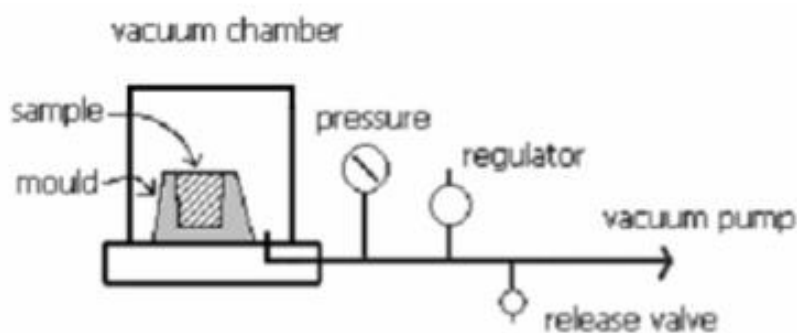
Figure 1.23: Schematic representation of RPT [12].

The reduction of pressure magnify the effect of dissolved gas on the opening of bifilms, in fact if the pressure is reduced to 1/100th of an atmosphere, it is expected that the air layer between the films would be expanded by approximately 100 times, converting an invisible defect into a visible one [12].

RPT is widely used in industrial field due to the advantages previously said, but the major disadvantage is that the results are non-quantitative. Dispinar in his work [12] gives a quantitative measurement of metal quality using a RPT sample for the first time, using the Bifilm index. In this work, such quality index is used in parallel with filtration and hydrogen measurement to find the best procedure to measure the quality of the molten metal in the easiest, fastest and cheapest way.

1.7 SAEN operating process

This work was carried out at SAEN foundry s.r.l. (Figures 1.24 and 1.25) a company working in diecasting field since 1971 located at Brugine (Pd, Italy). They not only produce tools for HPDC but also project and finally test them in their own foundry to ensure an high quality level of the products.

Figure 1.24: SAEN logo.

Figure 1.24: SAEN headquarters.

Since these trials are usually small and thier first purpose is not the castings production, the thsis activity was kindly hosted.

Foundry actually is composed by two HPDC machines of 750 and 300 metric ton and the relative gas furnaces sizes are 600 and 300 kg respectively, in which the burning gas is not in contact with the melt but just lap the crucible. The melting process starts at the end of each working day, when the furnaces are charged with scrap and some ingots, in particular 100 kg of both in the biggest one and 50 in the smallest. At 2 a.m. the furnaces start to melt the charge and temperature is set to 750°C. At 8 a.m temperature is rised to 800°C and 50 kg of ingots (7 kg each) are charged every hour during foundry trials. When the melting is complete operating temperature is set approximately to 690°C fo both furnaces. The ingots were loaded manually in the biggest furnace and semi-automatically in the smallest one to avoid high falls of temperature during production. Before to start, molten metal is treated by degassing with argon using a 12,5 mm diameter graphite lance and then adding fluxing salts onto the surface, to remove inclusions, oxides and dissolved gases. After treatment, the dross that had accumulated on the surface was skimmed off manually. Average duration of the foundry trial is 4-6 hours. During this time the state of metal changed: the surface oxide film was broken, re-oxidised and was submerged, introducing bifilms into the melt. Therefore, the quality was assessed using RPT, filtration and hydrogen measurement at each step of the process: after melting, after fluxing, and at the end of production.

1.8 MUSIC project

This thesis is also part of MUSIC project, the acronym of MUlti-layers control & cognitive System to drive metal and plastic production line for Injected Components. The project involves University of Padua (DTG) and University of Aalen (GTA), besides a lot of company like Audi, Frech, Magma, Enginsoft, RDS, Saen and more, as seen in Figure 1.25.

Figure 1.25: MUSIC partners.

The purpose of MUSIC about aluminium is to definitely reduce the high number of defects generated by high pressure die casting process. This process is one of the most defect generating and energy consumption processes in EU industry, but is strategic for the small and medium enterprises, because the productivity is very high so the costs can be spread on big number of pieces. Anyway a standard quality level of castings is hard to guarantee and so rejection of pieces is critical. The challenge of MUSIC is to transform a production-rate-dominated manufacturing field into a quality/efficiency-driven and integration-oriented one to exploit the enormous (and still underestimated) potential of HPDC (Figure 1.26).
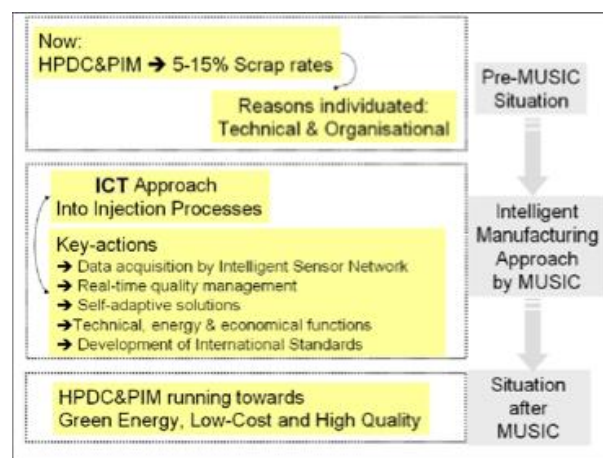
Figure 1.26: Music project flow chart.

Before to be loaded into the HPDC machine, aluminium is obviously melted and so the quality system has to be implemented from the beginning of the process, the melting stage. If the quality of the molten metal is not controlled, defects coming from the melting process cannot be distinguished from these occurred during the injection or solidification phase for example. Therefore en extreme effort on the machine operating could be even useless if initial condition is not monitored. The aim of this thesis is to build a procedure to evaluate quantitatively the quality of melt directly in industrial field.

CHAPTER 2

EXPERIMENTAL PROCEDURE

2.1 Alloys

In this thesis, three different European Standard Al-Si based alloys were considered: EN AC 46000, EN AC 47100 and EN AC 43400. They are commercially available and widely used in the automotive HPDC processes. Alloy used for the MUSIC project will be a variant of the standard EN AC 43400 alloy. SAEN foundry's internal batches were also considered, to verify if molten metal quality changed with the supplier. Finally, the chemical analysis of every foundry trial was taken.

2.2 Filtration

In this work a new filtration technique was developed in order to evaluate the melt cleanliness. The aim was to count the number of oxides and supply a quality assessment of the molten metal. Current techniques, such as Prefil, Podfa and Limca, are very expensive both for purchase price, time and cost to scan filter samples. Moreover, the most critical limitation is that they don't distinguish different type of oxides, according to their shape and dimension, so large or thick oxides are considered exactly like small or thin.

The new proposed method consists in pouring the molten Al alloy trough a filter, cutting it in two halves, polishing and scanning with an optical microscope to count the number of oxides trapped. Oxides were distinguished into several classes according to their dimension and shape, then a class was also assigned to each sample to describe the melt quality with a single qualitative value.

Once the filtration test had been established in the laboratory, the instrument was carried to the foundry, to sample the largest number possible of melts of the three different alloys. Specimens were taken before and after degassing, to evaluate benefits of the process, then during and at the end of foundry trials to verify quality change with time processing.

2.2.1 Laboratory test

A series of experiments was achieved at the DTG laboratory to assess the best system and operating conditions for filtration test.

1) Filtration system evaluation

The purpose of the filtration test was to find the best way to filter molten metal in terms of speed and filter full filling. 6 kg of EN AC 46000 alloy was melted in a 9 kg electric furnace. Once melted, the molten aluminium was kept at 690°C, then it was poured with a steel ladle in a steel cup (dimension in Figure 2.1) both pre-heated up to 70°C. Surface slag was skimmed off manually before each pouring. 20 and 30 ppi (pores per inch) FOSECO SIVEX FC® filters (Figure 2.2) were grounded manually to obtain the right shape to be putted into the cup. Filters were inserted first at room temperature and then pre-heated up to 70°C. In all cases, the metal did not pass through the filter because metallostatic pressure was too low, as seen in Figure 2.3.
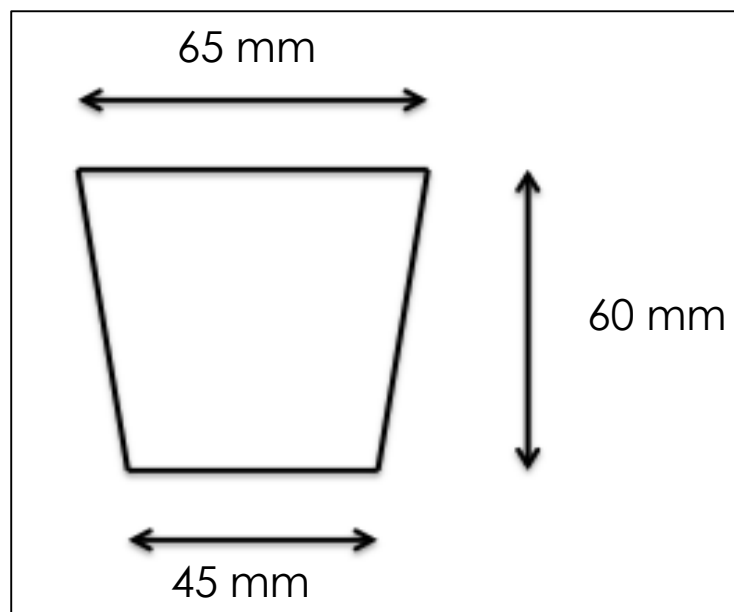
Figure 2.1: Steel cup representation.
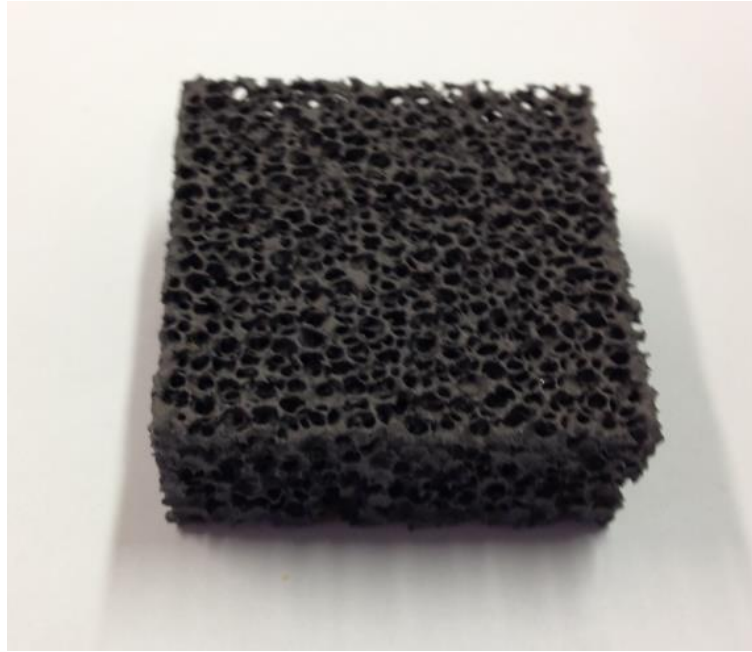
Figure 2.2: FOSECO SIVEX FC® graphite filter.

Figure 2.3: Filter filling failure.

To overcome this problem a suitable steel die was realized (Figures 2.4 a and b) with a pouring cup area of 60x40 mm² to facilitate the pouring operation and a cavity for the filter at the end of a 150 mm sprue, to ensure the metallostatic pressure. The die was composed by two parts, one flat and was closed using a clip to speed up opening and closing operations. Internal surfaces were coated with boron nitride spray to facilitate

removal of the specimen. The total dimensions of the die were 220x215 mm and weight was 10 kg, so it was easy to move and pre-heat, even into a foundry. Specimen for the tensile test was not evaluated in this thesis' work.
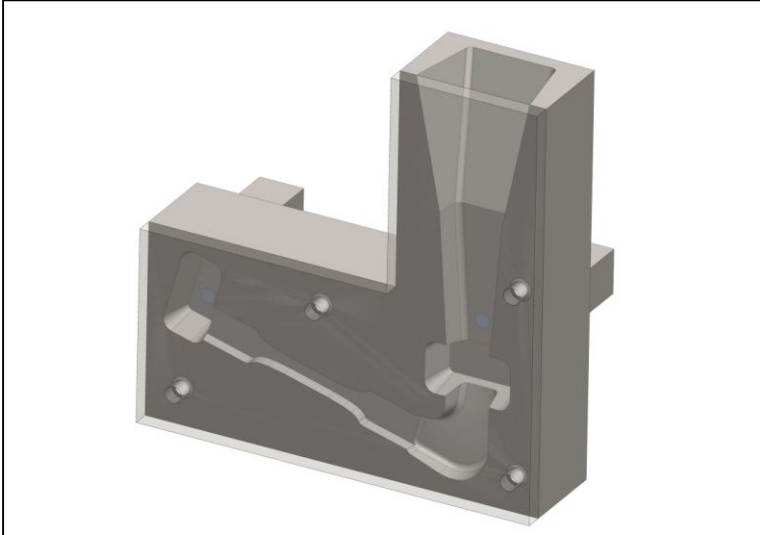
(a)

(b)

Figure 2.4: Die 3D representation (a) and photo (b).

2) Filter choice

Once the die has been made, type of filter and operating parameters were to be chosen. Filters had dimensions of 50X50 mm, so were halved, cut near the edges and grounded with 80 silicon carbide grade paper, to give them the right shape to be inserted into the die cavity. About 7 kg of EN AC 46000 alloy were melted in a 9 kg electric furnace. A pre-heated steel ladle was used to pour metal and surface slag was skimmed off manually before each pouring. Filter samples were taken keeping the melt temperature between 685 and 700 °C and the die temperature between about 155 and 170 °C. Filters of 20 and 30 ppi made by silicon carbide and graphite were used. Filter was inserted in the die cavity first at room temperature and then approximately at 70°C, pre-heating it on the furnace edge. The dwell time, in which filter was leaved in the cavity before pouring, was changed from 5 to 10 minutes, in order to find the best operating conditions. The goal was to choose the right pore size and time-temperature values to allow filter filling and the right material to be easily cut and grounded. To evaluate the filter filling X-ray technique was used.

3) Repeatability and reliability tests

The repeatability and reliability of the filtration technique were evaluated with two different tests. For both tests 6 kg of EN AC 46000 alloy were melted in a 9 kg electric furnace and kept at 695 °C; pouring conditions were the same as previous test. Filters were cut by a saw longitudinally along greatest dimension into halves and grounded up to 2400 grade paper. Then the specimens were polished with 6 μm and 3 μm diamond paste and finally with silica slurry. After lapping, samples were scanned with an optical microscope at 50 and 200x magnifications. Oxides were counted and divided in four different classes, from 1 to 4, according to their shape and dimension, as seen in Figure 2.5. Higher the class level, more dangerous should be the oxide. The 200x magnification was used to evaluate class 1 and 2 oxides, while lower magnification was used for counting class 3 and 4 oxides.
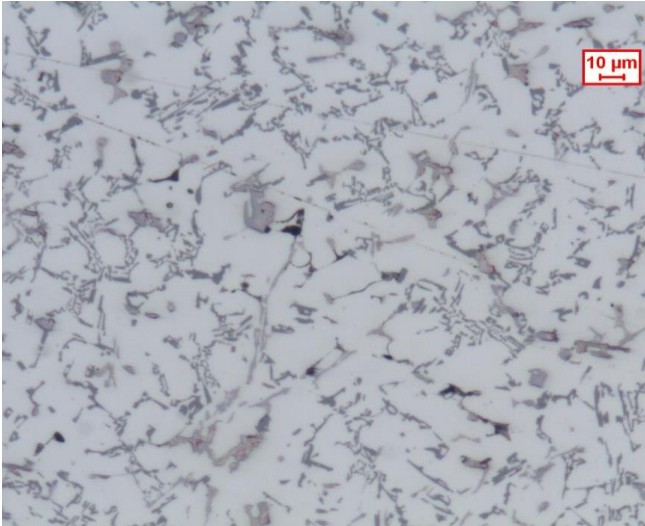
(a)
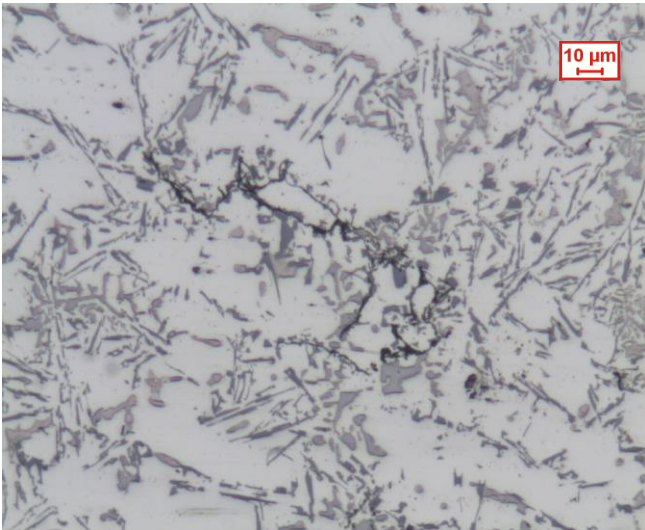
(b)
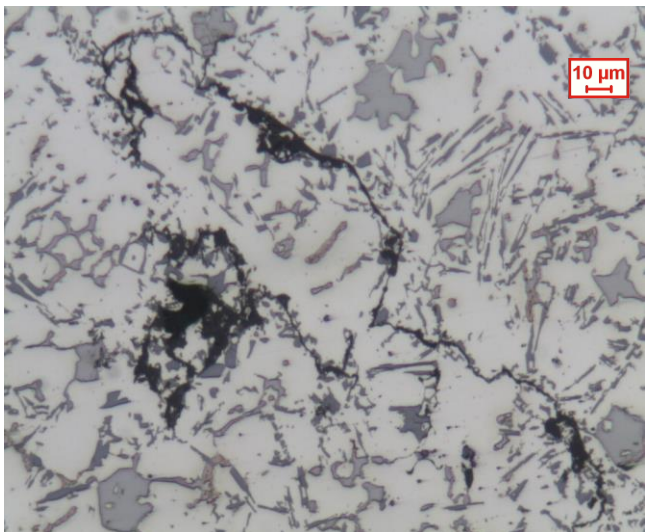
(c)
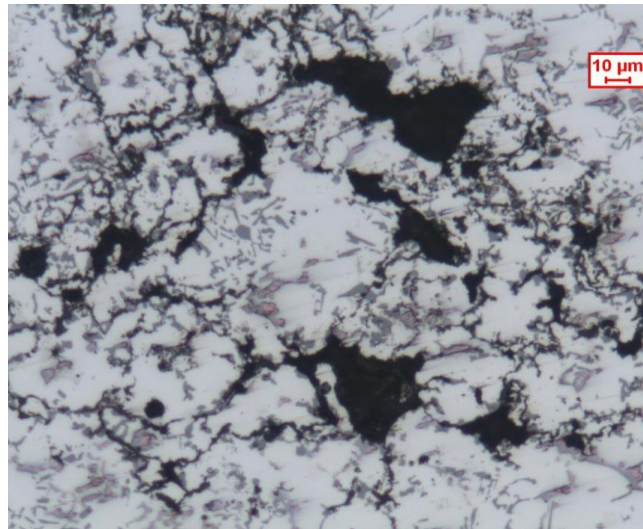
(d)

Figure 2.5: Optical micrographs of different oxides classes: 1 (a), 2(b), 3(c) and 4 (d).

In the first test, to assess the repeatability, two specimens were taken in succession from the same melt. A 20 mm² zone above each filter, in the middle of the sprue, was scanned with the microscope, Figure 2.6. At 50x magnification the analysed area was made up of 16 fields, at 200X of 256. This zone was chosen because molten aluminium should pass mainly through it, so most of the oxides should be trapped here. The number of oxides of each class was compared between the two samples to assess the repeatability.
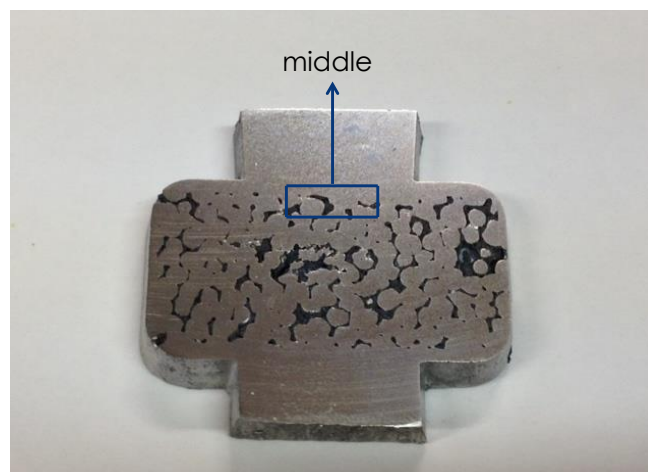
Figure 2.6: Middle-upper zone of the filter scanned with the optical microscope.

In the second test the reliability of the technique was assessed. One specimen was taken using the same operating condition of the first test, but three 20 mm^2 zones above the filter were scanned, instead of one, namely middle, left and right as seen in Figure 2.7. The purpose was to evaluate the distribution of different oxides, according to the 4 classes, in the superior part of the filter, to understand if the middle zone was significant to describe quality of the sample. Again the number of oxides of each class was compared for the three zones to evaluate reliability of the test.
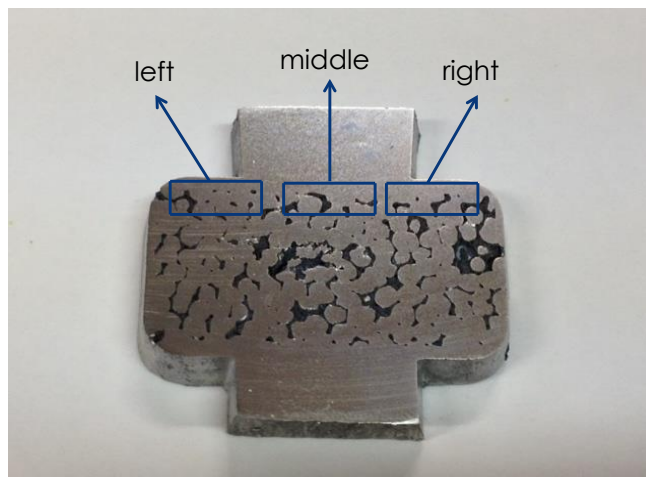
Figure 2.7: Left, middle and right upper zone of the filter scanned with the optical microscope.

2.2.2 Industrial operating procedure

During the industrial trials, the die and filters were pre-heated upon the edge of gas furnaces reaching the temperature of 70-90°C. Then a pouring without filter was carried out, in order to increase the die temperature up to 140-150°C. Filter was putted in die cavity and was left there for 5-10 min by closing the die. At this point, sampling could be start. The pre-heating pouring was done every time the die temperature fell below 130°C.

2.3 Reduce pressure test (RPT)

Reduce pressure test is one on the most diffused quality assessment technique in industrial field. It consists of a vacuum chamber, a rotary pump and a pressure regulator.

Actually a certain number of different indexes are used to evaluate melt cleanliness obtained from RPT specimens. In this work the most important indexes were evaluated and compared each other and with quality indexes from other techniques.

Once the RPT test had been established a lab scale, the same conditions were adopted in the foundry.

2.3.1 Laboratory test

A preliminary experiment was achieved in laboratory to assess repeatability and reliability of RPT, investigating on parameters that may affect the measurement. 7 kg of EN AC 46000 were melted in a 9 kg electric furnace and then melt was kept between 688 and 698°C. Specimens were taken with a steel ladle, pre-heated upon the furnace, and molten aluminium was poured into two steel cups with different shape and dimensions as seen in Figure 2.8.

Figure 2.8: Different steel cup used for RPT evaluation.

Cups were pre-heated initially until 70°C upon the furnace and further with a preliminary pouring. Steel cups were chosen instead of sand moulds because they are widely used in almost all industrial fields; manual forming is not required and steel does not have moisture absorption problems as sand [23]. Surface slag was skimmed off manually before each sample taking to avoid putting into the cups big oxides from the surface. 28 specimens (14 for every cup) were taken consecutively and for each a different quantity of metal was poured, to "simulate" the normal use in the industrial field. RPT pressure was

set to 100 mbar as suggested in the work [12]. For every specimen porosity percentage, density and Bifilm index were calculated, as explained in the following paragraphs. The aim of these tests was to evaluate if these *quality indexes* are affected by the specimens weight and shape of the cups.

2.3.2 Density measurement

In the reduce pressure test, pore formation is enhanced by the applied vacuum, therefore the melt quality may be related to the density of the RPT sample. For that reason, the density of each sample was calculated using Archimedes Principle (by weighing in air and in water), as show by Equation 2.1:

$$\rho = \frac{m_{air}}{(m_{air}-m_{water})\,\rho_{water}}$$

$$\text{(2.1)}$$

ρ: density of sample,

m_{air}: weight in air,

m_{water}: weight in water,

ρ_{water}: density of water.

The weighing was done on an electronic balance with 0,01g sensitivity. The corresponding ρ_{index} was also determined (Equation 2.2):

$$\rho_{index} = \frac{\rho_{atm} - \rho_{rp}}{\rho_{atm}} \cdot 100$$

$$\text{(2.2)}$$

ρ_{atm}: density of the sample solidified under atmospheric pressure

ρ_{rp}: density of the sample solidified under reduced pressure (RPT)

This index represent porosity percentage formed in the RPT specimen, obtained comparing its density (ρ_{rp}) with the density of the specimen solidified under atmospheric pressure (ρ_{atm}).

In addition, the Equation (2.3) ($r^2=0{,}961$) was used to evaluate density of the alloy by considering the effect of alloy chemistry on the specific gravity [24], instead of density of the specimen solidified under atmospheric pressure (ρ_{atm}):

$$\rho_n = 2{,}71-0{,}4Si+0{,}74Cu+0{,}3Fe+0{,}87Mg+0{,}09Mn+ \qquad (2.3)$$
$$0{,}06Cr+0{,}51Zn+0{,}56Ti$$

This value was called nominal density (ρ_n) and was compared with RPT specimen density (ρ_{rp}) to calculate the nominal density index, which represented a porosity percentage too (Equation 2.4):

$$Nominal\ density\ index = \frac{d_n - d_{rp}}{d_n} \cdot 100 \qquad (2.4)$$

The purpose was to verify if there was a difference between density of the sample solidified under atmospheric pressure and nominal density evaluated with Equation 2.3.

2.3.3 Image analysis

The RPT samples were cut by a saw longitudinally into two halves and ground up to 1200 grade paper. Images taken from the surfaces prepared in this way were digitized by a desktop scanner with a resolution of 1200 pixels per inch (pixel spacing approximately 20 µm). Then were processed with XnView® free software, changing resolution, contrast, brightness and gamma to facilitate subsequent Image Analysis as seen in Figure 2.9.

(a)   (b)
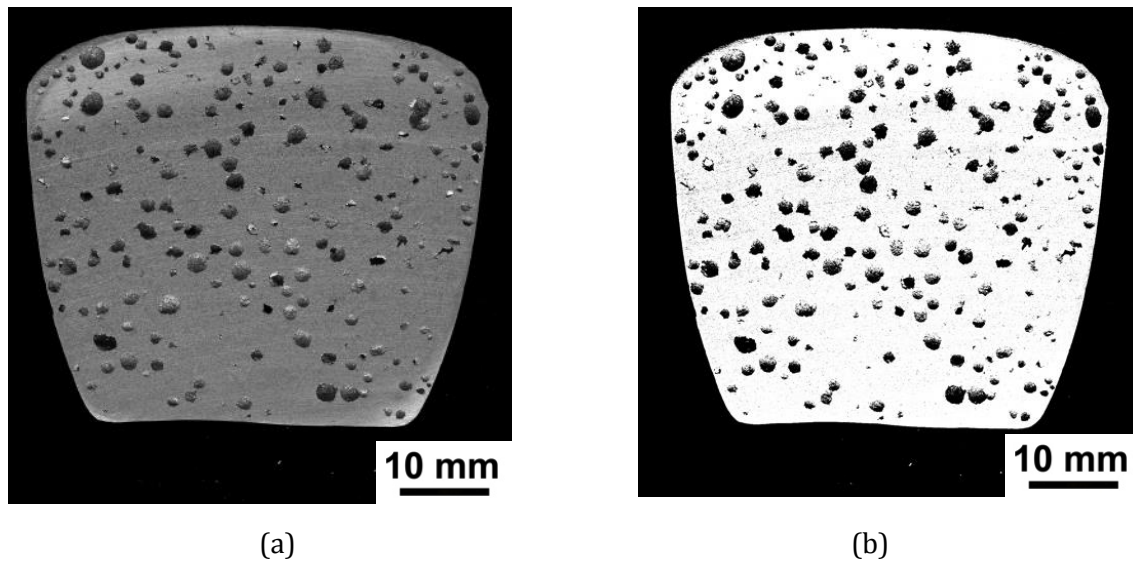
Figure 2.9: Sectioned RPT sample before (a) and after (b) image processing.

Resolution was reduced to facilitate subsequent operations from 1200 to 700 dpi, but was high enough to not generate measurement errors, as revealed in [12]. Images were subjected to Image Analysis to calculate the area and length of each pore and the area of the whole surface of the sample as seen in Figure 2.10. For each pore the maximum dimension between length and width was identified, and this dimension was summed for all pores to calculate the Bifilm index [12]. The software pack used was Leica Qwin®. To avoid errors, a filter was used in the Image analysis to discard defects with an area lower than 0,1 mm^2 because these are attributed to scratches or in general to surface defects during sample preparation.

Porosity percentage was also evaluated with image analysis using the equation:

$$porosity\% = \frac{\sum Area_{pore}}{Area_{sample}} \cdot 100 \qquad (2.5)$$

Area$_{pore}$ = area of the single pore

Area$_{sample}$ = area of the whole surface of the sample

(a)   (b)
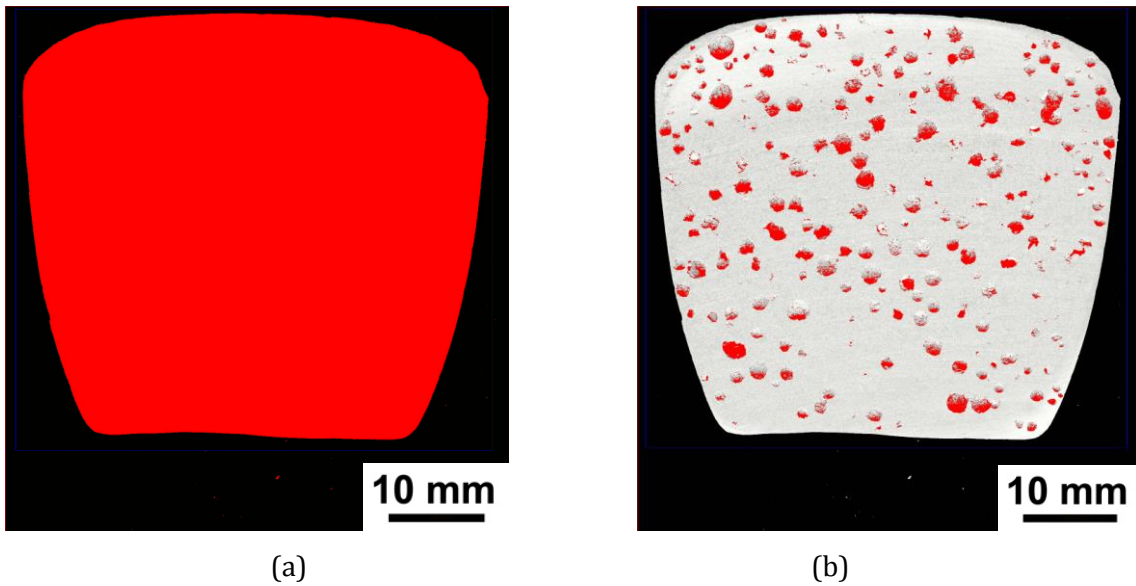
Figure 2.10: Specimen sectioned area (a) and porosity (b) binarization using image analyser.

2.2.4 Industrial operating procedure

During foundry experiments, a steel cup was pre-heated upon the edge of gas furnaces reaching temperature of 70-90°C. Before reduce pressure test was done a pre-heating pouring and specimen was allowed to solidify under atmospheric pressure to obtain the specimen for the calculation of density index. The molten aluminium was then poured with a steel ladle coated with boron nitride into the cup and the test was done at a pressure set up at 100 mbar.

2.4 Hydrogen measurement

In this work hydrogen content of the molten aluminium was measured with FOSECO Alspek-H®. In paragraph 1.6 has been explained in detail its working principle. The proper alloy had to be selected before to start with the measurement. Then the probe was pre-heated until 250-300°C and putted into the melt. After about 5 minutes, time needed for stabilization, temperature and hydrogen content were measured. The measurement accuracy of the hydrogen analyser is claimed to be approximately 0.01 mL/100g of Al. Alspek-H® can measures continuously hydrogen content, so it allows to evaluate its trend

during degassing process. Probe was pulled out from the melt before fluxing, to avoid damage during skimming, and putted in again after the treatment.

CHAPTER 3

RESULTS

3.1 Laboratory test

In this section results of tests achieved at DTG laboratory of Vicenza are reported. The purposes of the experiments were to find out the best operative conditions for measurements and choose right indexes to evaluate quality of molten aluminium.

3.1.1 Filter choice

The aim of this first test was the choice of the most appropriated type of filter and filtration operating parameters, in terms of oxides trapping, full filling and ease of polishing for subsequent scanning with microscope. Results are shown in Table 3.1.

Melt and die temperature were kept as constant as possible to remove their effect on the test. Variation was about 15°C for both, more than acceptable especially in industrial field where filtration technique was later applied. Contrary, changed variables were the filter material (graphite or silicon carbide), pore size (20 or 30 ppi), filter temperature and dwell time into the die.

Looking at X-ray radiography in the Table 3.1, the first observation is that 20 ppi filters (B1, B2, B6, B7) were always filled satisfactorily. Instead, for 30 ppi filters 5 minutes of dwell time and room temperature were unsatisfactory conditions as seen in B3. Samples B4 and B8, with 10 min of dwell time at room temperature and 5 min of dwell time at 70°C respectively, were limit situations, in which filling is not complete, but acceptable. Best conditions for full filling of 30 ppi filters were 8 min of dwell time and pre-heating up to 70°C (B5).

Thus in this work 30 ppi filters were chosen for their higher ability to trap smaller oxides compared to 20 ppi. In foundry, filters were pre-heated upon the edge of gas furnaces until temperature of 70-90°C, and a dwell time between 5 and 8 minutes was used. Graphite filters were chosen instead of silicon carbide for their lower hardness, that means faster and easier preparation (cutting and polishing operations).
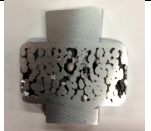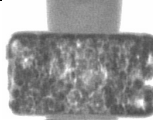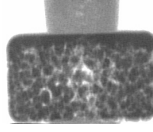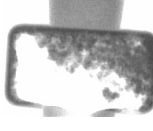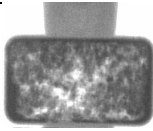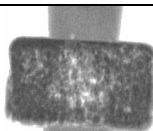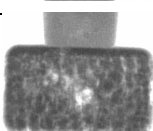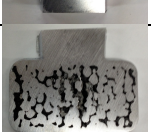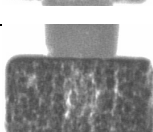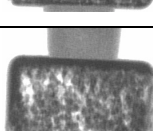
Sample	Filter material	T_{melt} [°C]	T_{die} [°C]	Filter type [ppi]	Dwell time [min]	T_{filter} [°C]	Filter image	Radiography
B1	G	690	158	20	5	26		
B2	G	685	153	20	10	26		
B3	G	685	169	30	5	26		
B4	G	690	164	30	10	26		
B5	G	700	160	30	8	71		
B6	G	692	165	20	8	70		
B7	SC	690	163	20	5	72		
B8	SC	691	162	30	5	70		

Table 3.1: Operating parameters and filling results of the filter choice test.

3.1.2 Filtration repeatability and reliability assessment

In order to assess the repeatability and reliability of filtration test, two different experiments were carried out. In the first one two consecutive specimens of the same melt were taken, then cut, polished and middle area of each filter was scanned with optical microscope at 200x and 50x magnification to count oxides. As seen in Figure 3.1, class 1 oxides were 32 for the first sample and 36 for the second, class 2 were 13 and 9, class 3 were 6 and 2 and finally class 4 were 2 and 0 respectively.
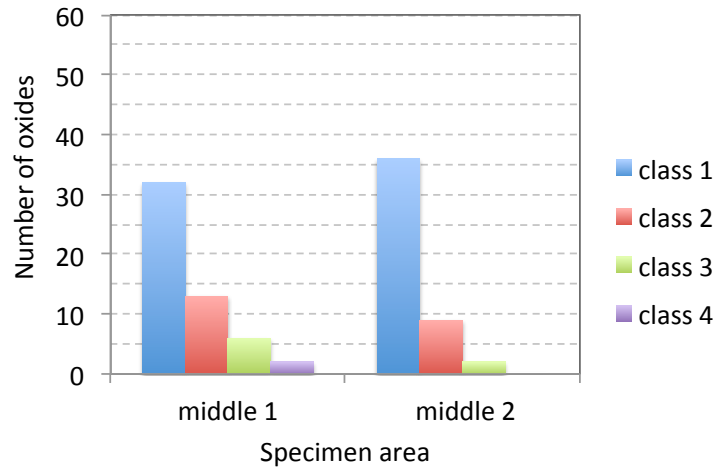
Figure 3.1: Number of oxides for each class counted in sample 1 and 2 middle area.

The most interesting finding was the coherency between the number of class 1 and 2 oxides, in contrast with the difference between bigger oxides of class 3 and 4. At first sight this difference seems negligible, but it has to be considered that the effect of bigger oxides is of course more harmful than smaller ones, so even a small difference can turn a clean sample in a dirty one.

The second test was carried out by scanning the three different zones of the same filter to verify if the middle area was representative of the entire sample quality. As seen in Figure 3.2, class 1 oxides were 49 in the left area, 57 in the middle and 53 in the right. Class 2 were 15, 16 and 20 respectively from left to right. Class 3 were 5, 2 and 3 and class 4 were 4, 0 and 1.
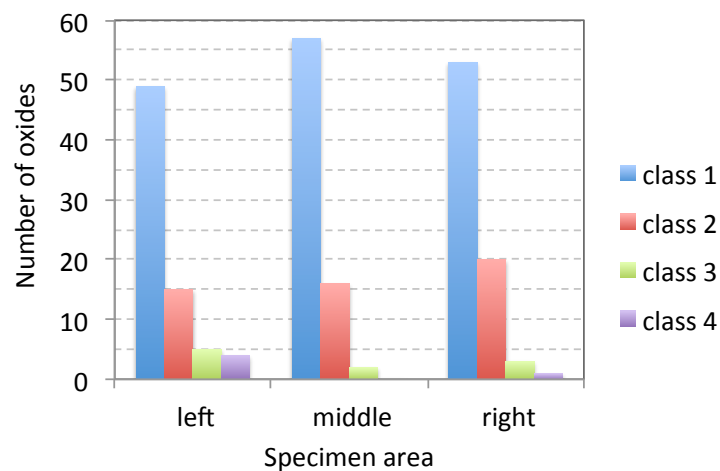
Figure 3.2: Number of oxides for each class counted in sample left, middle and high areas.

As previously, there was coherency between class 1 and 2, and difference between oxides of class 3 and 4 in the three zones respectively. This means that middle area is representative just for the number of class 1 and 2. Therefore, to assess quality of a sample correctly, middle area was scanned at 200x magnification, to evaluate number of class 1 and 2, and the entire area above the filter (left, middle and right) at 50x, to be sure to count properly the other classes. According to the number of oxides counted, a qualitative parameter to each class, from A to E as seen in Table 3.2, was assigned.

Oxide class	A	B	C	D	E
1	0 - 12	13 - 24	25 - 36	37 - 48	≥ 49
2	0 - 6	7 - 12	13 - 18	19 - 24	≥ 25
3	0	1	2 - 3	4 - 5	≥ 6
4	0	0	1	2	≥ 3
Description	Very clean	Clean	Medium	Dirty	Very dirty

Table 3.2: Oxides range and description for each qualitative class.

An example of a filtration sample analysis is given in Table 3.3.

Oxide class	#	Qualitative class
1	57	E
2	16	C
3	10	E
4	5	E

Table 3.3: Example of filtration test results.

As seen, there are four qualitative classes, but for simplicity are summarized in a single value obtained by comparing the four data. In this case final qualitative class of the sample is E, that means "very dirty".

3.1.3 RPT assessment study

The purpose of this experiment was to verify the repeatability and reliability of reduce pressure test. 28 specimens were taken consecutively from a molten bath of EN AC 46000. Weight of specimens was changed pouring different quantity of molten metal in two

different steel cups (Figure 2.8), to simulate a typical industrial use. Then, RPT was carried at 100 mbar. The obtained specimens were first weighed in air and water to evaluate density and later were cut, polished, scanned and image analysed to calculate the Bifilm index and porosity percentage.

Specimens from different cups were studied severely. Group 1 identified specimens coming from biggest cup, while group 2 from smallest one. At the beginning a study was carried out to find the distribution with the highest fit for density and Bifilm index results for each group.
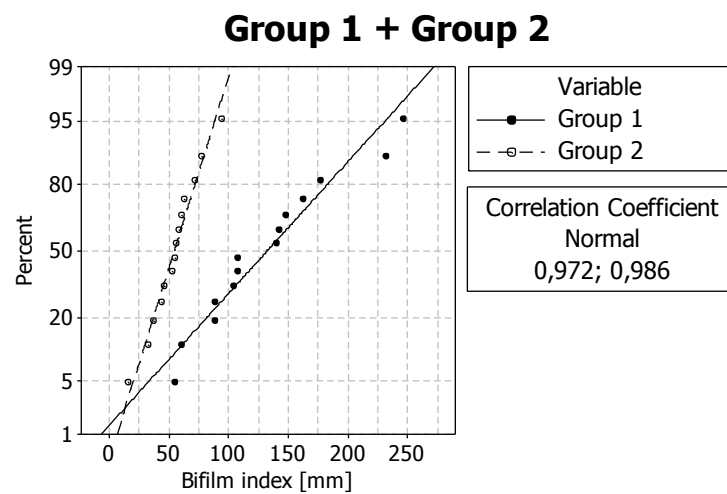
(a)
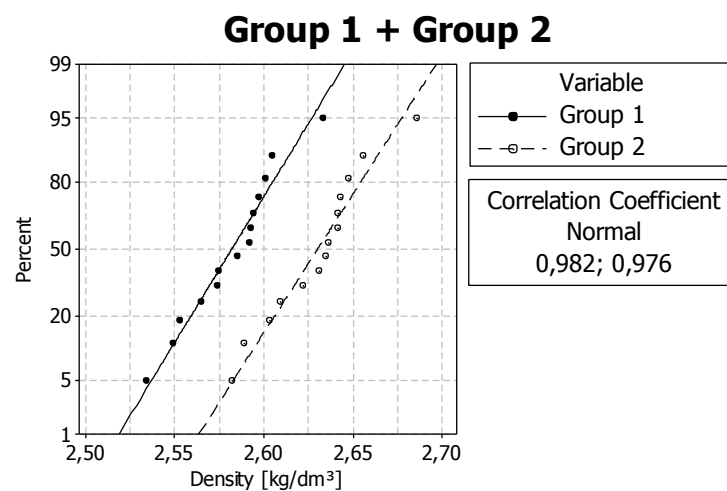
(b)

Figure 3.3: Density (a) and Bifilm index (b) normal distribution fit for group 1 and 2 joined together.

As seen in Figure 3.3 (a), the correlation coefficient of the normal distribution fit for density was 0,98 both for group 1 and group 2. Instead for Bifilm index was 0,97 for group 1 and 0,99 for group 2, as shown in Figure 3.3 (b). Since coefficients were high enough, Normal distribution was chosen to represent these two features.

The Normal distribution was built for the density and Bifilm index values of every group, as seen in Figure 3.4.

(a)   (b)

(c)   (d)
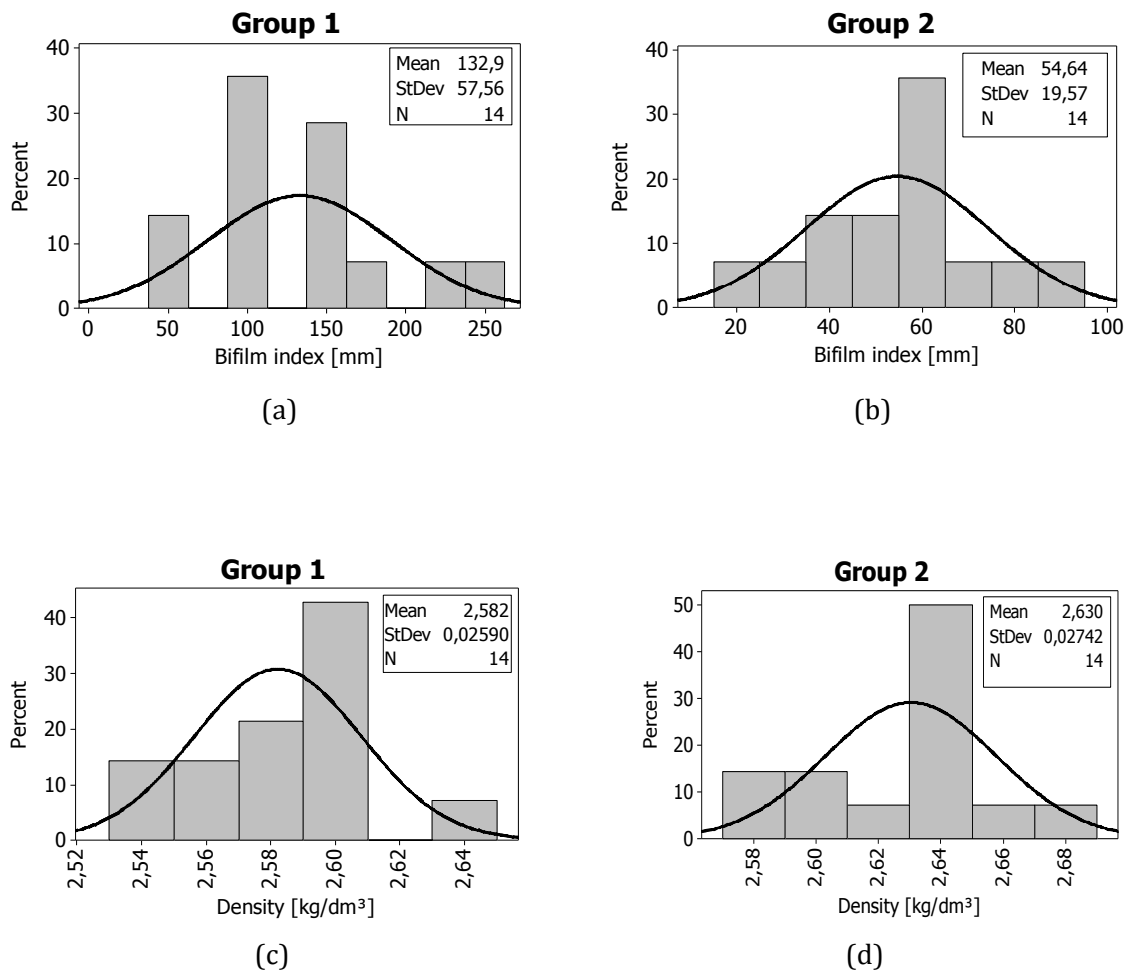
Figure 3.4: Normal distribution for Bifilm index (a,b) and density (c,d) values for group 1 and 2.

For group 1, the mean value of Bifilm index was approximately 133 mm and standard deviation 58 mm (a), corresponding to 43% of the mean value. Average density was 2,582 kg/dm^3 and standard deviation 0,026 kg/dm^3 (c), the 1%. For group 2 mean value of Bifilm index was 55 mm and standard deviation 20 mm (b), 36% of the mean value.

Average density was 2,630 kg/dm³ and standard deviation 0,027 kg/dm³ (d), approximately 1%. The first observation is that Bifilm index and density mean values were different between the two different groups, in particular group 1 specimen, from biggest cup, had higher average Bifilm index and so lower average density than group 2, from smallest cup. Bifilm index standard deviation was higher for group 1, instead density standard deviation was approximately the same for both groups. Thus, on average, quality of group 1 samples was worse than group 2.

To investigate about this difference, the graph of Bifilm index on weight was plotted for each group of samples, as seen in Figure 3.5. The purpose was to verify if weight had an influence on Bifilm index values.
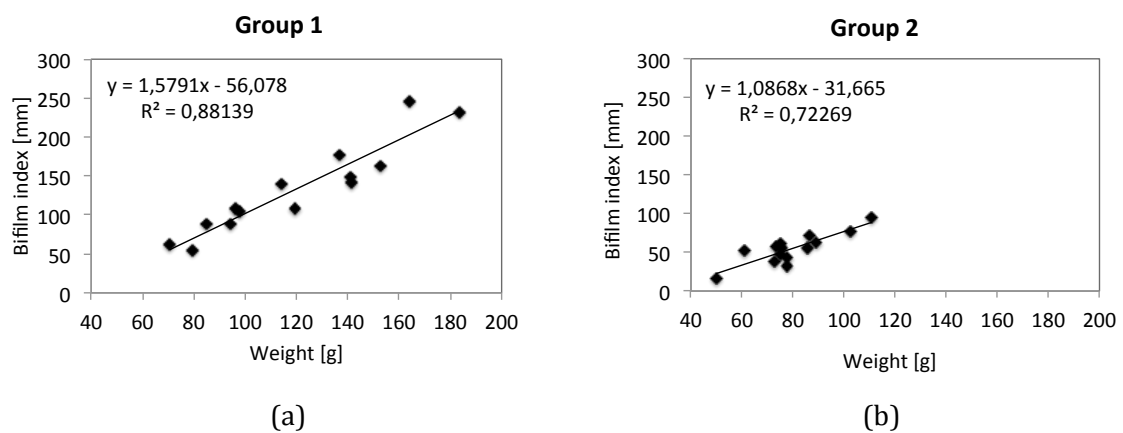
Figure 3.5: Bifilm index-weight relationship for group 1 (a) and 2 (b).

Looking at the graphs, the relationship between Bifilm index and specimen weight was clear, especially for group 1 where weight changes were higher than group 2, and so line building was easier, as suggest the square correlation coefficient of 0,88, Figure 3.5 (a). In Figure 3.5 (b) data were closer and so correlation coefficient dropped to 0,72 but the trend was similar.

The same graphs were built also for density to verify if depended on specimen weight too. As seen in Figure 3.6, the correlation found was similar to Figure 3.5, but with some differences. First of all slope of the line was significantly different between the two groups. Then the square correlation coefficient for group 1 was 0,48 (a) and for group 2 was 0,75 (b), far from each other and inverted compared to Figure 3.5. It's interesting to note that highest slope regarded group 2, so density of specimens that weighted less than 110 g

seemed to be more sensitive to weight variations compared to the density of heavier ones. In fact line of group 1 is much more flat than group 2. Therefore in this work, weight of specimens taken in industrial field was kept always higher than 110 g, trying to avoid any mass bother on density.

(a)   (b)
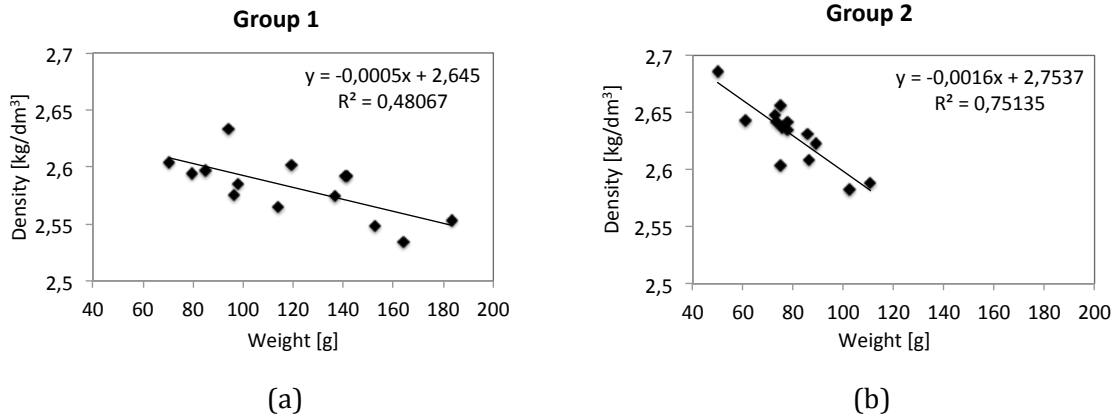
Figure 3.6: Density-weight relationship for group 1 (a) and 2 (b).

Focusing on Bifilm index, since the trends of graphs in Figure 3.5 were similar, they were joined together. The result is presented in Figure 3.7. As seen, Bifilm index definitely increased with weight increase ($R^2 = 91$). This behaviour was probably due to the higher quantity of bifilms caught in a bigger mass of molten aluminium.
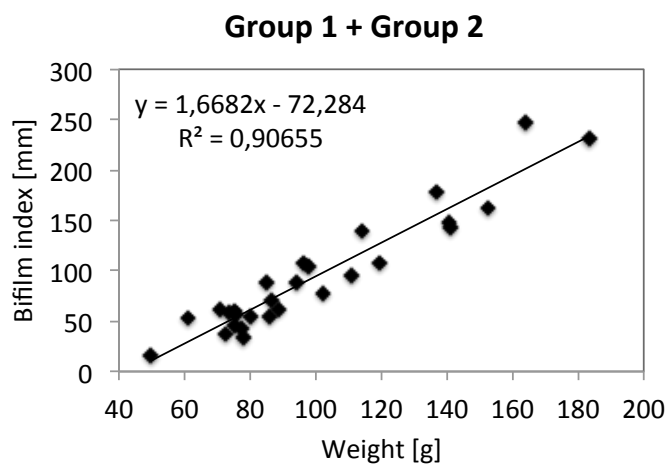
Figure 3.7: Bifilm index-weight relationship for group 1 and 2 joined together.

A way to depurate Bifilm index from weight influence was tried to find. Due to almost linear correlation between them, a new quality index was proposed in this work instead of Bifilm index and named Specific Bifilm index (SBI), as shown by the equation 3.1:

$$Specific\ Bifilm\ index\left[\frac{mm}{g}\right] = \frac{Bifilm\ index}{weight} \qquad (3.1)$$

Measurement unit of this index is [mm/g] that means millimetres of oxide contained in a gram of aluminium.

To compare the reliability of Bifilm index and SBI for specimens with a different weight, the normal distribution was built joining together the previous groups analysed.

(a)   (b)
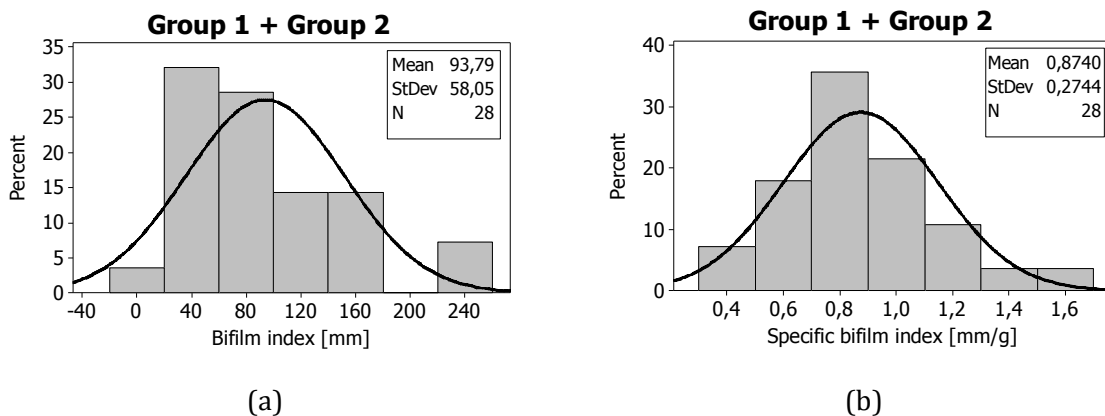
Figure 3.8: Normal distribution for Bifilm index (a) and Specific Bifilm index (b) for group 1 and 2 joined together.

As shown in Figure 3.8, the mean value of Bifilm index was approximately 94 mm and the standard deviation 58 mm (61% of the mean value). For the SBI, the average value was 0,87 mm/g and the standard deviation 0,27 mm/g (approximately 31%). So the standard deviation in percentage of Specific Bifilm index was half; the distribution of average Bifilm index was more homogeneous and closer to the average value. The probability plot in Figure 3.9 further verified this. SBI had a better fit with Normal distribution than Bifilm

index. It can be concluded that Specific Bifilm index was more accurate to describe the quality of specimens of different weight.

(a)   (b)
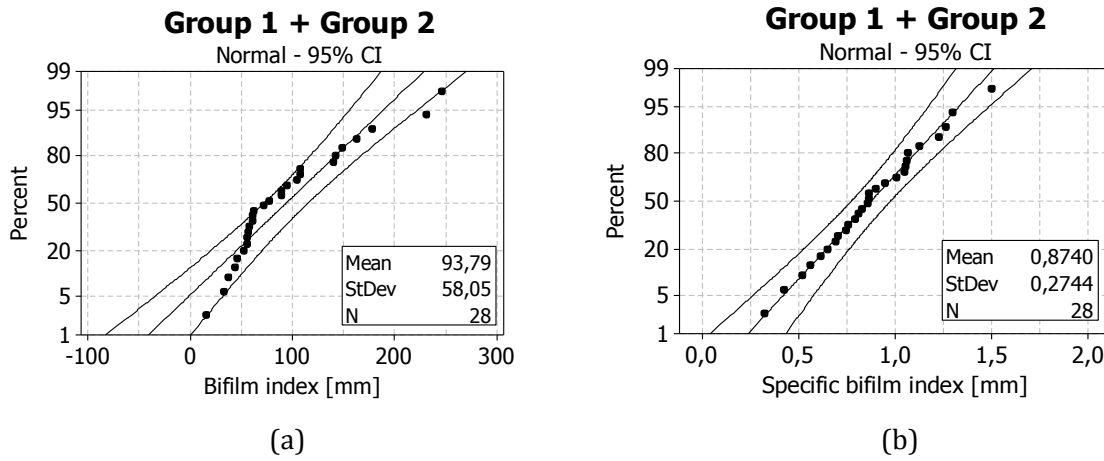
Figure 3.9: Normal distribution fit for Bifilm index (a) and Specific Bifilm index (b) for group 1 and 2 joined together.

Coming back to Figure 3.6, it was observed that density changed with specimens weight variation, similar to Bifilm index. So a graph was built plotting together density and Bifilm index.
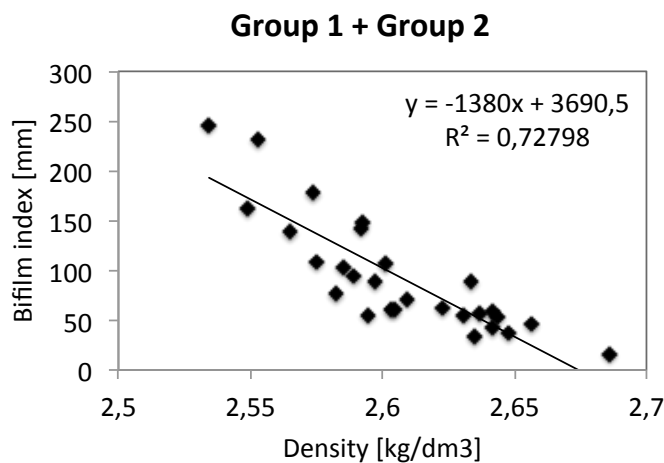
Figure 3.10: Bifilm index-density relationship for group 1 and 2 joined together.

As seen in Figure 3.10, the density decreased with Bifilm index increasing, as expected. Square correlation index was 0,73 due to slight scattering, but the trend was anyway clear. If the bifilms number increased, the probability of their opening to form porosity was higher and so the density of the specimens decreased. In order to assess if this correlation was verified also between Specific Bifilm index and density, the graph in Figure 3.11 was built.

Group 1 + Group 2
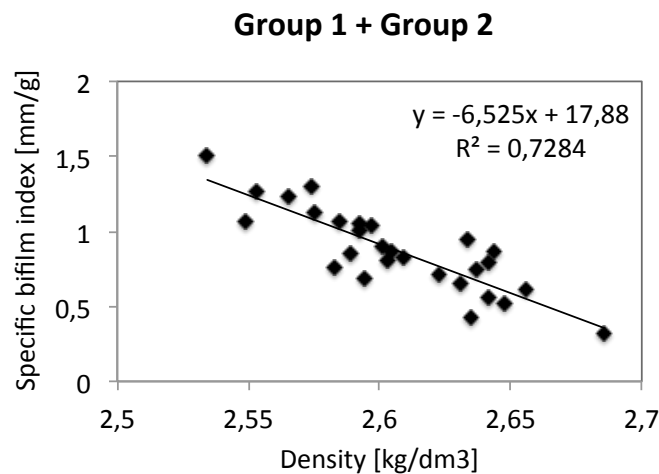
Figure 3.11: Specific bifilm index-density relationship for group 1 and 2 joined together.

As seen, square correlation index was again 0,73 and so the relationship was the same as Figure 3.10.

Finally to further verify the dependence of Bifilm index on weight, a short test was achieved in foundry. The purpose was to verify if there was any difference on experiments results changing scale of the furnace, compared to the laboratory test.

Operating conditions were the same as before, but melted aluminium was 250 kg instead of 9. The alloy was the same and the temperature was set to 695°C. Dimension of the cup was between those used for group 1 and 2. 5 specimens of different weight were taken consecutively from the melt. The results can be seen in Figure 3.12. The slope of the line is very similar to Figure 3.5, so Bifilm index on weight trend was the same regardless the furnace dimension. The square correlation index was 0,86, due to reduce number of tests.

Concluding, in this work Specific bifilm index was chosen to describe the quality of RPT specimens, avoiding errors due to different weight of specimens, but keeping the correlation with density as Bifilm index.
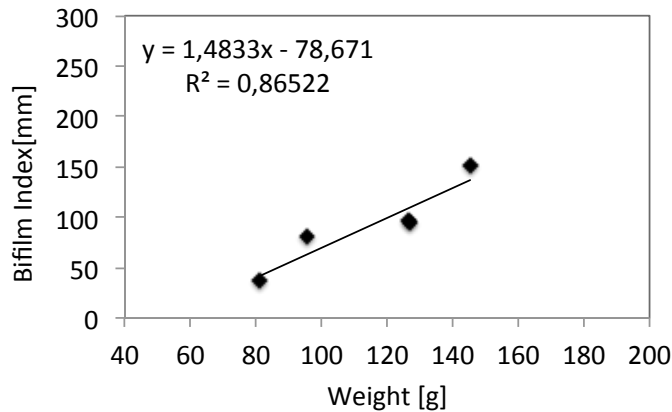
Figure 3.12: Bifilm index-weight relationship for foundry test.

3.1.4 Porosity percentage calculation assessment

Actually, the most used parameter to evaluate melt cleanliness in industrial field is the Density Index (DI), which represents porosity percentage in RPT specimens. Into the MUSIC project this index should be use to evaluate the melt quality, and maximum acceptable value is set at 2%. In this experiment DI was compared with Nominal density index (NDI) and porosity % calculated with image analysis to find the most accurate one to describe the melt quality. These three indexes were calculated for the 28 specimens of the previous test and the results are compared in Figure 3.13.

First observation is that Density index is close to Nominal density index, but constantly underestimates the porosity percentage. The error was systematic and due to the different density values chosen as alloy reference for the two indexes. Alloy reference means the ideal density value of a specimen without any porosity, which is compared with the density of the RPT specimen.

For NDI this value was obtained from chemical analysis of the melt and relative equation, as seen in paragraph 2.3.2. Instead, for Density index was obtained weighing on air and water a specimen solidified under atmospheric pressure. The problem was that its density depends on the solidification process. To demonstrate this, specimen solidified under atmospheric pressure was sectioned, polished and subjected to image analysis.

density was not the real density of the alloy, but was affected by an intrinsic error, and porosity % was underestimated.
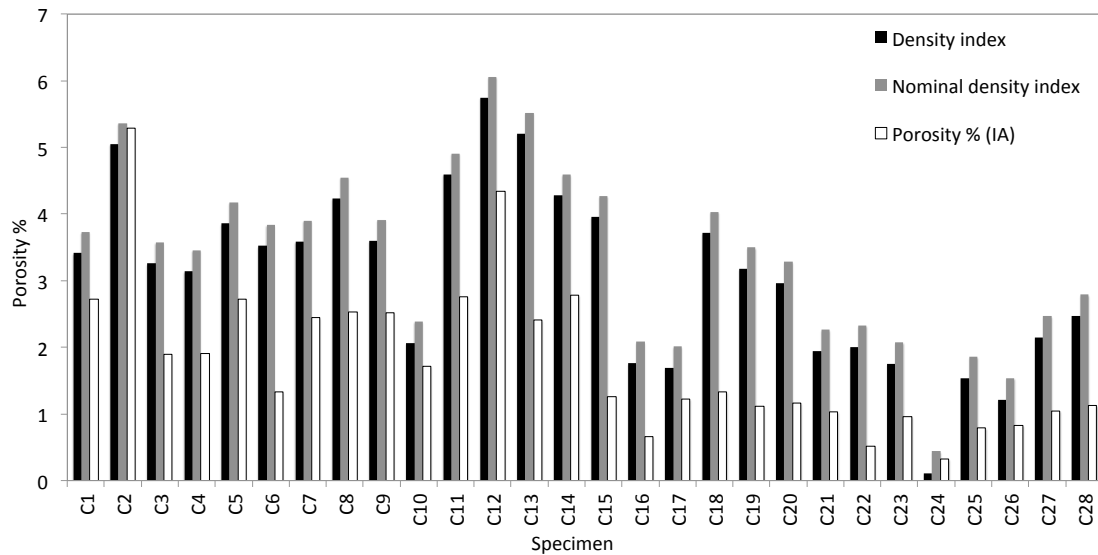
Figure 3.13: Porosity percentage evaluated with different tecniques.

As seen in Figure 3.14, a certain amount of porosity forms in the middle-high part of the sample, last region to solidify. If a specimen solidifies under atmospheric pressure, bifilms are not opened as under reduce pressure, but however there is a little opening action in the middle zone of specimen due to shrinkage and entrapped gas [12]. So specimen For the sample in Figure 3.14 porosity % was approximately 0,33%, not negligible amount. Therefore 0,33 was the systematic difference between DI and NDI seen in Figure 3.13.
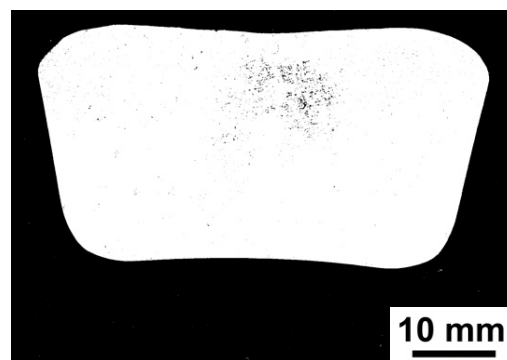
Figure 3.14: Sectioned and polished surface of a specimen solidified under atmospheric pressure.

Another possibility to evaluate percentage of porosity in RPT sample was to use image analysis. The total area of porosities could be calculated and divided for the entire surface

of the sample. The first problem of this technique was the condition of sample surface, in fact if not perfectly grounded, scratches could be source of errors. Another problem was the scanner light refection inside the pores, which depended on geometry of the pores and where pores were cut. Generally these problems caused an underestimation of porosity area, as seen in Figure 3.13. About this, the most interesting sample was C2 (a), because it was the only where the porosity % and Nominal density index are close (except for sample C24 that had very few pores). If C2 is compared with other sample, for example C13 (b), its surface appears more white after image correction, as seen in Figure 3.15. This was due to better polishing, so the contrast with the black of pores is higher and their evaluation is more accurate, compared with C13.

(a)   (b)
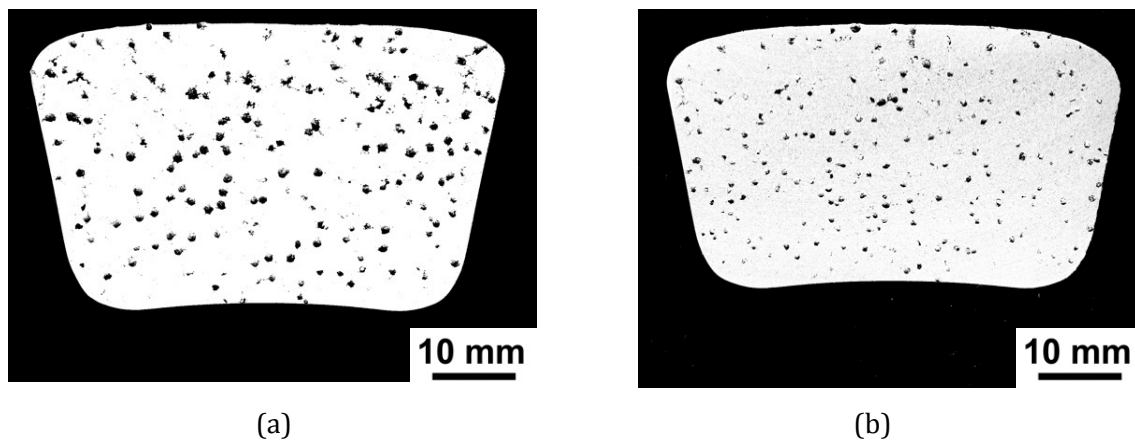
Figure 3.15: Sectioned and polished surface of sample C2 (a) and C13 (b).

Since just one sample out of 28 was correctly prepared, porosity evaluation with image analysis was discarded. Has to be noticed that Bifilm index (and consequently Specific Bifilm index) was much less affected by this underestimation error. In Figure 3.16 a porosity in which light reflection is not perfect (a) is shown and so binarized area is approximately half than real value (b). Calculating Bifilm index, and of course NBI, only porosity length was considered and so underestimation of the area was negligible, as seen in Figure 3.16 (c).

| (a) | (b) | (c) |
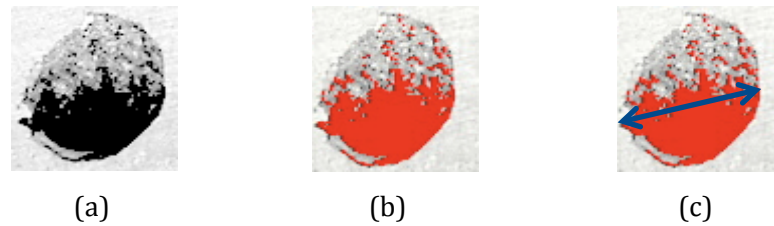
Figure 3.16: Porosity after image correction (a), after binarization (b) and Bifilm index evaluation (c).

3.2 Industrial trials

In this section, results obtained from industrial trials are reported and were used to evaluate suppliers, degassing process and quality changes with time processing, according to indexes presented before. Filtration, reduced pressure test and hydrogen measurement were applied together to assess the melt quality. During foundry trials were taken at least three specimens: first one after alloy melting, second after degassing and fluxing treatment and third at the end of the trial. The chronological sequence of instruments used for every sampling was:

- Alspek-H®
- Filtration test
- RPT

In Table 3.4 all information about foundry trials is given, including air humidity that was approximately the same every time and so was neglected in this work.

Foundry trial	Date	Furnace	Alloy	Batch (Supplier)	Degassing time	Degassing rate	Gas	Air humidity
D	02/07/13	600 kg	46000	14/13 (A)	12 min	12 l/min	Ar	68%
E	04/07/13	300 kg	46000	14/13 (A)	12 min	12 l/min	Ar	68%
F	09/07/13	300 kg	43400	07/13 (A)	12 min	10 l/min	Ar	64%
G	10/07/13	300 kg	46000	14/13 (A)	12 min	8 l/min	Ar	65%
H	19/07/13	600 kg	46000	14/13 (A)	12 min	10 l/min	Ar	67%
I	22/07/13	600 kg	46000	10/13 (B)	12 min	8 l/min	Ar	70%
L	24/07/13	600 kg	46000	10/13 (B)	12 min	14 l/min	Ar	68%
M	26/07/13	300 kg	47100	06/13 (B)	6 min	12 l/min	Ar	74%
N	26/07/13	600 kg	43400	11/13 (A)	8 min	12 l/min	Ar	60%
O	02/08/13	300 kg	46000	10/13 (B)	4 min	12 l/min	Ar	68%
P	02/08/13	600 kg	47100	06/13 (B)	8 min	12 l/min	Ar	66%

Table 3.4: Foundry trials operating conditions.

3.2.1 Supplier evaluation

The first specimen taken for every foundry trial was useful not only to assess initial condition of the melt before degassing, but also to evaluate different suppliers performance, since the foundry melting process was the same every time. The company was provided by two different suppliers, named A and B. In this work ingots from A and B were not mixed together during melting, to be able to assess the metal quality of each supplier.

Starting from RPT, the Nominal density index was the first index calculated. It involved just the two weighings and chemical analysis of the melt. In Figure 3.17 are given the results of all foundry trials.
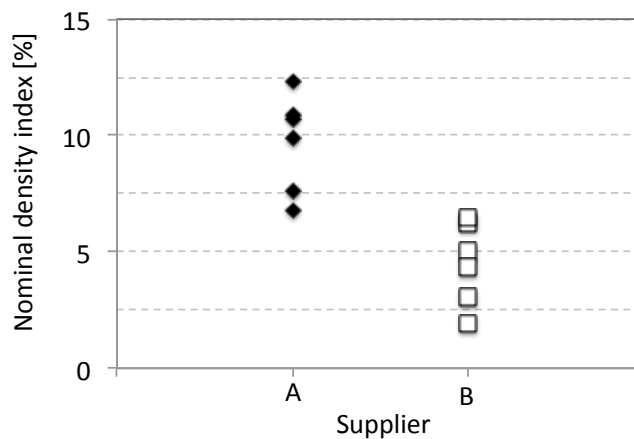
Figure 3.17: Nominal density index-supplier relationship for all foundry trials before degassing.

As seen, there is a substantial difference between them. NDI was between 7% and 12% for supplier A and between 2% and 6% for B, always lower and also less scattered.

Samples were cut, polished, scanned and subjected to image analysis to obtain Specific bifilm index values, plotted in the following graph. As shown in Figure 3.18, the values are between 2 and 4 mm/g for supplier A and approximately between 1 and 2 for B. The situation was the same, even if in this case there is a slight overlap between the two groups.
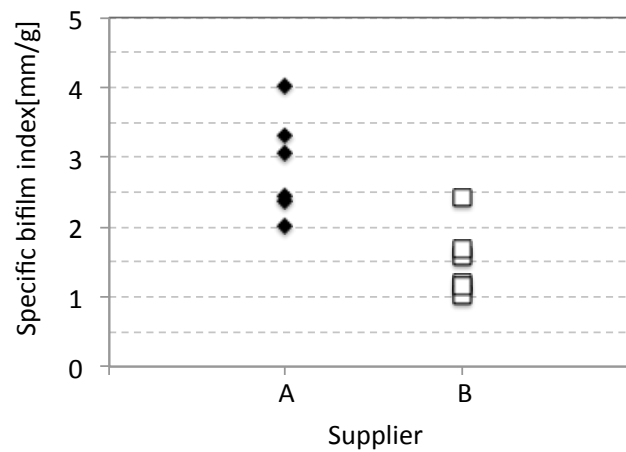
Figure 3.18: Specific bifilm index-supplier relationship for all foundry trials before degassing.

The hydrogen content was also considered, as shown in Figure 3.19.
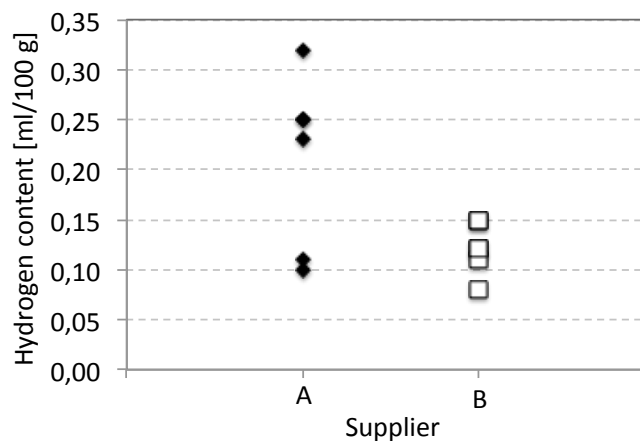
Figure 3.19: Hydrogen content-supplier relationship for all foundry trials before degassing.

The results confirm again what previously said, with hydrogen content between 0,10 and 0,32 for supplier A and between 0,08 and 0,15 for B. In this case overlap is more evident but has to be observed that scattering of A was much higher than B, so on average B specimens contained less hydrogen than A. If the initial hydrogen level is high, a high number of porosity is expected in the specimens.

The last technique used to evaluate the different suppliers was the filtration method. Samples were cut, polished and scanned with an optical microscope at 50 and 200x magnifications to count number of oxides. Then a qualitative class was assigned to every sample to describe the cleanliness level. As seen in Figure 3.20, in the horizontal axis there are the foundry trials, in the vertical axis the qualitative class of each samples evaluated with filtration test.
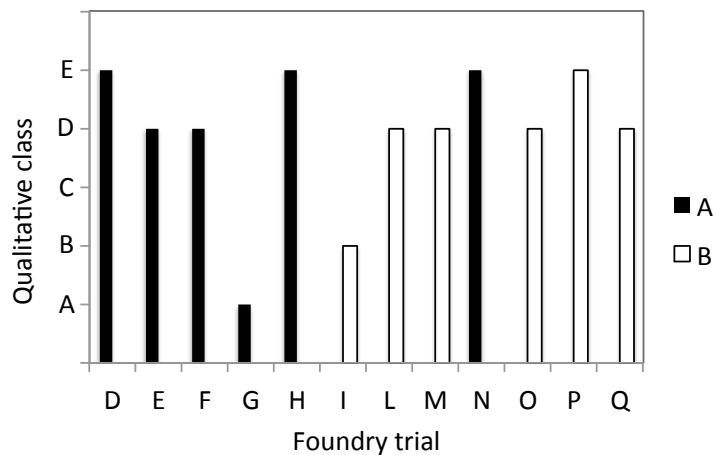
Figure 3.20: Qualitative class relationship with foundry trial and supplier.

In the samples a high number of oxides was find and so the most common classes were D and E. In this case difference between suppliers A and B was less clear because quality appears comparable, in contrast with previous results.

3.2.2 Degassing study

Degassing process was studied severely for 600 kg and 300 kg furnaces; by applying reduce pressure test, filtration and hydrogen measurement, to evaluate quality improvements. For every foundry trial in Table 3.4, the first specimen was taken after complete melting of the charge and was used also in the previous paragraph to evaluate suppliers. The second specimen was taken after degassing and fluxing and is compared with the first one in the next paragraphs according to all quality indexes.

Degassing process was ruled by acting on two parameters: flow rate and time. Foundry standard values were 12 l/min and 12 min for both furnaces. Gas used was argon. At the

beginning the duration of 12 min was kept constant and the flow rate was changed respectively to 14, 12, 10, 8 l/min for the biggest furnace and 12, 10, 8 l/min for the smallest one, as seen in Table 3.4. Then, flow rate was kept constant to 12 l/min and time was changed to find the best trade-off between the two variables for every furnace. For the smallest furnace durations of 6 and 4 minutes were tried, instead for the biggest one 8 minutes. In this work, the fluxing was not changed in terms of quantity and type of salts.

1) Nominal density index (NDI)

The nominal density index was the first to be calculated. In Figure 3.21 the results before and after degassing and fluxing treatment for 600 kg furnace are given. As seen, initial melt condition was scattered, from very dirty such as trial H sample before degassing, with a Nominal density index of 11%, to quite clean, such as trial I with 2%. As said in the previous paragraph, this scattering is due to the different ingots' quality of the suppliers. In particular, two groups could be identified: first one included trials D, H and N, supplied by A, in higher position than second group of trials P,L and I from supplier B. The first group had a NDI between 8% and 11%, the second between 6% and 2%. The difference between trial values before degassing of the same batch, like D and H or L and I, was probably related to the quality of the scraps charged into the furnace at the beginning of melting process.

The first observation about the degassing process is that the initial scattering was decreased, the Nominal density index after fluxing ranged between 2% and 7%, so in general the degassing was effective. It could be observed that the cleaning action with the extreme flow rates, 14 l/min of L and 8 l/min of I, was not so effective, because the NDI did not change much before and after degassing. Instead, using the medium flow rate values degassing performance was increased. In particular, for trial D, using the foundry standard parameters, the result was good, but the highest difference between starting and ending value was observed for trial H, using 10 l/min. Anyway, the driving force of the degassing cleaning action seems to be the initial quality condition of the melt, more than flow rate. If the melt is dirty before the degassing, the initial quality is strongly increased after the process; contrary the improvements are lower by starting with a clean melt. From trial H to I, the improvement decreased according to decreasing of Nominal Density index before degassing.
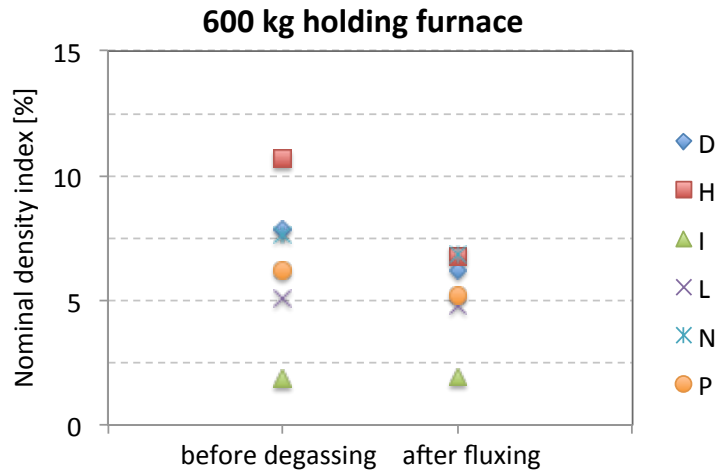
Figure 3.21: Nominal density index before degassing and after fluxing for the 600 kg furnace.

What said for the 600 kg furnace is also valid for the 300 kg one. As seen in Figure 3.22, the initial dispersion of data is approximately the same as before, with a NDI between 12% and 3%. Degassing and fluxing reduced scattering again. The Nominal density index values were between 6% and 2%, if trial O specimen before degassing was discarded.
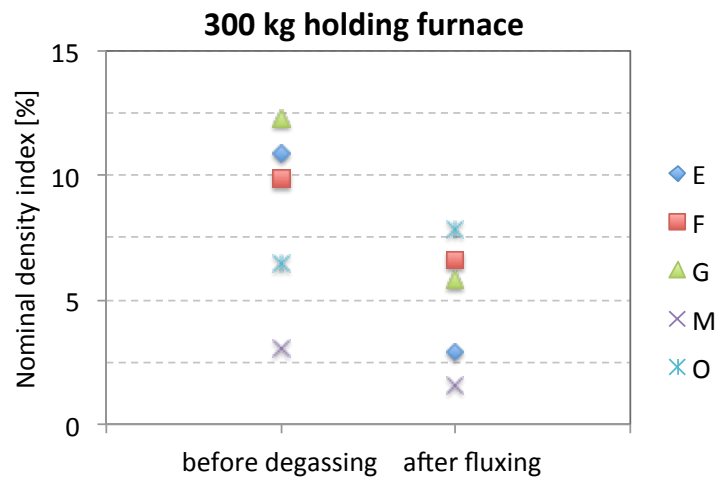
Figure 3.22: Nominal density index before degassing and after fluxing for the 300 kg furnace.

The highest improvement was obtained with a flow rate of 12 l/min for 12 min of trial E. In the case of the trial M, the initial NDI value was low so it was hard to improve it more.

Trial O is the only case in which the Nominal density index increased after degassing. Since flow rate was 12 l/min, the problem was the 4 min of degassing time, too short to clean the melt effectively and so had to be increased. It's interesting to note that the lowest NDI reached for both furnaces was approximately 2%. This value could be identify as the limit for this kind of degassing and fluxing treatment and explains why the improvement decreased with the initial NDI decreasing.

2) Specific bifilm index (SBI)

After Nominal density index evaluation, samples were cut, polished, scanned and subjected to image analysis to obtain Specific bifilm index value. In Figure 3.23 the results for 600 kg furnace are given. As seen, initial melt condition was scattered as for NDI data, from 4 mm/g of trial H specimen before degassing to 1 mm/g of trial I, due to different ingots quality. It is interesting to note that position of foundry trials H, D, L and I (all EN AC 46000 alloy) before degassing was exactly the same of previous graph, contrary trials N (EN AC 43400) and P (EN AC 47100) fell down. Such result is probably due to the different chemical composition of these alloys as seen in Table 3.4, which affects the NDI in addition to porosity. Furthermore, the different chemical composition changes also the solidification process and so the dimension and shape of porosities [7].

Specimens before degassing from supplier A had SBI between 2 and 4 mm/g and those from supplier B between 1 and 2,5 mm/g. The difference between the two suppliers was clear again even if the two groups were overlapped between trials L and N.
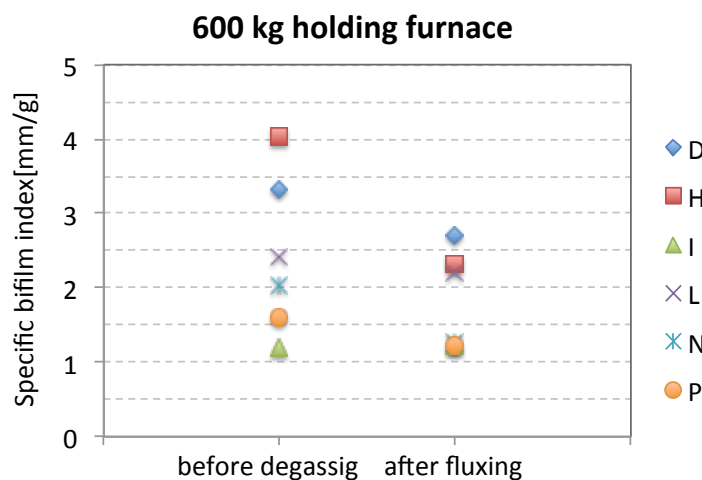
Figure 3.23: Specific bifilm index before degassing and after fluxing for the 600 kg furnace.

The degassing process decreased the initial scattering, so it was effective also in terms of SBI reduction. New range was between 2,5 and 1 mm/g. The cleaning action with extreme flow rates seems less effective than using medium flow rate values, as observed in the previous paragraph. But the main driving force of cleaning action was again the initial Specific bifilm index value. Anyway, the most interesting finding was the existence of the same limit for the degassing process as in the case of Nominal density index. This limit of 1 mm/g was reached by specimens of trials N, P and I after degassing, even if the alloy and the initial SBI value were different (Table 3.4).

As seen in Figure 3.24, for the 300 kg furnace, the initial values were less scattered than Figure 3.23, in fact range was between 1 and 3 mm/g. As in Figure 3.21, the degassing reduced scattering, except for trial O, in which SBI was increased. The most interesting aspect was the final value of trials E, F and G closed to 1 mm/g, even if the flow rate and alloy were different. This value seems to be the limit achievable by the degassing process if the initial metal quality was poor, but in the case of trial M, 1 mm/g was further reduced to 0,5. So in the smallest furnace the driving force of the process is once again the starting melt conditions, but, in contrast with the results of the biggest one, the lower limit could be overcame if the initial melt quality was high enough.
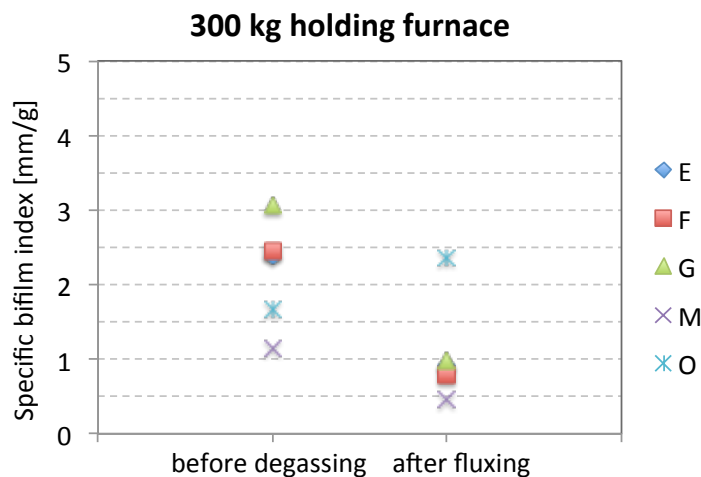
Figure 3.24: Specific bifilm index before degassing and after fluxing for the 300 kg furnace.

3) Hydrogen content

To evaluate the degassing process the hydrogen content was also considered in this work. It was measured before degassing, continuously during degassing and after fluxing. In Figure 3.25 hydrogen levels before degassing and after fluxing for 600 kg furnace are presented. As seen, the starting range was between 0,25 and 0,1 ml/100g of Al. Consistently with previous quality indexes results, specimens before degassing of trials D and H, were in the highest position, but other values were close to each other and between 0,15 and 0,1. After fluxing, the scattering was reduced and the final hydrogen content range was decreased between 0,2 and 0,1. Also for the hydrogen removal, the main driving force was the initial content, more was high more improvement was visible. Lower limit for hydrogen level was 0,1 ml/100 g.
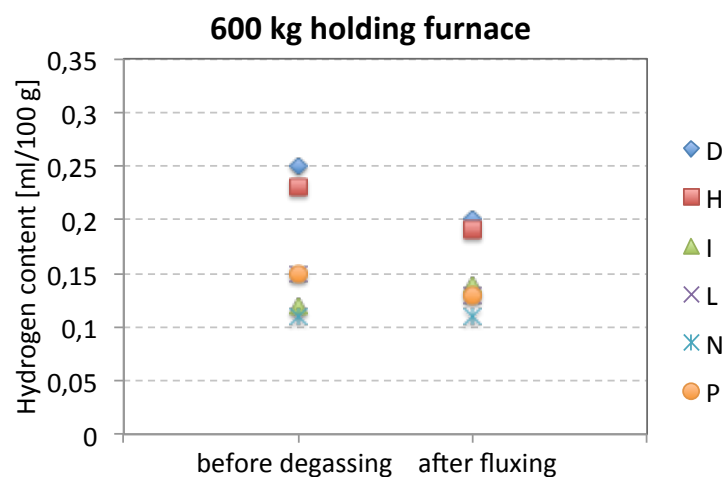
Figure 3.25: Hydrogen content before degassing and after fluxing for the 600 kg furnace.

The typical trend of hydrogen content during degassing of the 600 kg furnace is shown in Figures 3.26 (a) and (b). The degassing of trial H started at 10.08 and finished at 10.20, for trial L started at 08.22 and finished at 08.34. After degassing probe was putted off and fluxing was carried out. As seen in the graphs, after an initial adjustment period, the hydrogen level remained constant, even during the degassing, changing the flow rate or increasing the temperature as in Figure 3.26 (a). Instead a strong oscillation of hydrogen content was expected during the degassing, especially using high flow rate, as in the case of trial L with 14 l/min, or changing the temperature, but the variations observed were

minimal or absent. The real improvement, that reduce the initial scattering and so the hydrogen content, as seen in Figure 3.25, was reached after the fluxing operation.

(a)

(b)
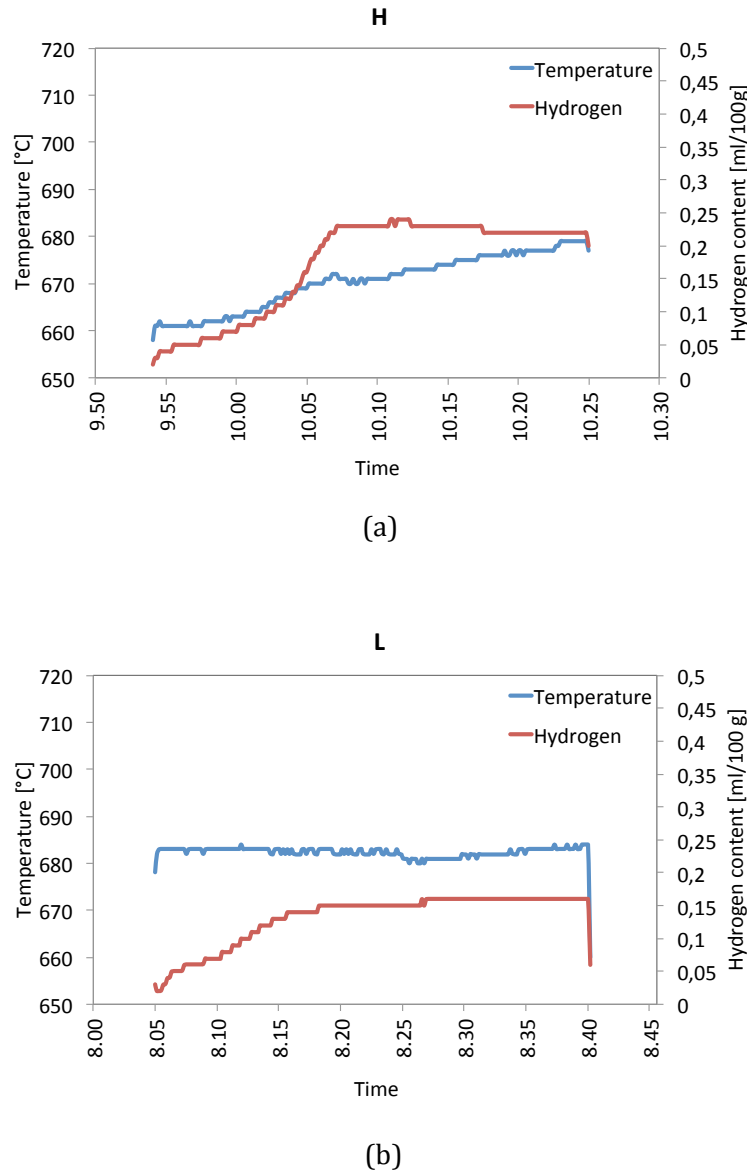
Figure 3.26: Hydrogen concentration and melt temperature during degassing process of trial H (a) and L (b).

For the 300 kg furnace, the initial scattering was higher than 600 kg one, with a range between 0,3 and 0,1 ml/100g of Al, as seen in Figure 3.27. The hydrogen content before degassing of trials E and F was high, consistently with previous results, but trial G was the lowest value, in contrast with the previous indexes. After fluxing the hydrogen level range

was reduced between 0,2 and 0,1 ml/100g of Al. The degassing was effective in general, except for trial G, in contrast with Figures 3.22 and 3.24. As in the 600 kg furnace, the lowest hydrogen level achievable was approximately 0,1 ml/100 g Al.
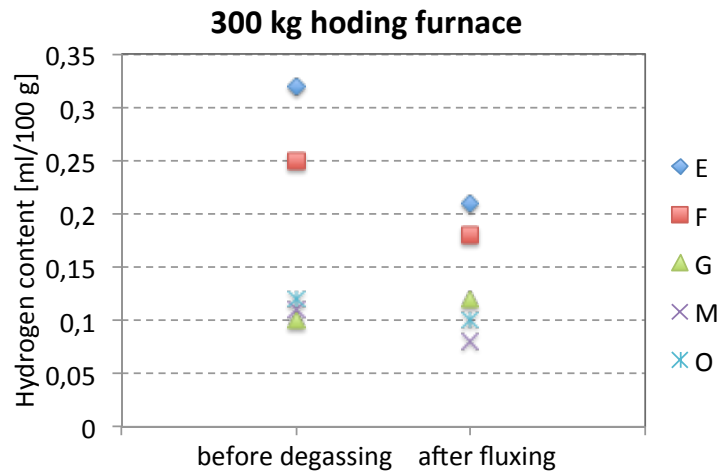
Figure 3.27: Hydrogen content before degassing and after fluxing for the 300 kg furnace.

Examples of the trends of the hydrogen content during degassing in the 300 kg furnace are shown in Figures 3.28 (a) and (b). For trial G degassing started at 10.36 and finished at 10.48, for trial E started at 10.28 and finished at 10.40. First observation is that hydrogen level remained constant for degassing G, but decreased for degassing E, which contained initially more hydrogen, as seen in Figure 3.28.

(a)

(b)
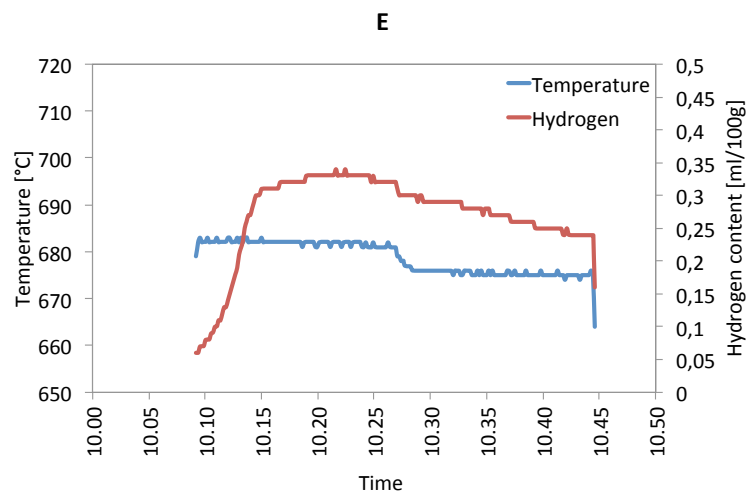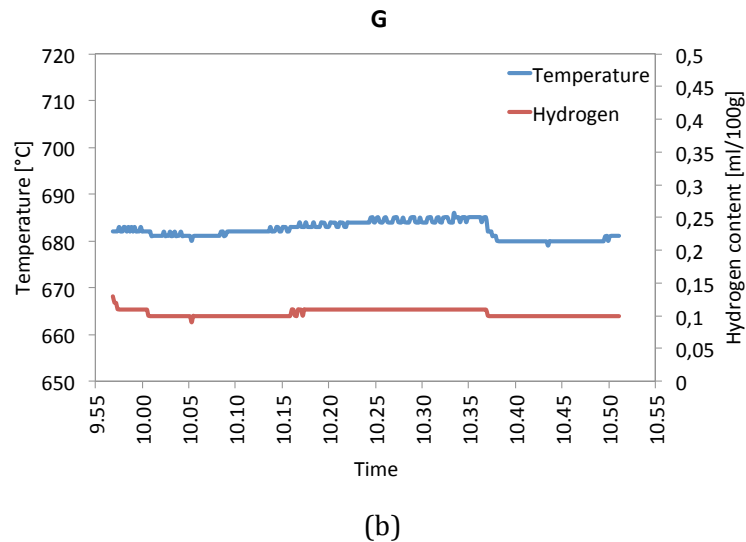
Figure 3.28: Hydrogen concentration and melt temperature during degassing process of trial E (a) and G (b).

Once again, the driving force of the treatment seems to be the initial hydrogen content of the melt. Finally it was observed that in the smallest furnace the hydrogen content during the process seems to follow the temperature variation more than in the biggest one.

4) Filtration test

The filtration test was the last technique applied to assess the degassing process improvements. In Table 3.5 results for the 600 kg furnace are presented. For every specimen is given the number of oxides counted and the resulting final qualitative class.

Foundry trial	Sample	Class 1	Class 2	Class 3	Class 4	Qualitative class
D	before degassing	10	20	6	5	E
	after fluxing	26	17	5	2	D
H	before degassing	41	8	2	3	E
	after fluxing	25	16	3	2	D
I	before degassing	10	4	2	0	B
	after fluxing	7	5	3	0	B
L	before degassing	11	4	3	2	D
	after fluxing	12	4	2	1	C
N	before degassing	5	25	5	4	E
	after fluxing	11	17	5	2	D
P	before degassing	29	26	3	3	E
	after fluxing	13	7	4	1	D

Table 3.5: Oxides number for each class and relative qualitative class before degassing and after fluxing for the 600 kg furnace.

In Figure 3.29, the qualitative class of specimens taken before and after degassing were graphically compared. First observation is that results of EN AC 46000 trials (D, H, I, L) were coherent with the Figures 3.21 and 3.23. The most dirty samples before degassing were in trial D, characterised by an high presence of oxides of classes 3 and 4, and in trial H with high number of classes 1 and 4. In the specimens before degassing of trials N and P were found a lot of oxides, especially of class 4, in contrast with SBI and hydrogen content results. This behaviour, as said before, was probably due to different chemical composition, that changed solidification and also dimension and shape of oxides.

600 kg holding furnace
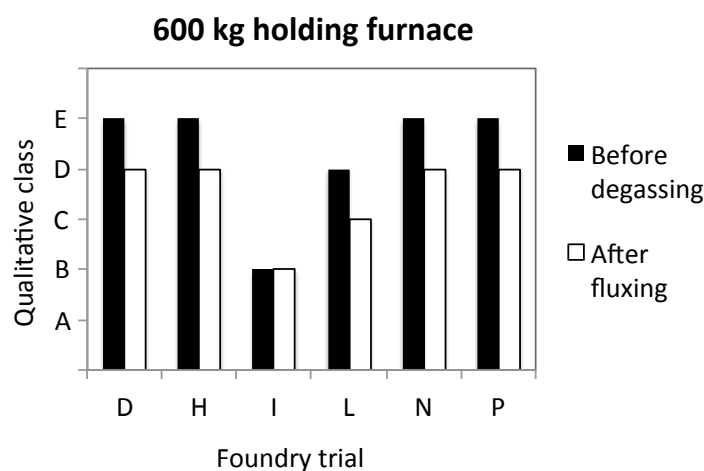
Figure 3.29: Qualitative class relationship with foundry trial before degassing and after fluxing for the 600 kg furnace.

In general degassing reduced the number of oxides, except for trial I, which had the cleanest sample before degassing, with no class 4 oxides. Therefore the degassing process did not improve quality further because reached its limit.

In Table 3.6 results for 300 kg furnace are presented and in Figure 3.30 are graphically compared. As seen, foundry trials E and F results are coherent with NDI and SBI values. Also the trend of trial O is consistent with these two indexes because starting class got worse after degassing and fluxing, so degassing increased oxides number. Degassing of trial M did not improve qualitative class, but, like in trial P (Figure 3.29), were found more oxides than expected, looking results of NDI and SBI. This means that the different chemical composition and consequently the solidification have to be considered comparing sample of different alloys.

Foundry trial	Sample	Class 1	Class 2	Class3	Class 4	Qualitative class
E	before degassing	26	9	4	1	D
	after fluxing	22	9	3	0	B
F	before degassing	2	3	3	2	D
	after fluxing	2	3	0	1	B
G	before degassing	16	3	0	0	A
	after fluxing	31	7	0	0	B
M	before degassing	8	12	4	2	D
	after fluxing	61	14	3	1	D
O	before degassing	22	6	5	2	D
	after fluxing	21	4	4	3	E

Table 3.6: Oxides number for each class and relative qualitative class before degassing and after fluxing for the 300 kg furnace.
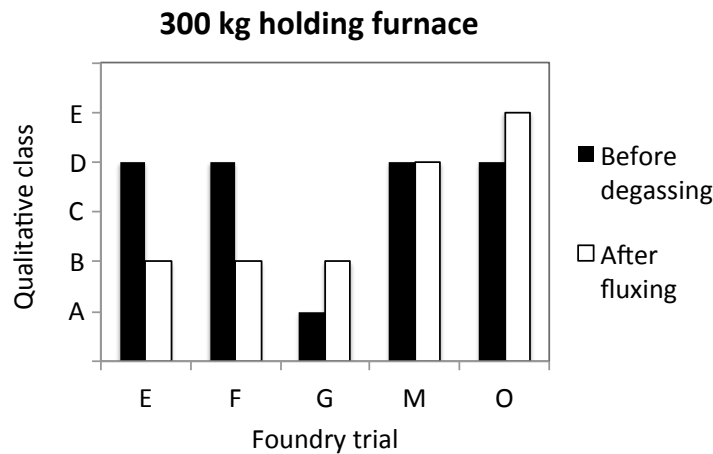
Figure 3.30: Qualitative class relationship with foundry trial before degassing and after fluxing for the 300 kg furnace.

3.2.3 Effect of gas-type on the degassing process

The last experiment about degassing involved the type of gas used during the process. Argon, usually used by foundry, was replaced with nitrogen and quality improvement was evaluated applying the previous four indexes. As seen in Table 3.7, EN AC 47100 from supplier B was used; the degassing time and rate were 10 minutes and 10 l/min in the biggest furnace. The air humidity level was comparable with the previous measures and so was neglected again.

Foundry trial	Date	Furnace	Alloy	Batch (Supplier)	Degassing time	Degassing rate	Gas	Air Humidity
R	02/09/13	600 kg	47100	06/13 (B)	10 min	10 l/min	N	76%

Table 3.7: Foundry trial R operating conditions.

In Figure 3.31 Nominal density index results are given before and after degassing and fluxing treatment. Initial value was approximately 4%, lower than the average value of the other trials seen in Figure 3.21, while the final value was 3%. Porosity level was reduced although initial value was low and furnace was the biggest.
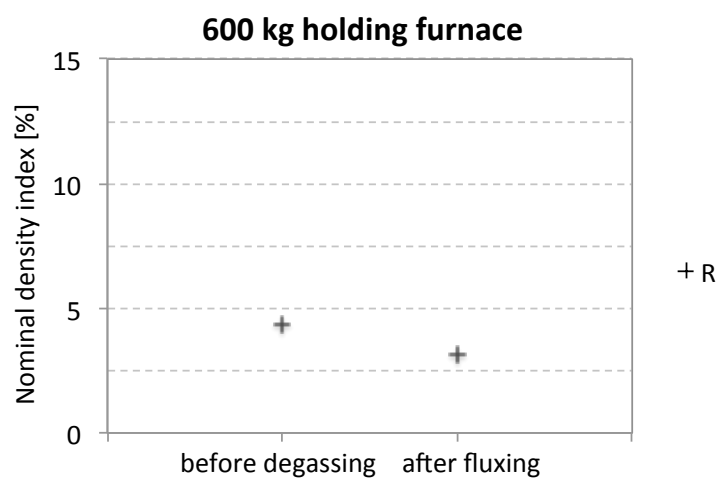
Figure 3.31: Nominal density index before degassing with nitrogen and after fluxing for the foundry trial R.
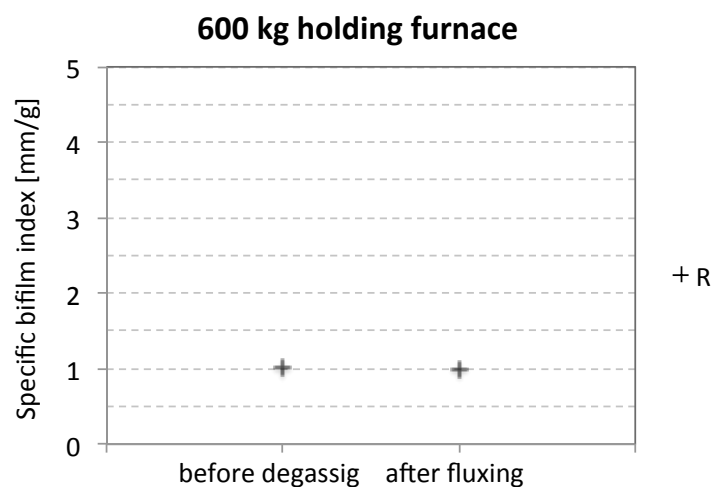
Figure 3.32: Specific bifilm index before degassing with nitrogen and after fluxing for the foundry trial R.

The Specific bifilm index was evaluated. As seen in Figure 3.32, it was 1 mm/g before and after degassing, exactly on the limit of the process. There was not any improvement consistently with the previous degassing results for specimens with initial SBI near the limit. This result was not coherent with NDI trend shown in Figure 3.31.

In Figure 3.33 hydrogen content of the melt are plotted before and after fluxing and degassing. First value was 0,8 ml/100g of Al, and after treatment was 0,12. This growing trend was in contrast with what observed in Figures 3.31 and 3.32.
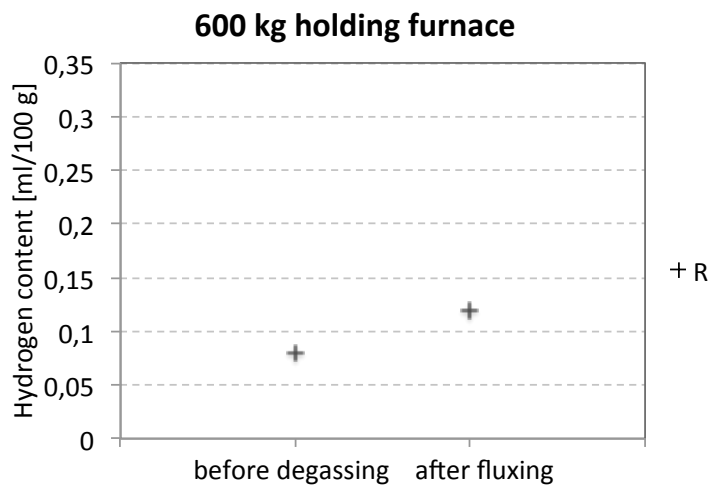
Figure 3.33: Hydrogen content before degassing with nitrogen and after fluxing for the foundry trial R.

In Table 3.8 filtration test results are shown and in Figure 3.34 are graphically compared. A reduction of oxides for each class was observed and consequent the qualitative class increased from D to B. Such behaviour was coherent with the NDI but not with SBI and hydrogen content.

Foundry trial	Sample	Class 1	Class 2	Class3	Class 4	Qualitative class
R	before degassing	16	5	2	2	D
	after fluxing	3	0	1	1	B

Table 3.8: Oxide number for each class and qualitative class before and after degassing for the foundry trial R.

600 kg holding furnace
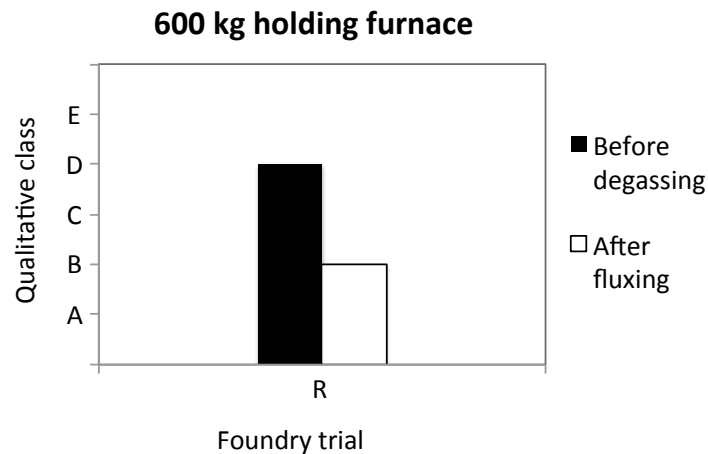
Figure 3.34: Qualitative class relationship with foundry trial R before degassing and after fluxing.

3.2.4 Melt quality changing with time processing

During foundry trials, and in general during HPDC production, the metal quality changes were expected with time processing. As seen in Chapter 1, oxide layer protects molten the metal from further oxidation and becomes thicker after an incubation time, changing its structure from amorphous to crystalline. During production, surface oxide film was broken by HPDC cup and ingots charged, so parts of it were submerged introducing bifilms into the melt. Then, the opened surface re-oxidized, increased thickness, was submerged again and so on. Therefore the metal quality was affected by the time and surface breaking action of HPDC ladle and ingots charged. Bigger oxides were expected to find into the melt with time processing.

In the SAEN foundry, the melt did not stay into holding furnaces for a long time because die pre-industrial trials were small and alloy was changed as frequently as dies for most of cases. The initial point chosen to monitor quality changes was the end of fluxing process. Samples were taken in the middle and at the end of casting trial, if higher than 100 pieces, or just at the end if lower than 100. Results were divided into two groups: 600 and 300 kg furnace, because the difference between the two HPDC machines and processes. The melt surface exposed to atmosphere was different, the dimension of cups was changed and ingots charging method was manual in the biggest furnace and semi-automatic in the smallest one, so oxide breaking and submerging actions were expected to have different impact on quality. Similar to the paragraph 3.2.2, quality test applied were the RPT, filtration test and hydrogen measurement. NDI, SBI, filter qualitative class and hydrogen content were used as quality indexes.

1) Nominal density index (NDI)

Nominal density index was the first index to be calculated. As seen in Figure 3.35, for 600 kg furnace, initial point, on time 0, was the value measured after degassing and fluxing treatment. Last specimen was taken at the end of every foundry trial, but for trial D another one was taken also half an hour before the last one.

The trend of trials D and H was similar, but it is interesting to note that in the case of trial D, 30 minutes later the second sampling, index value decreased. Trial I was the only case in which the NDI increased and so cleanliness worsened.

It was observed that, unexpectedly, Nominal density index seemed not changed much with time processing in the biggest furnace.
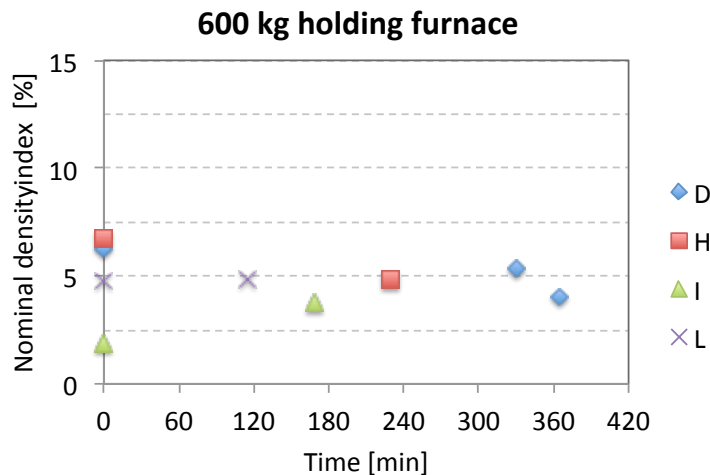
Figure 3.35: Nominal density index variation with time processing for the 600 kg furnace.

In Figure 3.36 results for the 300 kg furnace are presented. The initial NDI of trials E, M, and O was approximately the same also at the end of the casting. Different was trial F, in which after 240 minutes index value decreased from 6,5% to 5% and in the last 30 minutes reached 3,5%.

Consistently with what was previously said for 600 kg furnace, Nominal density index seemed to remain constant with time processing, except for trial F in which slightly decreased.

300 kg holding furnace
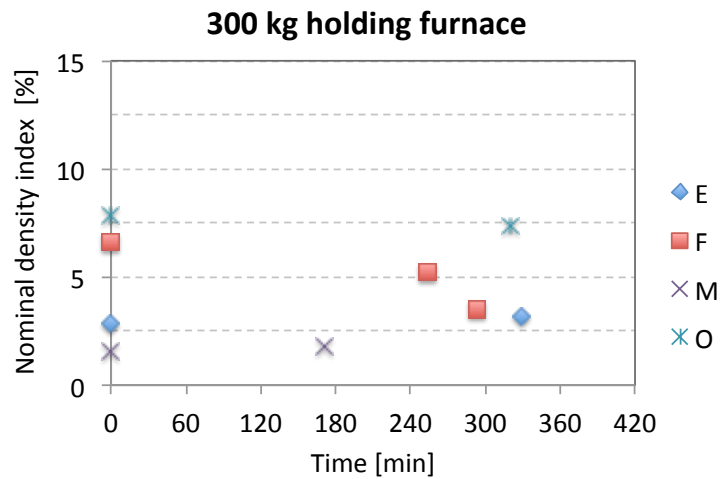
Figure 3.36: Nominal density index variation with time processing for the 300 kg furnace.

2) Specific bifilm index (SBI)

After NDI evaluation, Specific bifilm index was calculated. In Figure 3.37 the results for 600 kg furnace are given. These are substantially coherent with Figure 3.35, especially for trials D, H and I.

600 kg holding furnace
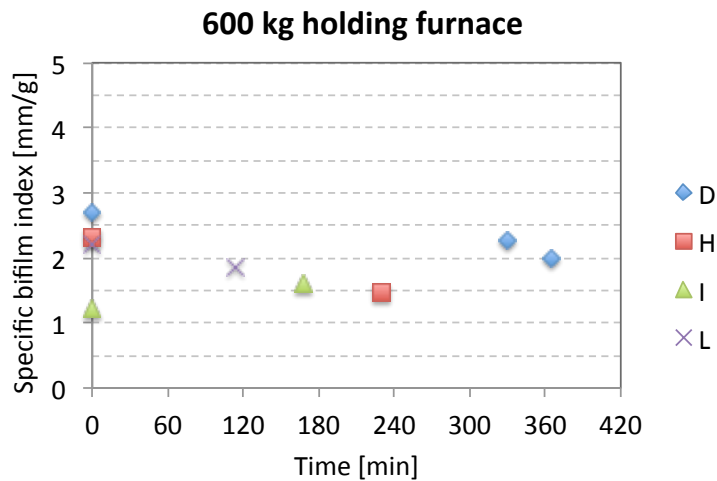
Figure 3.37: Specific bifilm index variation with time processing for the 600 kg furnace.

In Figure 3.38 are reported SBI values for the 300 kg furnace. Trend of trials E and O is comparable with Figure 3.36. In the case of trial M Specific bifilm index increased from 0,5 to 1 in 180 minutes, instead NDI was constant with time processing, as seen in Figure 3.36.

Trial F quality was improved with time processing, but looking at SBI results in Figure 3.36, the trend is opposite. The last observation is that, contrary to NDI results, SBI seems to slightly decrease with time processing for the 300 kg furnace.
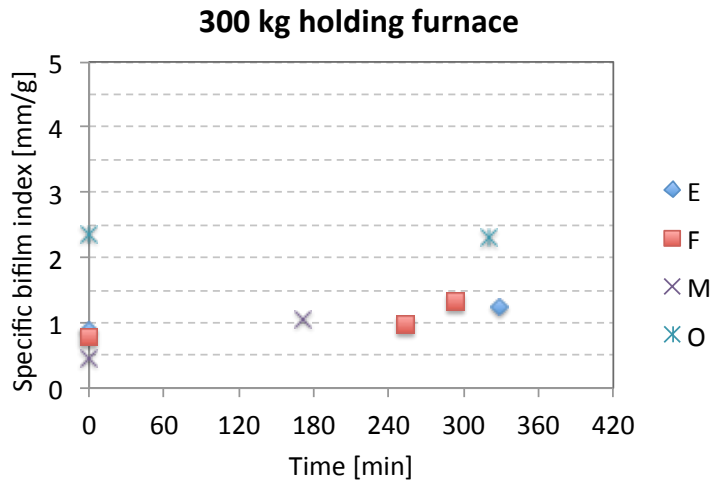
Figure 3.38: Specific bifilm index variation with time processing for the 300 kg furnace.

3) Hydrogen content

In Figure 3.39 hydrogen contents are presented at the beginning and at the end of foundry trials for the 600 kg furnace. As seen, the hydrogen trend with time processing was confined between 0,1 and 0,2 ml/100 g of Al, definitely a low level. The sudden rise to 0,3 ml/100 g of Al of the last specimen of trial D is not understood.
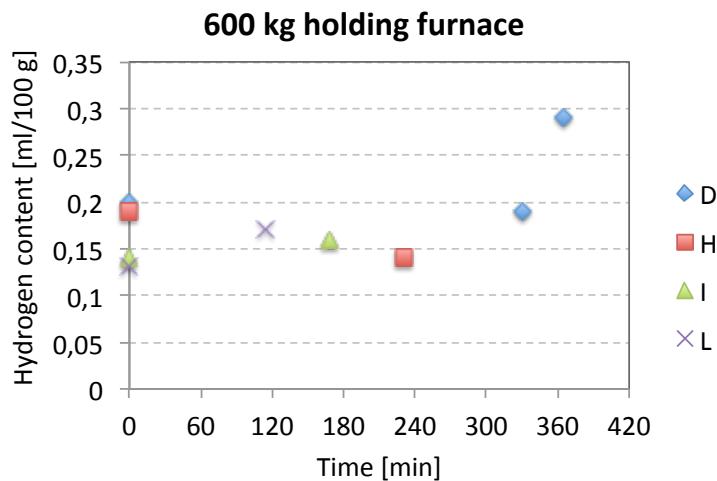
Figure 3.39: Hydrogen content variation with time processing for the 600 kg furnace.

In Figure 3.40 the results for 300 kg furnace are shown. The most important observation is that, also for 300 kg furnace, hydrogen content was approximately confined between 0,1 and 0,2 ml/100 g of Al during foundry trials.
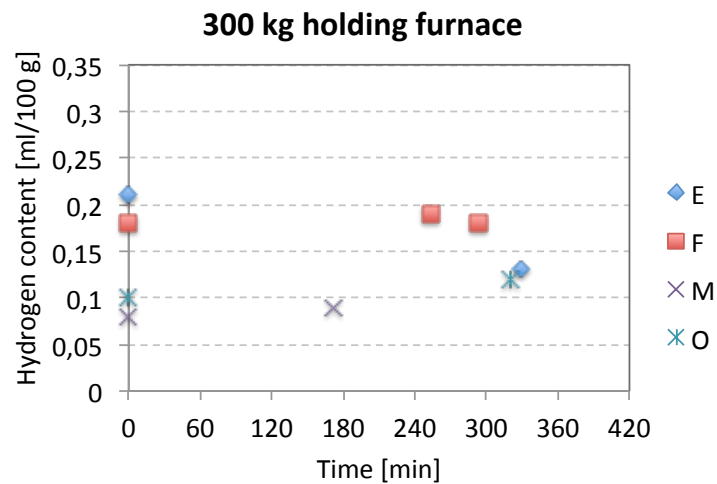
Figure 3.40: Hydrogen content variation with time processing for the 300 kg furnace.

4) Filtration test

Filtration test was the last technique used to assess quality changings during time processing. In Table 3.9, results for the 600 kg furnace are presented, including the sampling time indication.

Foundry trial	Sample	Time [min]	Class 1	Class 2	Class 3	Class 4	Qualitative class
D	after fluxing	0	26	17	5	2	D
	during trial	330	14	7	2	2	D
	end of trial	365	18	24	3	4	E
H	after fluxing	0	25	16	3	2	D
	end of trial	230	12	5	2	1	C
I	after fluxing	0	7	5	3	0	B
	end of trial	168	48	7	1	0	B
L	after fluxing	0	12	4	2	1	C
	end of trial	114	20	12	3	1	C

Table 3.9: Oxides number for each class and relative qualitative class variation with time processing for the 600 kg furnace.

In Figure 3.41 qualitative classes of specimens are graphically compared. Black is used for the specimens taken after fluxing, on time 0, grey for those taken during foundry trial, and white for the specimens taken at the end of trials. Trial D initial qualitative class remained constant after 330 minutes, but in the last 35 minutes the number of oxides increased, especially classes 3 and 4, so the qualitative class worsened. This result is in contrast with Nominal density index and Specific bifilm index, but coherent with the hydrogen content seen in Figure 3.34. In the case of trial I, after 168 minutes, class 1 oxides increased almost of seven times but class 3 oxides decreased by 2 and so the qualitative class remained B. Contrary, in Figures 3.35, 3.36 and 3.37 cleanliness of the trial I seemed to decrease with time processing.
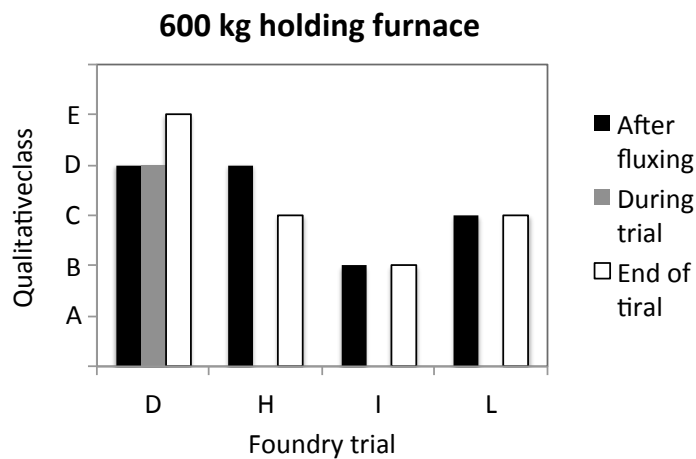
Figure 3.41: Qualitative class relationship with foundry trial after fluxing, during trial and at the end of trial for 600 kg furnace.

In Table 3.10 results for the 300 kg furnace are presented and in Figure 3.42 are graphically compared. The trend of trial E was coherent with the NDI and SBI results in Figures 3.36 and 3.38. In the case of trial F, data were in contrast with the NDI and hydrogen (Figure 3.20) content, but quite coherent with SBI. Trial M qualitative class move from D to B with time processing, completely in contrast with the other quality indexes. Trial O was the dirtiest specimens after fluxing, in fact qualitative class remained E after 320 minutes, consistently with Figure 3.36 and 3.38.

Foundry trial	Sample	Time [min]	Class 1	Class 2	Class 3	Class 4	Qualitative class
E	after fluxing	0	22	9	3	0	B
	end of trial	329	33	5	1	0	B
F	after fluxing	0	2	3	0	1	B
	during trial	254	0	0	0	0	A
	end of trial	294	1	0	0	0	A
M	after fluxing	0	61	14	3	1	D
	end of trial	172	6	0	0	1	B
O	after fluxing	0	21	4	4	3	E
	end of trial	320	32	17	3	4	E

Table 3.10: Oxides number for each class and relative qualitative class variation with time processing for the 300 kg furnace.
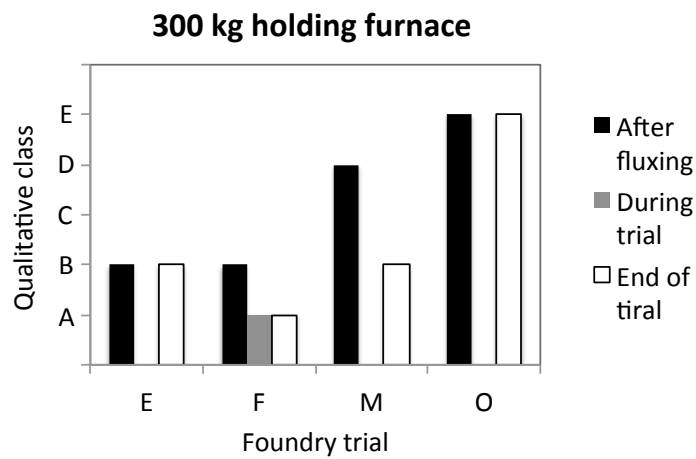

Figure 3.42: Qualitative class relationship with foundry trial after fluxing, during trial and at the end of trial for 300 kg furnace.

CHAPTER 4

DISCUSSION

4.1 Quality assessment methodology

The main purpose of this thesis was to achieve a procedure to assess the molten aluminium quality in industrial field. In order to be really applied, it has to be cheap, easy and quick, even accepting a slight error. Among the three instrument used, the only one that has these characteristics is reduce pressure test. Therefore hydrogen and filtration results were tried to correlate with RPT ones, as seen in Figure 4.1.

FILTRATION   **ALSPEK-H®**

RPT

Figure 4.1: Schematic illustration of ideal correlation between RPT and both filtration and Alspek-H® results.

Starting from hydrogen content, the first observation is that its value was less than 0,2 ml/100 g in almost all cases, and the degassing had reduced it further. Moreover during the industrial production had not changed much so its effect on quality could be neglected. Anyway, looking at results, it seems that there was consistency between hydrogen content and both Specific bifilm index and Nominal Density index of the most dirty specimens. These were samples before degassing of trials D and H for 600 kg furnace and trials E and F for 300 kg. For other specimens the hydrogen level was grouped on lower values and remained constant after degassing. To verify the existence of any kind of correlation between hydrogen content and both SBI and NDI, the relative graphs were built in Figure

4.2 and 4.3. It can be noticed the presence of a sort of trend, but the data are very scattered for both graphs.

What said in the paragraphs 3.2.2 and 3.2.4 is now confirmed, since almost all values were between 0,1 and 0,2 ml/100 g, hydrogen content is not clearly correlated with other quality indexes and so it is negligible.
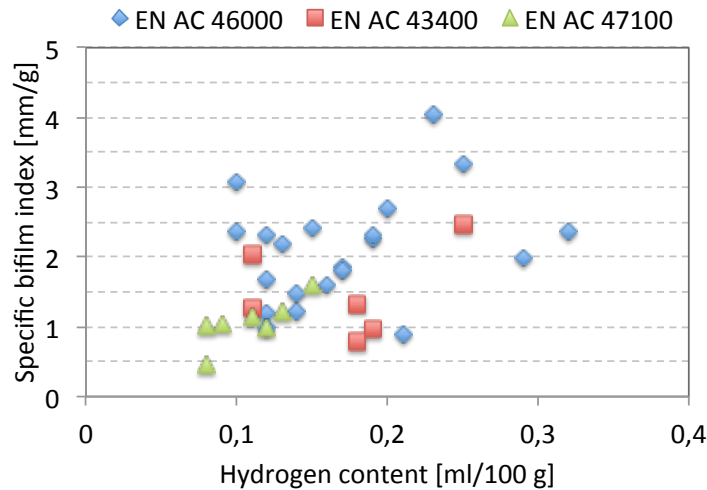
Figure 4.2: Specific bifilm index-hydrogen relationship for all the analysed specimens.
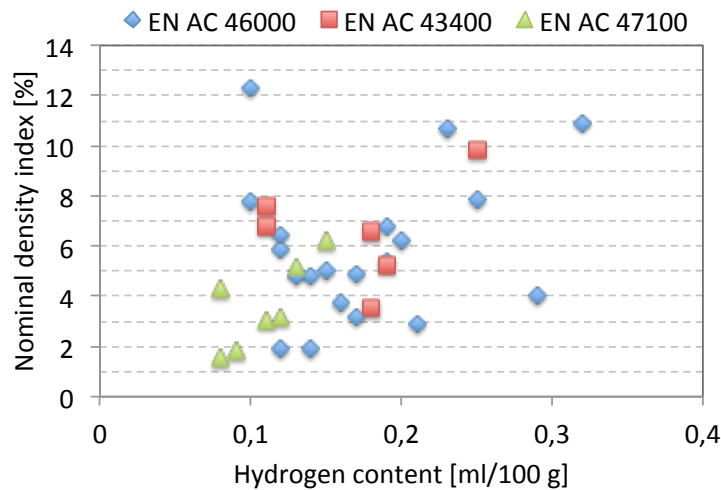
Figure 4.3: Nominal density index-hydrogen relationship for all the analysed specimens.

About filtration, for EN AC 46000 alloy a certain relationship between qualitative class and both SBI and NDI was observed. Also for other alloys this correlation seemed to exist, but as said before, the number of specimen taken for EN AC 43400 and EN AC 47100 was too

low to give robust conclusions. As in the case of the hydrogen content, same graphs were built to compare NDI and SBI with qualitative class, but this time keeping alloys separated, as seen in Figure 4.4 and 4.5.

(a)

(b)

EN AC 47100

(c)
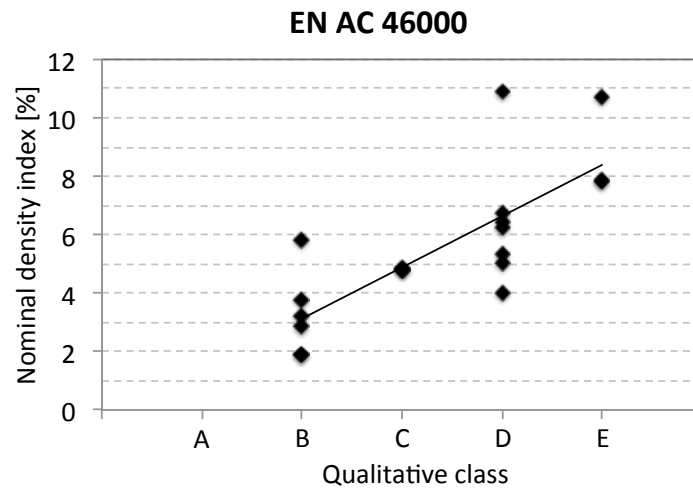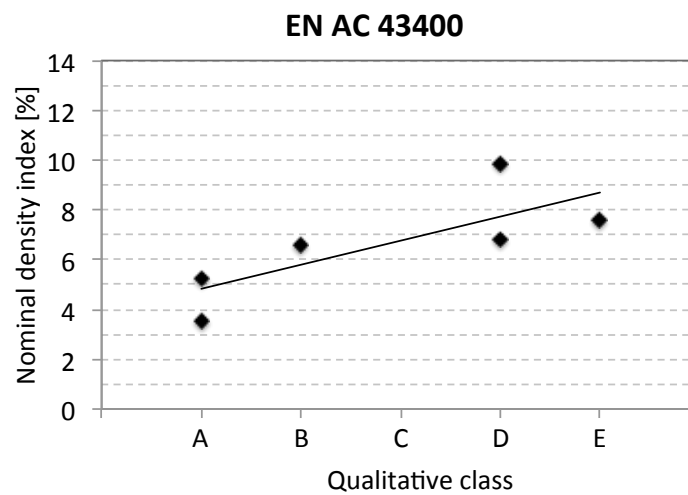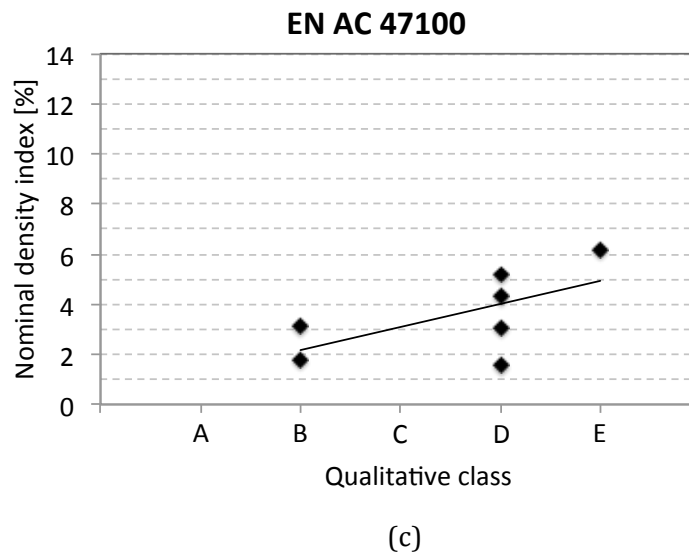
Figure 4.4: Nominal density index-qualitative class relationship for EN AC 46000 (a), EN AC 43400 (b) and EN AC 47100 alloy (c).

EN AC 46000

(a)

EN AC 43400

(b)

EN AC 47100

(c)
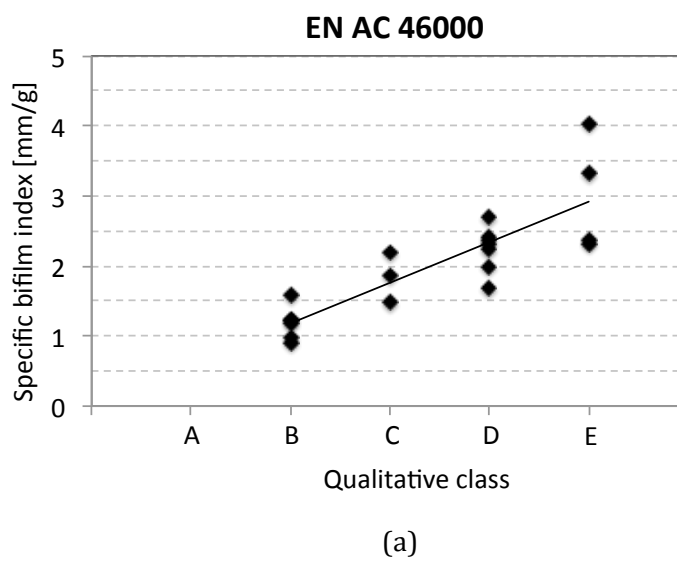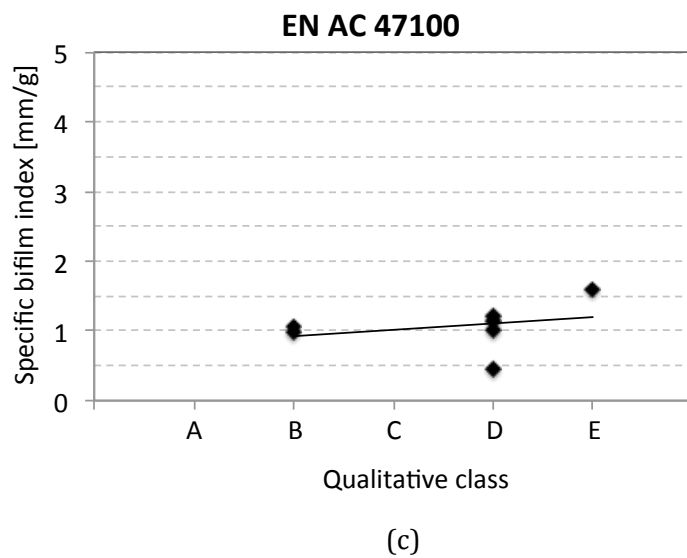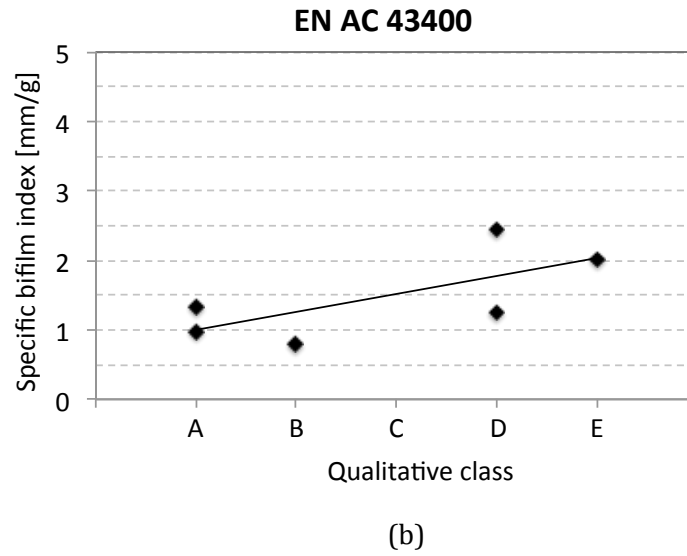
Figure 4.5: Specific bifilm index-sample class relationship for EN AC 46000 (a), EN AC 43400 (b) and EN AC 47100 alloy (c).

As shown in figure 4.4 (a), it seems to be some coherency between two indexes for EN AC 46000 alloy. It is clear that qualitative class increased with Nominal density index increasing, so it can be concluded that they are correlated. In fact, similar relationship was observed for EN AC 43400 and EN AC 47100 alloys in Figure 4.4 (b) and 4.4 (c), even if trend slope is quite different. Comparing now Figure 4.4 (a) and 4.5 (a) it is seen that scattering was reduced and so the sample class was strongly correlated with SBI, more

than with NDI. It can be further observed that the scattering increased with sample class increasing and so with cleanliness decreasing. Finally what said for graphs 4.4 (b) and 4.4 (c) is also valid for 4.5 (b) and 4.5 (c). Therefore, EN AC 46000 alloy qualitative class is correlated with NDI, accepting a slight scattering, and more strongly with SBI. Changing the alloy, slope of the line is not the same and so the correlation changes, so specimens of different alloys are not comparable between each other. To confirm this, more sampling should be done and it is necessary to build specific oxides number classes for every alloy. Concluding, hydrogen measurement is not a reliable technique to assess the molten metal quality because cannot detect small quality changes and so it can be use just as macro-assessment. As if that was not enough, the hydrogen measurement instruments are expensive too. Conversely, the filtration test allows to know exactly what is contained in the melt and it is correlated with RPT indexes results. But its biggest problem is the time needed to prepare and scan samples, totally unacceptable in any industrial environment. Therefore reduce pressure test is the only usable instrument in industrial field not only for its ease of use, quickness and low cost but also for robustness of results.

4.2 Nominal density index or Specific bifilm index?

From RPT specimens both Nominal density index and Specific bifilm index were obtained, which were studied in this thesis and here they are finally compared to understand which can describe better the molten aluminium quality. A substantial consistency was observed between them during industrial test, therefore they were plotted together in a graph considering all specimens analysed in this work. As seen in Figure 4.6, especially for EN AC 46000 alloy, trend is clear, even if scattered. The NDI increased with SBI increasing, as expected. In fact if a specimen contained a big number of oxides, the probability of the porosity formation is high and so NDI increased. For the other two alloys, scattering is higher and is hard to find a trend line, also because the specimens are too few. Anyway it can be observe that the group of EN AC 47100 alloy samples occupy lowest zone of the graph, near origin, therefore it seems to be more clean than the others. The EN AC 43400 alloy specimens are exactly under EN AC 46000 alloy ones, so for the same NDI values have lower SBI on average.
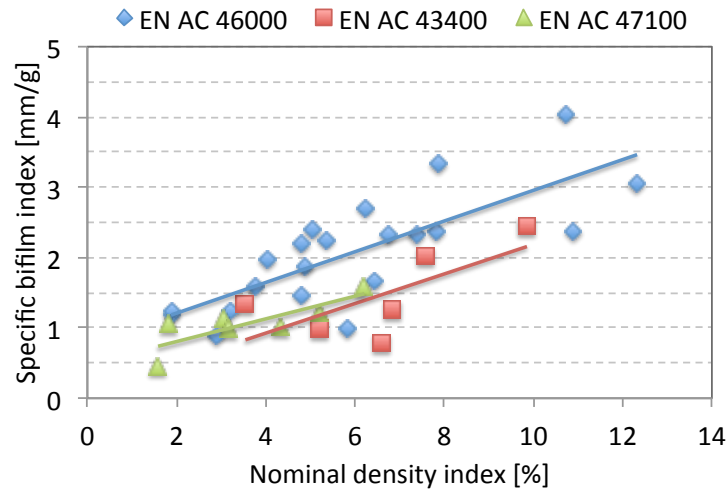
Figure 4.6: Specific bifilm index-Nominal density index relationship for all the analysed specimens.

The differences among the alloys are probably caused by different solidification mechanism, which affect quality indexes and play a fundamental role in quality assessment. For example, solidification of eutectic alloy, like EN AC 47100, is characterized by a grain growth ruled by thermic differential [7]. During growth, grains push oxides to specimen centre that should be the last part to solidify, as seen in Figure 4.7. So cutting RPT specimen a big porosity in the middle was found, probably containing some oxides that could not be correctly quantified (Figure 4.8). For this kind of alloys, specimens taken are too few so more work has to be done in order to be able to compare them with EN AC 46000 alloy ones.
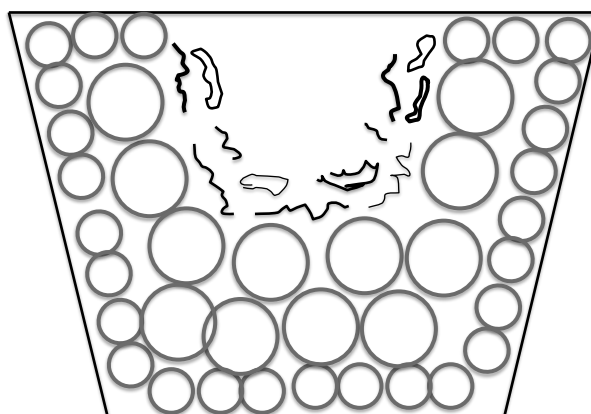
Figure 4.7: Schematic illustration of grain solidification into an EN AC 47100 alloy RPT specimen.
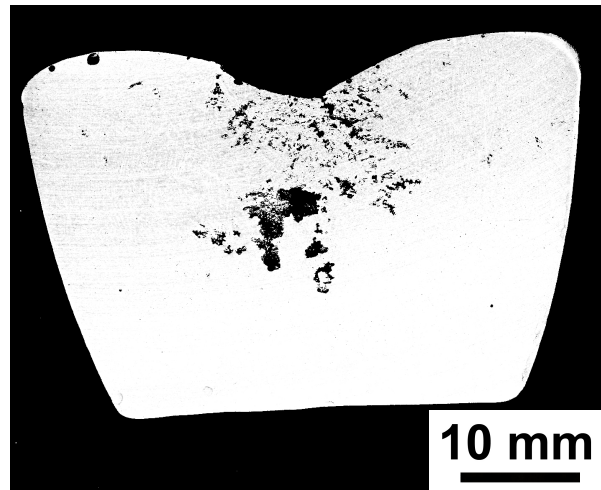
Figure 4.8: Sectioned and polished surface of a 47100 RPT specimen.

As shown by graph in Figure 4.6, the EN AC 46000 alloy results are however quite scattered. A possible explanation is that Nominal density index is a three-dimensional measurement because refers to the entire volume of the specimen, instead Specific bifilm index is two-dimensional because is relative to a specific sectioned surface. From this point of view, with the second one, some information about oxides extension are lost and their length could be underestimated. An example of this behaviour was observed in the specimen shown in Figure 4.9, where SBI was quite low but NDI was high.
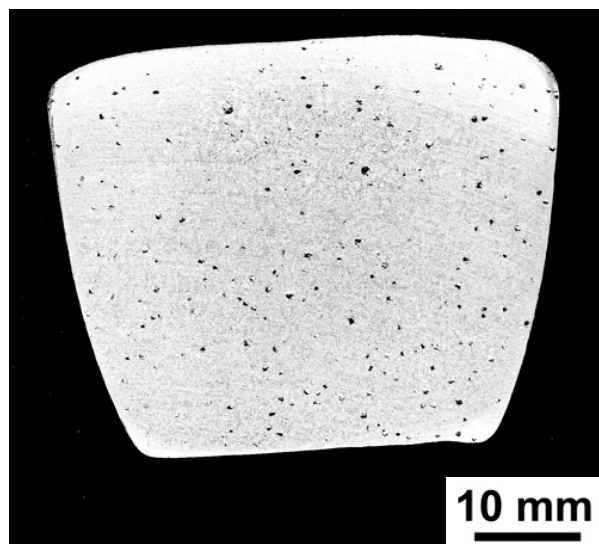
Figure 4.9: Example of underestimation of oxides presence in a sectioned and polished RPT specimen.

The Nominal density index could underestimate the bifilms' presence; in fact if they don't open to form an extended porosity, density is not much affected by them. Even if close, they act exactly like a crack and mechanical properties of the final product will be poor. An example of this type of pores was found in the specimen shown in Figure 4.10.
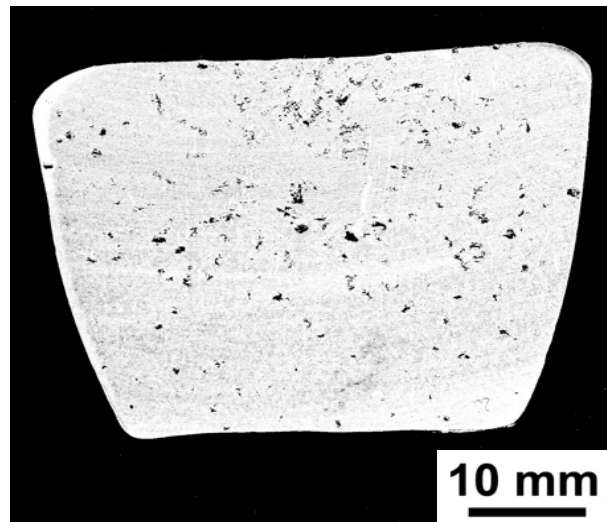
Figure 4.10: Example of crack-like pores in a sectioned and polished RPT specimen.

The last possible cause of scattering was that only Bifilm index was corrected from weight influence, contrary density was not, even from specimens with different weight, as seen in paragraph 3.1.3. In this work the specimens taken weighted between 110 g and 150 g to simulate industrial RPT use, but in general to be able to compare correctly NDI and SBI, weight variations should be minimal. The suggestion is to keep the weight as constant as possible and always over 110 g, to minimize density sensibility to weight variations.

Concluding, both indexes are characterised by weaknesses and strengths, but Nominal density index has a big advantage because is less time consuming and it could be evaluated directly inside the foundry. Therefore is recommended for frequent quality checks, instead Specific bifilm index should be calculated occasionally, if a particularly accurate measurement is required or to analysed the porosities morphology.

4.3 Supplier evaluation

Quality assessment methodology proposed in this work was applied not only to check the melt cleanliness during foundry trials but also to evaluate the suppliers, keeping constant the melting process variables. Looking at the results of paragraph 3.2.1, the first observation is that NDI and SBI values were coherent. The hydrogen content followed the two RPT indexes, even if slightly more scattered. Finally, with the filtration test was found a high number of oxides in most specimens so particularly differences between the two suppliers were not noticed. Probably classes were too rigid to compare them correctly, but having found many oxides it can be concluded that initial metal condition was poor for both suppliers. Since NDI and SBI were coherent between them and also with hydrogen content, it can be concluded that quality of supplier B ingots was definitely better than supplier A.

Has to be said that the comparison concerned all the analysed alloys together, divided of course by supplier, but actually only the EN AC 46000 alloy was provided by both suppliers, in fact EN AC 43400 alloy was supplied only by A and EN AC 47100 alloy only by B. So the same graphs seen in paragraph 3.2.1 were built just for EN AC 46000 alloy. As shown in Figure 4.11, the results were the same even considering only this single alloy. Therefore what was said previously was definitively confirmed: the quality of supplier A was worse than supplier B.

(a)   (b)

(c)   (d)
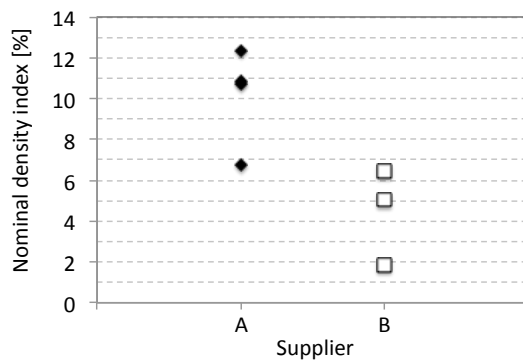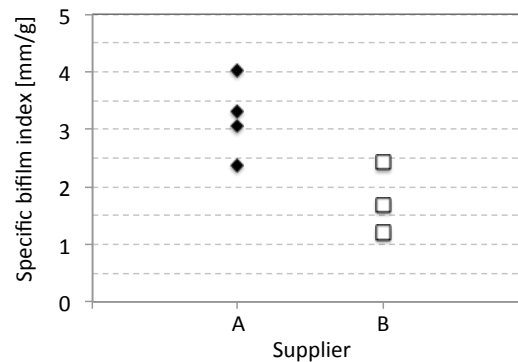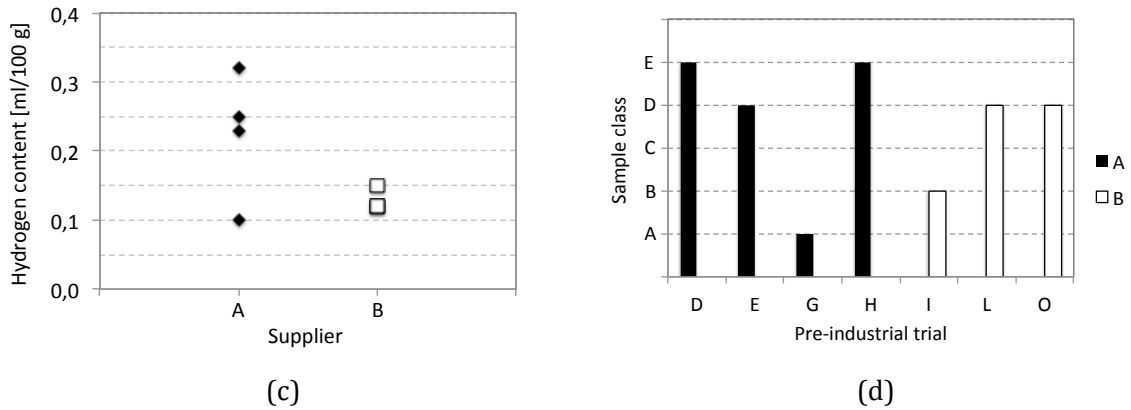
Figure 4.11: Nominal density index (a), Specific bifilm index (b), hydrogen content (c) and sample class (d) of EN AC 46000 alloy from supplier A And B.

4.4 Degassing study

The first observation about degassing and fluxing treatment is that was generally effective, because reduced the scattering and improved quality index values on average. However the hydrogen content, NDI and SBI have not changed during the degassing. The real improvement was obtained after the fluxing and skimming. This behaviour can be easily explained for RPT indexes, in fact taking specimen during the degassing, a lot of oxides, carried to the surface by bubbles, are caught with the ladle and brought into the cup. About hydrogen content some assumption can be made. The first one is that the drossing fluxes had a degassing effect on the melt due to the sodium, calcium and phosphorus content. For example it is known that sulphur hexafluoride is one of the best gas for degassing but unlikely is very polluting for atmosphere [7]. Another explanation is that since opened floating bifilms were caught by the drossing salts during fluxing, they were even closed and tangled together so the hydrogen trapped inside flowed outside of the melt. Probably the combination of these two effects is the cause of the quality improvement after fluxing.

Another interesting founding is the identification of the process limit. This value is related to the operating conditions of degassing process, in particular the use of lance and fluxing after degassing. Modern degassing stations use a rotor in the last part of the lance to break big bubbles in smaller ones and fluxing is done during degassing to trap oxides from all the metal mass and not just from the surface. The result is a better degassing performance and so achievement of a lower limit. It is interesting to note that such limit did not strongly depend on gas flow rate. The increasing of degassing performance observed with medium

flow rates seems less important than the initial quality level of the molten metal. In fact this parameter was the real driving force of the entire process, because more dirty was the melt, more effective was the degassing, in relative terms. If the melt cleanliness was near the limit, degassing was almost useless, especially for the bigger furnace.

Since were not observed particular changes with different flow rates, degassing time was then studied. When the process duration was very low, degassing had worsened initial cleanliness level. In fact the oxides were not completely carried to the surface and so the superficial fluxing did not remove those floating in the melt. It can be concluded that the degassing duration had a strong impact on the process performance, therefore SBI on degassing time graph was plotted for 600 kg furnace, as seen in Figure 4.12.

The first value, on time 0, is the SBI before degassing and the second value refers to the specimen taken after fluxing. The process limit line was drown on 1 mm/g, consistently with chapter 3 results, then were built the theoretical trend lines passing through the two points to understand time needed to reach the process limit value. Lower was initial SBI more flat was the theoretical line. For trials D, H, I and L, all of EN AC 46000 alloy, 12 min was not sufficient to reach a SBI of 1 mm/g, and probably not even 20 minutes were enough. Instead for trials N and P, 12 and 15 minutes it seemed sufficient.

The same graph was built also for 300 kg furnace in Figure 4.13. As seen, the situation is different because in all cases, except for trial O, the limit was reached after fluxing and in the case of trial M was even improved.
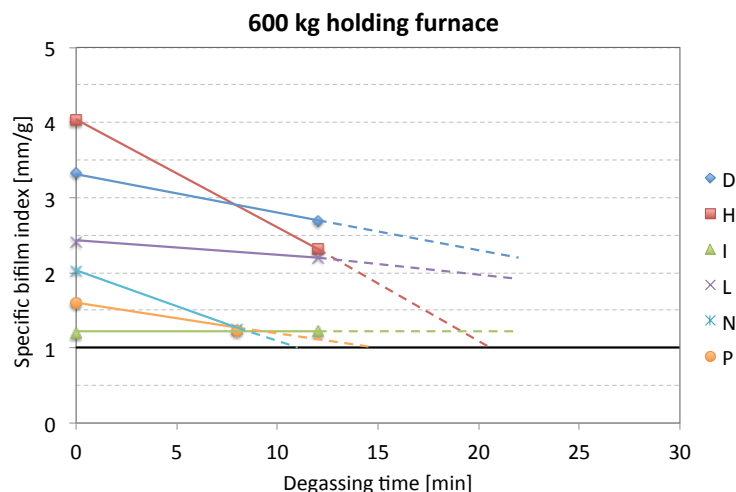
Figure 4.12: Theoretical trend of the Specific bifilm index increasing degassing time for 600 kg holding furnace.

300 kg holding furnace
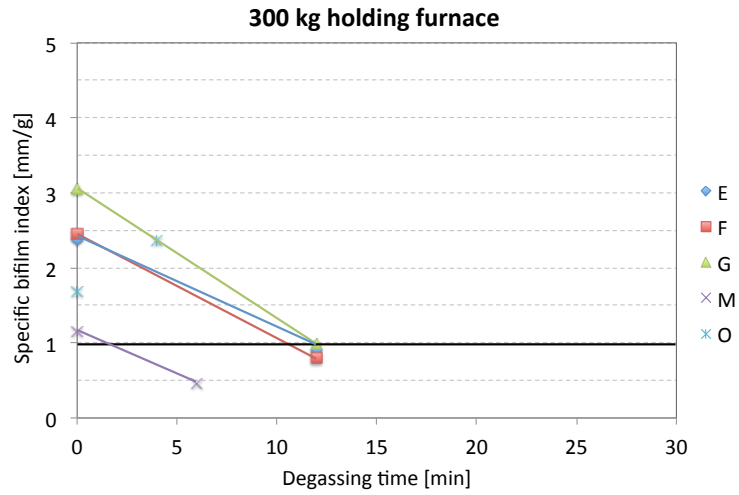
Figure 4.13: Theoretical trend of the Specific bifilm index increasing degassing time for 300 kg holding furnace.

600 kg holding furnace
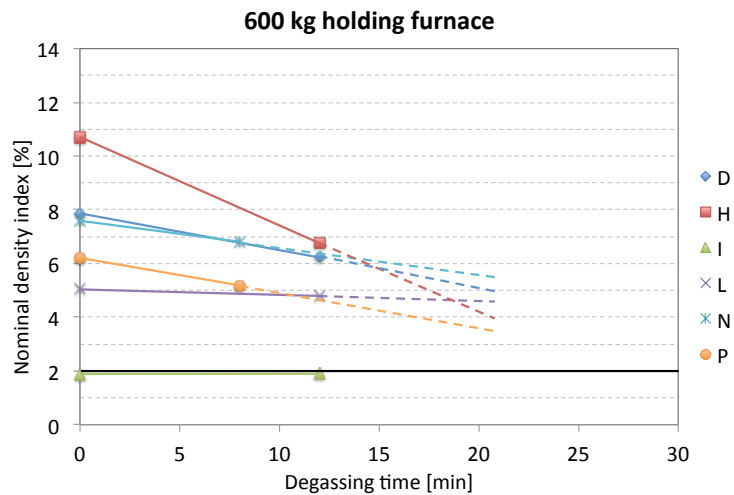
Figure 4.14: Imaginary trend of Nominal density index increasing degassing time for 600kg holding furnace.
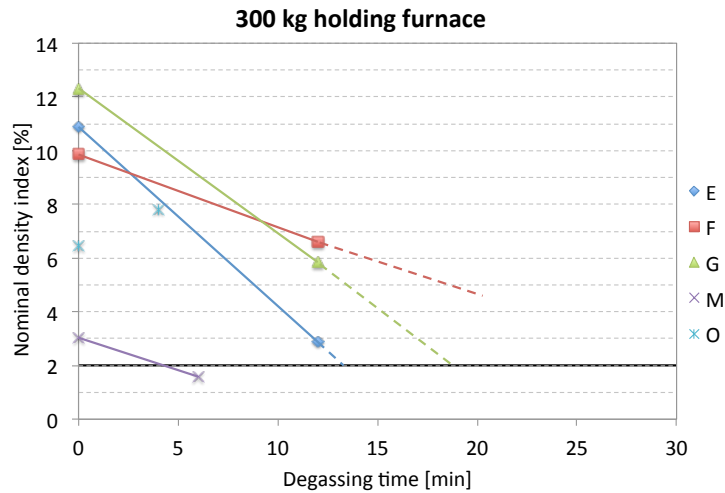
Figure 4.15: Imaginary trend of Nominal density index increasing degassing time for 300kg holding furnace.

The Nominal density index on degassing time was plotted for both furnaces. The results for 600 kg, in Figure 4.14, were coherent with Figure 4.12 for EN AC 46000 alloy trials (D, H, I and L). Contrary, trials N and L did not reach the process limit of 2% after the degassing. The 300 kg results in Figure 4.15 were coherent for the trials E and M, but quite different for trial F, where the degassing seemed not so effective and for trial G where the limit is reached after approximately 20 minutes instead of 12. As said previously, probably SBI values were underestimated, but in both cases the degassing and fluxing treatment appeared more effective in the smallest furnace because the slope of theoretical lines was higher.

A possible explanation of such behaviour is that the degassing lance was effective only for a certain volume of metal, close to the lance itself. In fact, without rotor or diffuser, the gas bubbles are bigger and during rising tend to remain near the lance [7], as shown in Figures 4.16. Thus the effective degassing volume, which was the volume of molten metal cleaned effectively by degassing, covered almost all the volume of the smallest crucible but proportionally half the volume of the biggest one, as seen in Figure 4.17. Therefore is strongly recommended to use a diffuser or at least move the lance during degassing of the biggest furnace to increase the effective volume. Furthermore the fluxing salts should be putted on the melt before degassing, to be submerged by bubbles and trap more oxides from deeper metal.
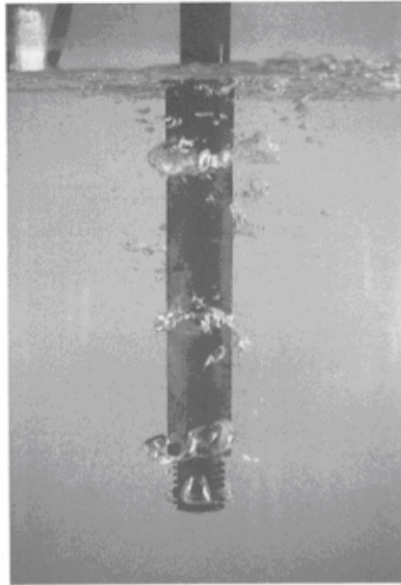
Figure 4.16: Large bubbles produced by use of a graphite lance in a water model study of degassing [7].
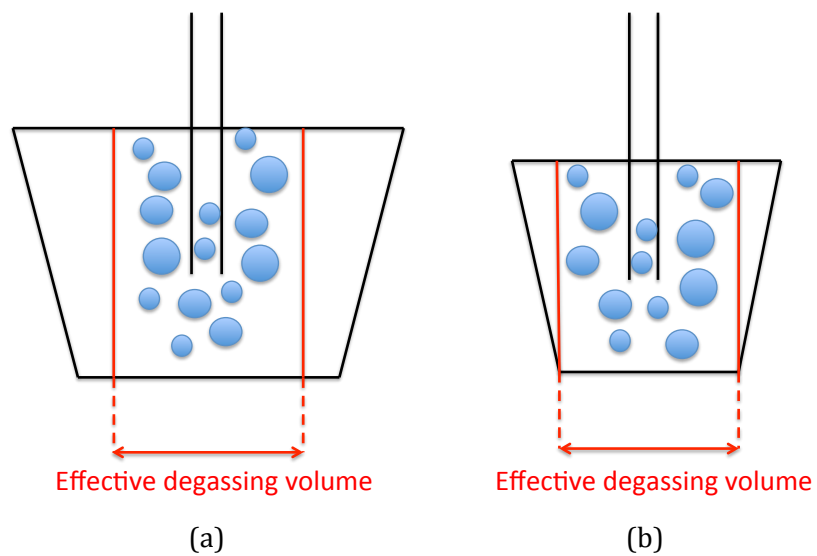
Figure 4.17: Effective degassing volume for the 600 kg (a) and 300 kg (b) holding furnaces.

4.5 Nitrogen or argon?

The nitrogen is widely used in industrial filed because it could be taken free from tanks no longer usable for HPDC machines. Main problem is that its bubbles are bigger compared to argon and rise farther between them, so the clean effect is less because small oxides slips over bubbles and only extended ones are carried on surface [7], as seen in Figure 4.18.

Nitrogen   Argon

(a)   (b)
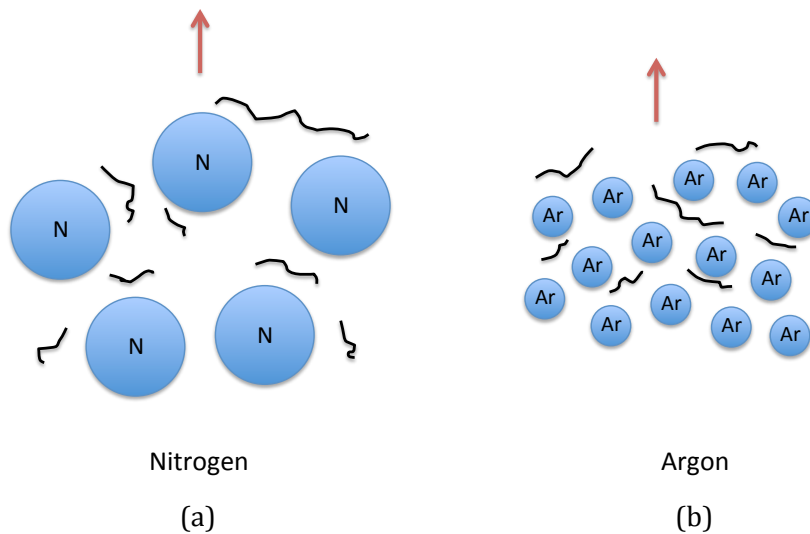
Figure 4.18: Bifilms feed to the surface of the melt by (a) nitrogen bubbles and (b) argon bubbles.

Moreover, the big bubbles may cause higher turbulence in the surface with the risk to introduce bifilms into the melt. From the obtained results, it seems that using nitrogen instead of argon, cleanliness however slightly increased, especially looking at the Nominal density index and filtration sample class. It should be considered that just one degassing was carried out with nitrogen and alloy was EN AC 47100. Therefore this single result is not sufficient to evaluate the degassing process with nitrogen for this kind of treatment.

4.6 Metal quality with time processing

At first sight, it seems that quality not changed much with time processing. As previously said, the decreasing of melt cleanliness seems to be due to the surface oxide film breaking by HPDC ladle and ingots charge. Furthermore it was expected to find bigger oxides in

filtration sample due to the microstructure changing from amorphous to crystalline as time goes by. None of these effects was observed in the results, instead values measured remained into specific range. The Nominal density index between 2 and 4%, Specific bifilm index between 2 and 1 mm/g, hydrogen between 0,2 and 0,1 ml/100 g and also the filtration results were constant or even improved. It was observed a slight increasing trend, so a decreasing in cleanliness, especially for SBI, in the smallest furnace. In the biggest, trend is opposite; the cleanliness seemed to increase with time processing. This behaviour could be explained starting by Stokes law that describes frictional force of a spherical small particle in a continuous viscous fluid.

$$F = 6\pi\eta Rv \qquad\qquad (4.1)$$

$F =$ frictional force

$\eta =$ dynamic viscosity

$R =$ radius of the spherical particle

$v =$ particle's velocity

Comparing with the force that causes the motion of particle, the sedimentation velocity can be obtained:

$$v = \frac{2}{9}\frac{(\rho_p-\rho_f)}{\mu}g\,R^2 \qquad\qquad (4.2)$$

ρ_p = density of the particle

ρ_f = density of the fluid

μ = dynamic viscosity

g = gravitational acceleration

R = radius of the spherical particle

As seen in Equation 4.2, to start moving is necessary a density difference between the particle and fluid. Since the oxide density (2.5 - 3.5 gr/cm^3) and liquid aluminium density (2.5 g/cm^3) are very close, bifilms should float in the melt. However there is another force

that may help the oxides moving. If they are heavy, because the air gap between bifilms was consumed to further oxidize bifilms themself (and of course made them thicker), these oxides will sink in the bottom of furnace according to the Stokes low. On the other hand if the air gap is big, bifilms may rise toward the surface always according to the Stokes low. It should be considered that these situations are valid only in the case of laminar flow, i.e. without convection that increases turbulence, as in the smallest furnace. Decreasing quality with time processing could be due to rising oxides that were caught from the surface by the ladle. If there is convection, like in the biggest furnace, due to its width, oxides moves inside the melt in various pathways, not rising, so the probability to catch them is lower. In fact the quality seemed to increase with time processing.

4.7 Quality assessment procedure

The ultimate purpose of this thesis was to write down a procedure to assess molten aluminium quality in industrial field. This procedure includes not only a list of instruments and instructions, but also all the correct operating parameters and chronological sequence of actions to apply the procedure properly. Tools used are: steel ladle, steel cup (not too small and possibly with thin walls), RPT, die for the chemical analysis, Archimedean balance and quantometer.

1) Pre-heat, at least up to 70°C, the ladle, RPT steel cup, and die for the chemical analysis. The fastest way is on the edge of furnace.
2) Pour aluminium in the cup and leave it solidify under atmospheric pressure, just to pre-heat it more. Discard the specimen.
3) Skim off the surface oxide film with the ladle bottom, fill the ladle, pour metal in the cup, carry it with care and leave it solidify under a pressure of 100 mbar. Leave the RPT pump running.
4) During wait, pour metal in the die for the chemical analysis for two times. Discard the first specimen.
5) Remove the RPT specimen from the cup and weight the specimen in air and then in water.
6) Calculate density with the following equation:

$$d = \frac{m_{air}}{(m_{air} - m_{water})\rho_{water}}$$

7) Grind the specimen for the chemical analysis with zirconium oxide paper.

8) Do the chemical analysis with the quantometer.

9) Calculate the nominal density with the following equation:

$$d_n = 2,71\text{-}0,4Si\text{+}0,74Cu\text{+}0,3Fe\text{+}0,87Mg\text{+}0,09Mn\text{+}0,06Cr\text{+}0,51Zn\text{+}0,56Ti$$

10) Calculate the Nominal density index with the following equation:

$$Nominal\ density\ index = \frac{\rho_n - \rho_{rp}}{\rho_n} \cdot 100$$

At this point the first quality index is calculated and it can be used to assess the melt cleanliness. The next part is for those which want go deeper in the quality evaluation, calculating Specific bifilm index and compare it with the previous result.

11) Cut the specimen in two halves, better using a grinding wheel.

12) Polish the surface with 180, 600 and 1200 silicon carbide papers.

13) Scan the sample at 1200 dpi.

14) Adjust the image colours and reduce to 700 dpi.

15) Do the image analysis.

16) Calculate Bifilm index with the following equation:

$$Bifilm\ index = \sum(pore\ lenght)$$

17) Calculate Specific bifilm index with the following equation:

$$Specific\ bifilm\ index = \frac{Bifilm\ index}{weight}$$

Now all the information about quality is collected. The two indexes can be compared to evaluate possible differences and the RPT specimen surface can be analysed to know pores morphology and choose the most reliable index.

CHAPTER 5

CONCLUSIONS

In this work three different measurement techniques have been evaluated to assess the molten metal quality. Hydrogen measurement was the most unreliable for this kind of melting process because the results were often scattered and it was unable to measure slight quality changes of the melt. A connection with the RPT data was not found. The filtration method seems to be more accurate but it is very time consuming both for the sample preparation and the scanning with optical microscope. Moreover it is a semi-quantitative test (qualitative classes). RPT was the most reliable measurement instrument in terms of accuracy, quickness and cost, and so it is strongly recommended.

Among the different quality indexes analysed for the RPT specimens, ρ_{index} and Nominal density index (NDI) do not need any metallographic preparation of the sample so they the quickest to carry out, but the morphology of the pores remains unknown. ρ_{index} underestimates systematically the true density; contrary the NDI is more robust and accurate. However specimen's weight should be higher than 110 g. Porosity content evaluated with image analysis is strongly dependent on metallographic preparation, so the repeatability is low and it cannot be applied in industrial field. The Bifilm index is a very accurate index if the analysed specimens have the same weight; from the laboratory test it was found that its result linearly depend on specimens' weight. It means that dividing Bifilm index for the weight (Specific bifilm index), the melt quality can be quantified independently from the quantity of molten metal used in the reduce pressure test.

Foundry trials have shown that the driving force of the degassing process is the initial quality of the melt. If it is poor, the treatment is more effective than starting with a clean melt. An effectiveness limit was also found for the degassing process studied. It was approximately an NDI value of 2% and an SBI value of 1 mm/g. This limit can be potentially evaluated for every furnace-degassing equipment system, and, knowing the initial condition of the melt (with the quality assessment procedure), it can be decided if carry out degassing process or not. As seen in this work, the degassing process of a clean melt did not give any benefit and so it was a waste for the foundry. Contrary, if the melt is dirty, knowing the system limit and the furnace dimension, the degassing time can be estimated using the theoretical trend lines proposed in this thesis. Actually, degassing in foundry is a standardized process, in terms of operating parameters setting, here it is suggested to adjust it according to the initial cleanliness of the molten bath. The

potential advantages for the companies are the reduction of annual cost of the treatment gas (in the case of argon) and fluxing salts, as well as time saving if degassing is not required. This means reduction of downtime and productivity increasing. The most important advantage is the potential elimination of all "non-quality costs" that affects foundries. In fact, if the initial quality of the melt is low and degassing is not sufficient to improve it enough, the produced castings could be rejected, wasting time, raw material and mostly energy.

Results of the degassing process with nitrogen, instead of argon, are too few to give robust conclusions.

During time processing it was unexpectedly not observed any particular quality changing of the melt, except for a slight cleanliness decreasing in the smallest furnace, probably due to lower convection compared to the biggest one.

The proposed quality assessment method allows to evaluate also the quality of different suppliers, keeping constant the melting parameters. In this work, a substantial difference was found between the two suppliers analysed.

The different chemical composition, solidification, oxide and porosity morphology may affect the quality measurement indexes. In the future, more work and efforts have to be done in such direction.

REFERENCES

[1]   Campbell, J.: "Castings". 2nd ed., Elsevier Butterworth-Heinemann, Oxford 2003.

[2]   Timelli, G.: "Innovation in Metallurgical production: Innovation on Design and properties", slides.

[3]   www.alueurope.eu

[4]   Akhtar, S., Timelli, G., Bonollo, F., Di Sabatino, M., Arnberg, L.: "A comparative study of defects and mechanical properties in High pressure die cast and gravity die cast aluminium alloys", International Foundry Reserch/Giessereiforschung 61 (2009) No.2, pp 2-14.

[5]   Akhtar, S., Dispinar, D., Arnberg, L., Di Sabatino, M.: "Effect of hydrogen content, melt cleanliness and solidification conditions on tensile properties of A356 alloy", International Journal of Cast Metals Research (2009), Vol 22, pp 22-25.

[6]   Espinoza-Cuadra, J., Garcia-Garcia, G., Mancha-Molinar, H.: "Influence of defects on strength of industrial aluminium alloy Al-Si 319", Materials and Design (2007), Vol 28, pp 1038-1044.

[7]   Gruzleski, J. E., Closset, B. M.: "The Treatment of Aluminium-Silicon Alloys". American Foundreymen's Society, Inc., Illinois 1990.

[8]   Kaufman, J. G., Rooy, E. L., "Aluminum Alloy Castings: Properties, Processes and Applications". ASM International, 2004

[9]   S. Impey, D.J. Stephenson, J.R. Nicholls, A study of the effect of magnesium additions on the oxide growth morphologies on liquid aluminum alloys. Microscopy of Oxidation, 1991: p. 238-244.

[10]   R. Fuoco, E.R. Correa, M. de A Bastos, L.S. Escudero, Characterization of some types of oxide inclusions in aluminum alloy castings. AFS Transactions, 1999. 107: p. 287-294.

[11]   L.P.H. Juergens, W.G. Sloof, F.D. Tichelaar, E.J. Mittemeijer, Thermodynamic stability of amorphous oxide films on metals: Application to aluminum oxide films on aluminum subtrates. Physical Review B, 2000. 62(7): p. 4707-4719.

[12]   Dispinar, D.: "Detrermination of Metal Quality of Aluminium and its Alloys". University of Birmingham, 2005.

[13]   Fisher, J.C., The fracture of liquids. Journal of Applied Physics, 1948. 19 (November): p. 1062-1067.

[14]   Bangykhan, K., "Effect of oxide film, Fe-rich phase, Porosity and their interaction on tensile properties of cast Al-Si-Mg alloys". University of Birmingham, 2005.

[15] P.S. Mohanty, F.H. Samuel, J.E. Gruzleski, Experimental study on pore nucleation by inclusions in aluminum castings. AFS Transactions, 1995. 103: p. 555-564.

[16] Akhtar, S.: "Hydrogen Porosity in Al-Si Foundry Alloys". NTNU, 2010.

[17] D. Emadi, J.E. Gruzleski, M. Pekguleryuz, Melt oxidation behavior and inclusion content in unmodified ad Sr-modified A356 alloy- their role in pore nucleation. AFS Transactions, 1996. 104: p. 763-768.

[18] Divandari, M., Campbell, J.: "Morphology of oxide films of Al-5Mg alloy in dynamic conditions in casting". Internation Journal of Cast Metals Reserch (2005), Vol. 18, pp 187-192.

[19] Anyalebechi, Prince N., Analysis of the effects of alloying elements on hydrogen solubility in liquid aluminum alloys. Scripta Metallurgica et Materialia, 1995. 33(8): p. 1209-1216.

[20] Lee, P. D., A. Chirazi and D. See, Modeling microporosity in aluminum-silicon alloys: a review. Journal of Light Metals, 2001. 1 (1): p. 15-30.

[21] X. Cao, J. Campbell, The nucleation of Fe-rich phases on oxide films in Al-11.5Si-0.4-Mg cast alloys. Metallurgical and Materials Transactions A, 2003. 34A (July): p. 1409-1420.

[22] N. Unlu, M.G. Drouet, Comparison of salt-free aluminum dross treatment processes. Resources, Conservation and Recycling, 2002. 36: p. 61-72.

[23] J. Campbell: "Complete casting handbook" Elsevier Butterworth-Heinemann, Oxford 2011.

[24] Makhlouf, M., Apelian, D., Wang, L.: "Microstructures and properties of Al die casting alloys", NADCA, Illinois 1998.

CV Andrea Gnesotto

PERSONAL DATA

First name / Surname	Andrea Gnesotto
Date and place of birth	25 March 1988, Bassano del Grappa (Italy)
Nationality	Italian
Address	Via Guido Agnolin 7, 36061 Bassano del Grappa (Italy)
Phone	+39 340 0065236
E-mail	andrea.gnesotto@gmail.com

EDUCATION AND QUALIFICATIONS

2011 – 2013	University of Padua, **Master Degree in Economics and Industrial Engineering**, with specialisation in logistics and industrial metallurgical applications.
2007 – 2011	University of Padua, **Bachelor Degree in Economics and Industrial Engineering**, with a specialisation in Management and Organisation.
2002 – 2007	Liceo Jacopo da Ponte, Scientific High School Degree in Bassano del Grappa.

FORMATIVE EXPERIENCE

May-September 2013	**Internship** at **SAEN snc** for graduation thesis. The work consists in development of an innovative method to evaluate aluminium melt cleanliness into high pressure die casting process foundry.
2012	**Logistic Game** National session in Vicenza, during Logistic Meeting on 04th of May. Classified 3rd within University of Padua and in the top ten among all other Italian universities. About 20 teams of students of Department of Management and Engineering in Vicenza, had competed in a game of logistical and manufacturing construction of an industrial plant. A virtual simulation of an "Internal Supply Chain" with a production system, a material handling system and an assembly system. The aim of the game was to plan all activities to reach a given level of service, using least possible amount of money. Scores allowed to draw up a national ranking.
2008	Short summer experience in the warehouse of a company of leather handbags near Vicenza. With tasks of loading/unloading, client orders and shipments control.

LANGUAGES SKILLS

Italian	Mother tongue.
English	**Certification: 2007 Test of language ability (TAL), level B1** **Written: Fluent Spoken: Fluent**

COMPUTER SKILLS

Very good knowledge of Microsoft Office, Mysql, Adept V+, CES EduPack, Arena.
Good knowledge of GAMS, Pro Engineering, MatLab.

CHARACTERISTICS AND MOTIVATIONS

Determined, dynamic and well-disposed for team work as proven during my Logistic
Game experience. Open-minded and always ready to learn from new opportunities and
experiences from all over the world. Available to move for medium-long periods.
Interested in industrial metallurgical application, continuous improvement of processes
and problem solving.

OTHER ACTIVITIES AND INTERESTS

I like travelling, music, reading and I practice amateur football and snowboarding.

Bassano del Grappa, 12th December 2013.

Andrea Gnesotto